Structural and Stress Analysis of a High Temperature Geothermal Wellhead

Árni Ólafsson

Faculty of Industrial Engineering, Mechanical Engineering and Computer Science
University of Iceland

Structural and Stress Analysis of a High Temperature Geothermal Wellhead

Árni Ólafsson

60 ECTS thesis submitted in partial fulfillment of a
Magister Scientiarum degree in Mechanical Engineering

Advisors
Dr. Magnús Þór Jónsson
Dr. Halldór Pálsson

Faculty of Industrial Engineering, Mechanical Engineering and Computer Science
School of Engineering and Natural Sciences
University of Iceland
Reykjavik, September 2011

Structural and Stress Analysis of a High Temperature Geothermal Wellhead
60 ECTS thesis submitted in partial fulfillment of a *Magister Scientiarum* degree in Mechanical Engineering

Faculty of Industrial Engineering, Mechanical Engineering and Computer Science
School of Engineering and Natural Sciences
University of Iceland
VR-II, Hjarðarhaga 2-6
107 Reykjavik
Iceland

Telephone: 525 4000

Bibliographic information:
Árni Ólafsson, 2011, *Structural and Stress Analysis of a High Temperature Geothermal Wellhead*, Master's thesis, Faculty of Industrial Engineering, Mechanical Engineering and Computer Science, University of Iceland

Reykjavik, Iceland, September 2011

Abstract

High temperature geothermal wellheads have to be designed to withstand very high pressure and temperature loads. The complex geometry of wellhead equipment make it difficult to analyze it structurally using conventional methods. In this project a finite element model of a geothermal wellhead was developed and tested using realistic load data from measurements of a well while charging. This model incorporates nonlinear material properties, taking into account the decreasing of strength with temperature, as well as yielding in the gaskets in the flange connection.

Útdráttur

Búnaður við topp á borholum á háhitasvæðum þarf að vera hannaður til að þola mjög hátt þrýsti- og varmaálag. Margbrotið form búnaðarins veldur því að erfitt er að álagsgreina hann með hefðbundnum aðferðum. Í þessu verkefni er gert einingareiknilíkan (e. finite element model) af borholutoppi og prófað með raunhæfum álagsgildum sem mæld voru við blástur borholu. Líkanið hermir m.a. ólínulega efniseiginleika, þar með talið minnkun á styrk með auknu hitastigi og flot í þéttingum flangsatenginga.

Table of Contents

List of Figures

List of Tables

Acknowledgements

This thesis was written under the guidance of Dr. Magnús Þór Jónsson and Dr. Halldór Pálsson, professors of mechanical engineering at the Faculty of Industrial Engineering, Mechanical Engineering and Computer Science at the University of Iceland. Their assistance and support is greatly acknowledged. Further acknowledgements go to Arnar Bjarki Árnason and Kristinn Ingason at Mannvit, Birta Svavarsdóttir and Gunnar Skúlason Kaldal at the University of Iceland, Geir Þórólfsson at Hitaveita Suðurnesja, Ólafur Árnason at Almenna verkfræðistofan, Sigurjón Fjeldsted, Sæmundur Jónsson and Þorleikur Jóhannesson at Verkís, and Sverrir Þórhallsson at Iceland GeoSurvey. Finally, acknowledgements go to GEORG (GEOthermal Research Group) for financial support, and Verkís for providing the author with excellent working facilites.

Árni Ólafsson

Faculty of Industrial Engineering, Mechanical Engineering and Computer Science
University of Iceland
VR-II, Hjarðarhagi 2-6
Reykjavík, September 2011

1 Introduction

Geothermal wells that have been drilled to reach reservoirs deep down in the earth have to be strong enough to withstand very high pressures and temperatures. These kinds of wells are often 2-3 kilometers deep, where the temperature of the geothermal system can be 200 to 350°C, and the pressure 110-130 bar. Normally a mixture of steam and water flows through a high temperature geothermal well, with the steam portion increasing with rising altitude. The flow is dependent upon the pressure at the top of the well, and this pressure can be controlled within certain levels. High temperature geothermal wells are usually operated at a 10-20 bar wellhead pressure. Under certain circumstances this pressure can get considerably higher, and there have been cases where the wellhead pressure in a closed well has been 100-110 bar [1].

The most common design procedure for wellheads is to estimate the highest probable temperature and pressure at the top of the well, and then to choose equipment accordingly, using standards and simple design models to assist in the design process. Some of the parts are standardized equipment from manufacturers (such as the main valve) and some are specially made (such as the restraining bars and sometimes the expansion spool). Since wellhead equipment has to withstand high pressures, temperatures, vibration, corrosion and other extreme load cases it is vital that the wellhead design is analyzed properly before construction begins. Due to the geometry of wellheads, and the complex load combination subjected to them, it can be difficult to analyze them structurally with conventional methods. Therefore, it would be of great assistance to designers to have a realistic model to analyze the equipment during the design phase.

1.1 Objective

The objective of this project is to construct a finite element model that can be used to analyze wellheads with more accuracy than conventional methods can offer. With the model the design could be safer and more economical. Also, it could provide guidance in the assembly of such equipment, for example how much the bolts holding the wellhead together should be pretensioned.

A high temperature geothermal wellhead design will be analyzed in general, and a model made of one wellhead in particular; a wellhead at the top of borhole HE-46 at Hellisheiði in Iceland. The model is made with the finite element method, using the commercial program ANSYS. This model is used to analyze the wellhead focusing on the structural integrity of the structure during several load cases often encountered during the service life of a wellhead. Measurements made of wellhead HE-46 during charging and the subsequent operating phase are used to assist in the placement of boundary conditions.

1.2 Content

In chapter 2 geothermal energy, geothermal systems in Iceland and the Hellisheiði power plant are discussed briefly. High temperature well and wellhead design is considered, and the service environment of such equipment discussed. Potential problems relevant to a wellhead analysis in general are looked upon.

In chapter 3 the finite element method is introduced and formulated. Nonlinearity is discussed and some solution methods introduced.

In chapter 4 the modeling of a geothermal wellhead with the finite element method is discussed. Geometry, material properties, elements, meshing, boundary conditions, loads and the function of the model are presented.

In chapter 5 case studies are made. Pretension analysis is made of the wellhead in order to see the response of the gaskets and flanges to bolt pretension load. The pretensioned model is then subjected to temperature and pressure loads encountered during operation. Finally, the model is tested using the pressure and temperature loads that the main valve is rated for.

In chapter 6 the conclusions of the thesis are discussed and presented.

2 High Temperature Geothermal Wellheads

2.1 Geothermal Systems and Power Production

Geothermal energy originates from volcanic activity due to movement of the plate boundaries of the Earth. Iceland lies on the boundary between the American and European tectonic plates, that move from each other at an average rate of two centimeters per year producing a gap that is filled with molten lava [1]. The heat contained in these lava pockets can be a valuable resource, if it can be extracted from the earth. When the earth above these volcanic areas is permeable enough, and groundwater is able to move through cracks in it, geothermal systems can be formed. Cold water sinks down towards the heat source below, heats up and rises upwards again, now containing more energy than before. To reach this energy in valuable quantities it is necessary to drill down into the earth.

Geothermal areas are usually divided into low temperature and high temperature areas, the former being areas where the temperature of the earth is below 200°C at a depth of 1000 meters, and the latter where it is above 200°C at the same depth [1]. High temperature areas are more valuable for energy extraction, because of the higher energy content of the geothermal fluid below. Geothermal power plants are usually constructed in high temperature geothermal areas. On figure 2.1 a geothermal map of Iceland can be seen. It shows how the high temperature areas of the country are spread over the boundary of the American and European tectonic plates. It also shows the location of the geothermal power plants in Iceland (2008) [2].

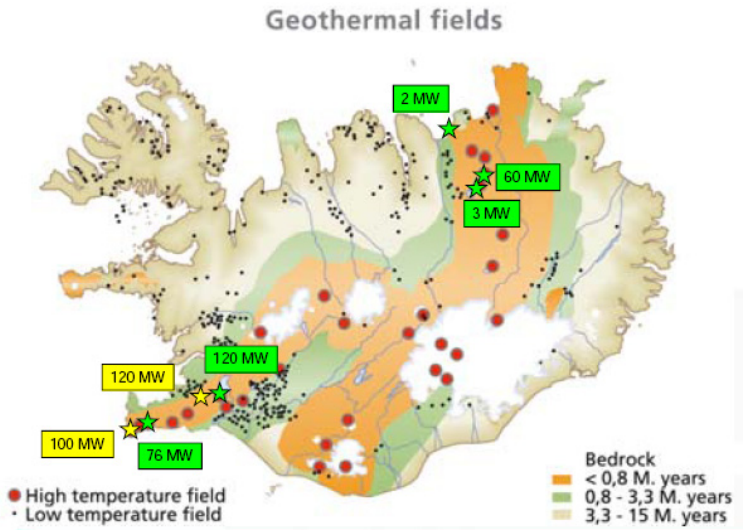

Figure 2.1 Geothermal fields in Iceland [2]

In the south-western part of Iceland there is a large geothermal area called Hengilssvæðið (e. Hengill area). In this area two major geothermal power plants are located; Nesjavallavirkjun (e. Nesjavellir power plant) and Hellisheiðarvirkjun (e. Hellisheiði power plant). These power plants produce electricity with steam turbines through electric generators, and then direct hot water to the geothermal heating system of Reykjavík. Hellisheiðarvirkjun started producing electricity in 2006, and was expanded to a co-generation plant (i.e. producing both electricity and delivering hot water to a district heating system) a few years later. Further expansion of the power plant is scheduled (2011) [3].

Hellisheiðarvirkjun uses energy from a geothermal system with a reservoir temperature of 250°C to 280°C [2]. The plant will produce 300 MW_e of electricity, and 400 MW_{th} of hot water for the district heating system when fully expanded [3]. There are about 50 geothermal wells connected to the power plant. One of these 50 wells, well HE-46, will be used as a reference for the model made in this project, with the main emphasis on the wellhead.

On figure 2.2 the production cycle of Hellisheiðarvirkjun can be seen.

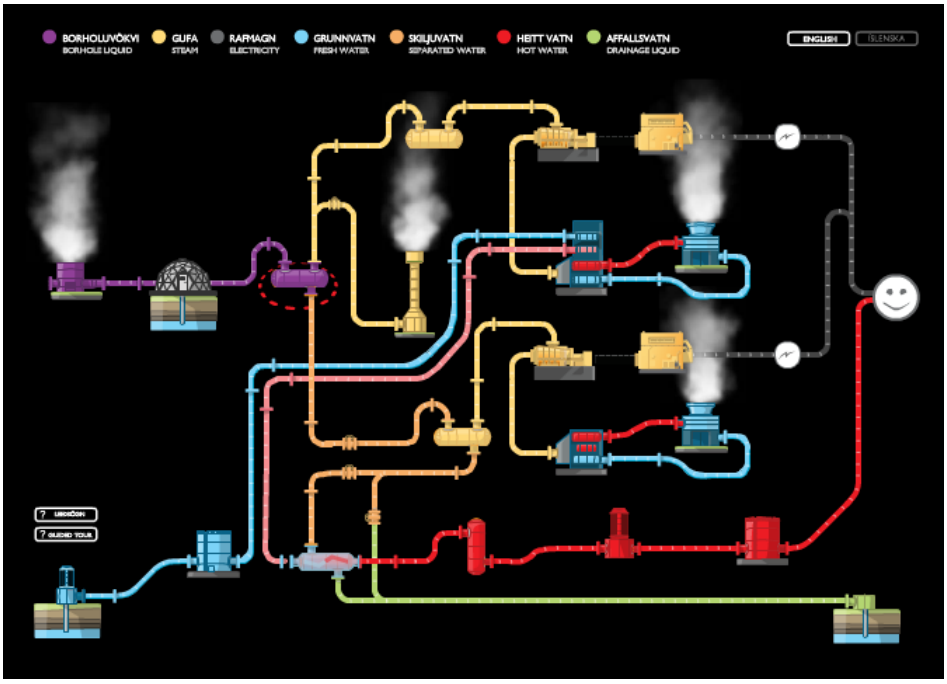

Figure 2.2 The production cycle of the Hellisheiði power plant [3]

The cycle can be described as follows: A mixture of steam and water flows from the wells and into steam separators, which separate the steam and water. From there the steam is sent through a moisture remover, and then through the turbines of the power plant, which turn the generators that produce electricity. The steam is condensed in a condenser and then used to heat up water for the district heating system of Reykjavík [3].

2.2 Wells and Wellheads

2.2.1 Wells

Conventional geothermal wells consist of several steel casings; a surface casing, a production casing and a slotted liner. The surface casing commonly reaches a depth of about 10-100 meters and the production casing a depth of about 800-2500 meters. The slotted liner hangs down from the production casing, and is permeable so the geothermal fluid can flow into the well. Sometimes other casings are also used, such as a conductor at the top of the well. The casing diameters vary with regard to the depth of the wells [4]. This casing program can be seen on figure 2.3, which also shows how the wellhead is stationed on top of the casings.

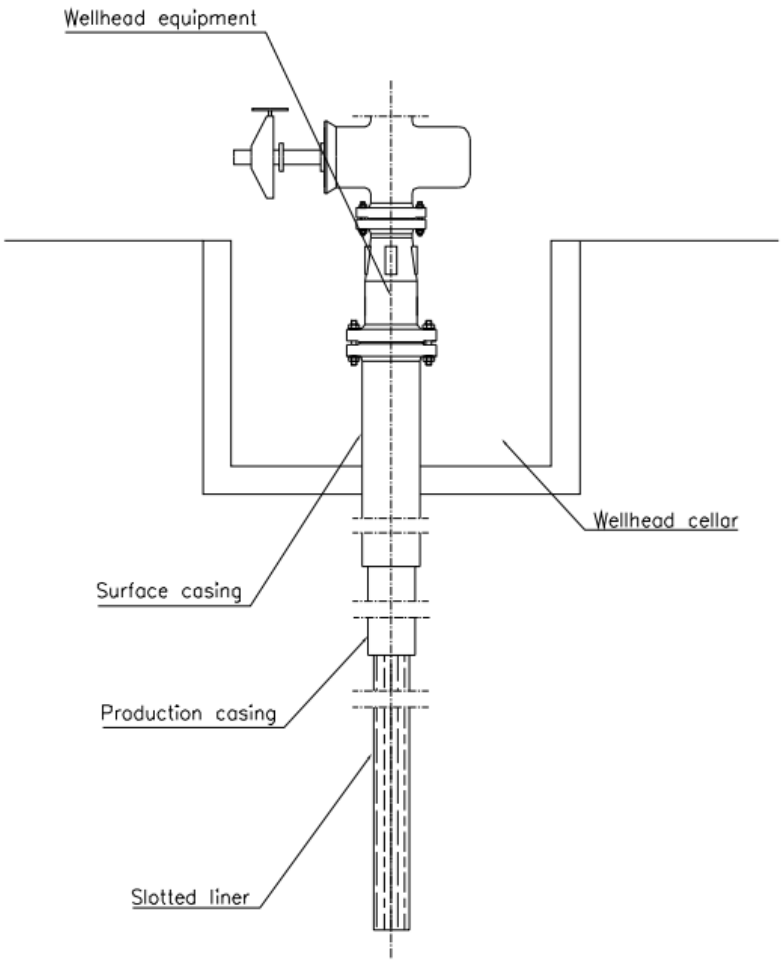

Figure 2.3 Casings and wellhead

2.2.2 Wellhead Design

Wellheads consist of several components; the most notable ones being the main valve which controls the flow of the geothermal fluid, the expansion spool which gives the production casing space for thermal expansion, and the necessary flanges, gaskets and bolts. A wellhead with a 12“ Class 900 gate valve and an expansion spool can be seen on figure 2.4, and a closer look of the inside of the expansion spool can be seen on figure 2.5. A wellhead of this type is modeled and analyzed in this project[1]. The wellhead is described in more detail in chapter 4.

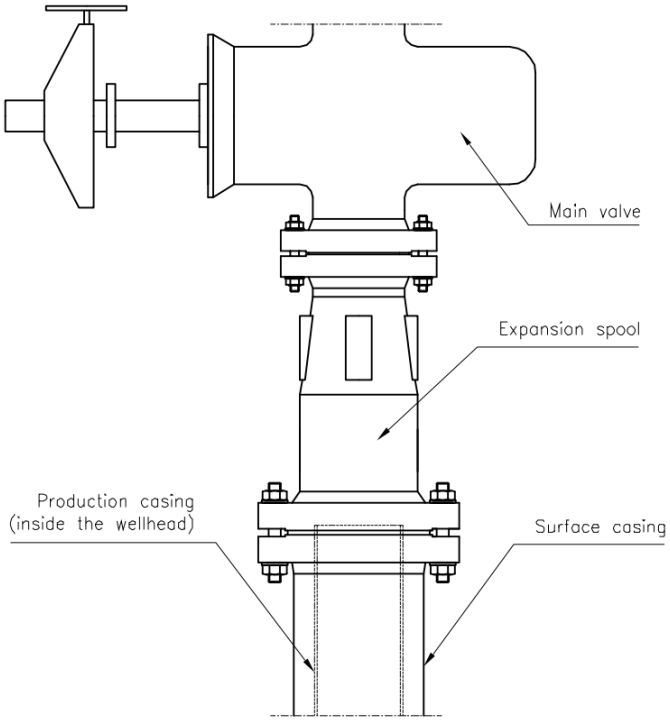

Figure 2.4 Wellhead with a 12” Class 900 valve and an expansion spool

[1] Figures are based on drawings of a similar wellhead as HE-46 (see section 2.1), which were provided by Mannvit with kind permission to use in this project. A sample of the original drawings can be seen in the Appendix.

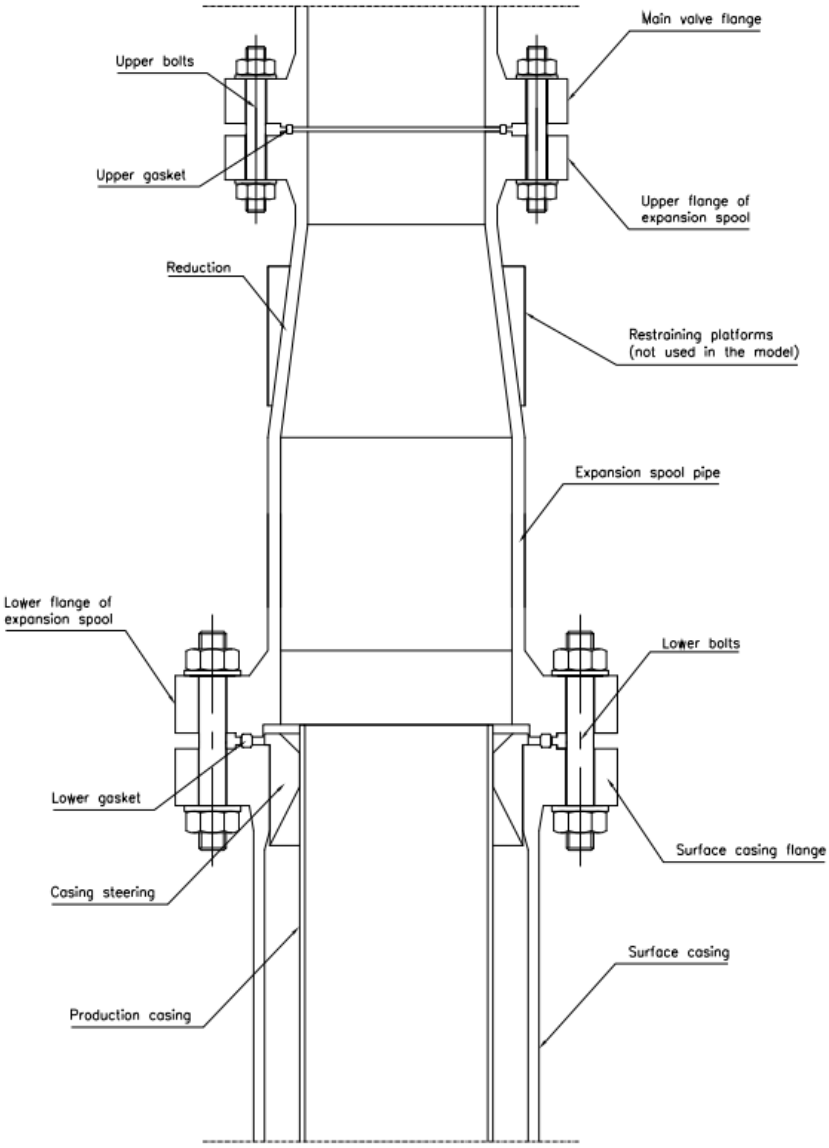

Figure 2.5 Inside the expansion spool

Wellheads are designed according to codes of practice. These include standards for pressure vessels and piping systems. The wellheads should, among other things, be designed to withstand the maximum pressure and temperature exposure under static and flowing conditions [5].

The main valve is usually chosen by using pressure rating charts, such as the one shown on figure 2.6, which rate different valve types according to pressure and temperature tolerance [6]. The 12" Class 900 valve seen on figure 2.4 is an expanding gate valve, and is designed to withstand 100 bar inner pressure, at 300°C temperature. Other wellhead equipment should be chosen or designed accordingly.

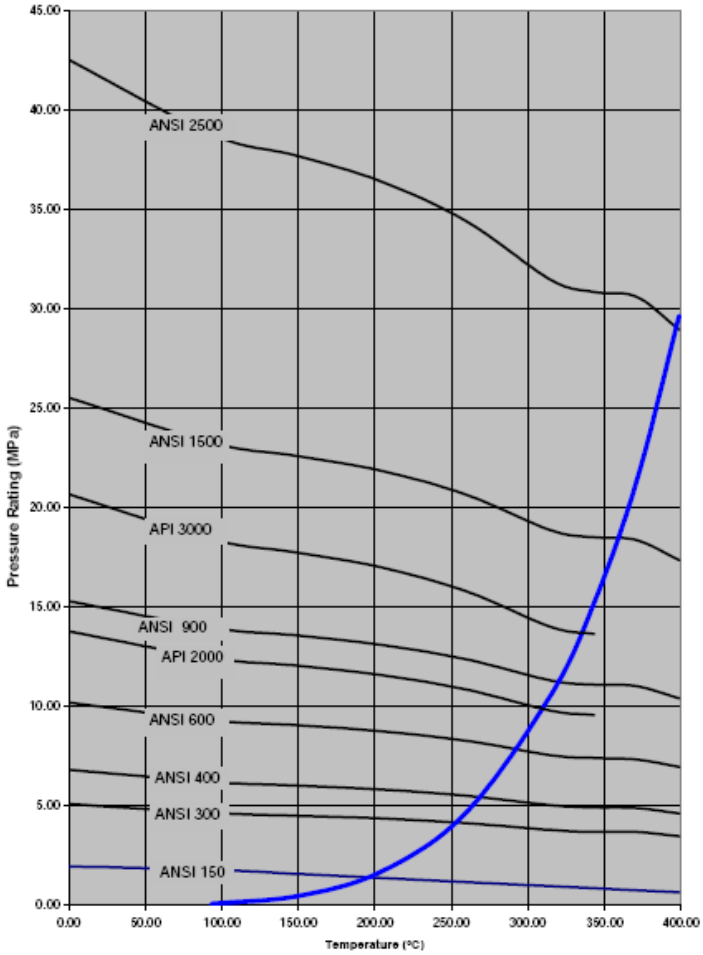

Figure 2.6 Wellhead working pressure derated for temperature [6]

2.2.3 Wellhead Operating Environment

Pressure and temperature

The pressure and temperature inside wellheads can range from 10-100 bar and 0-300°C, depending on the pressure and temperature in the geothermal system below, and if the well is flowing or not flowing. Normally wellheads are operated at about 10-20 bar pressure, but when the wellhead is closed the pressure can rise up to 80-100 bar, especially if gases from the geothermal fluid build up at the top.

The well that is under consideration in this project, HE-46, reaches a depth of 2444 meters and the average water/steam flow in the well is about 45 kg/s, with about 1130 kJ/kg of energy content. The usual wellhead operating pressure is 18-20 bar [7].

To calculate the temperature of the geothermal fluid inside the wellhead, it is necessary to take some thermodynamic relations into account. It can be assumed that the energy content of the fluid flowing up through a geothermal well is constant. Thus, if the energy content of the reservoir fluid has been found, the state of the fluid at the surface can be calculated as a function of wellhead pressure by following constant enthalpy lines on a T-s diagram [8]. Using the production figures found in [7] it can be calculated that the reservoir

temperature is about 260°C, and the temperature of the geothermal fluid at 18 bar at the surface is 212°C.

Therefore, in the analysis of wellhead HE-46 the model will be subjected to a temperature load of 212°C and a pressure load of 18 bar when simulating operating conditions. Also, in the case of an extreme case analysis of a closed wellhead the model will be subjected 100 bar pressure load. Using figure 2.6 for the main valve and following the rule that other wellhead equipment should be designed accordingly, the extreme temperature value is set to be 300°C.

Fluid flow and vibration

Although pressure and temperature are the most important design values for wellheads, other loads have to be considered. When the well is flowing a mixture of steam and water travels at high speed through the wellhead. Due to the different properties of the two phases the steam travels much faster than the liquid phase. The liquid tends to flow at the wall of the production casing and the steam in the middle of the well. Since there are constant phase changes on the way up, this flow tends to be very unstable, causing bubbles to form and can be difficult to analyze [9]. This, along with the high speed of the flow itself makes the wellhead vulnerable to induced vibration caused by this flow, if not accounted for in the design.

To account for this the wellhead is usually well brazed with stiffening bars and beams. If this is done properly vibration should not be a problem. For the wellhead shown in figures 2.3-2.5, the expansion spool is equipped with beam platforms where stiffening bars are mounted. Because vibration is time-dependent and the model made in the project steady-state, no account will be taken to vibration in the analysis in this project.

2.2.4 Wellhead Problems

Effect of pressure and temperature

The high pressure inside the wellhead causes stresses that can damage wellhead equipment. At high temperatures the strength of steel is reduced, which makes the wellhead material especially vulnerable to stress failure. Another problem associated with temperature loads is temperature gradient and thermal expansion. When the wellhead material heats up the steel expands, causing thermal stresses, which combine with the stresses caused by the inner pressure. Because the wellhead will never be at a completely uniform temperature, due to convection at the outer surface of it, there will always be formed a thermal gradient, which also causes stresses. [10]

Flange connections, pretension and leakage

Wellhead flanges are held together by pretensioned bolts. The pretension load is obtained by twisting the nut until the bolt is elongated almost to the elastic limit. The torque required to reach this pretension force can be found with the following equation [10]:

$$T = K \cdot F_i \cdot d \tag{2.1-1}$$

where

T = torque required [Nm]
K = torque coefficient [-]
F_i = pretension force [N]
d = tension diameter of the bolt or stud in question [m]

The torque coefficient, K, is based upon the size of the bolt or stud, and the friction factor of the material it is made of, and is here assumed to be 0.3 [10].

The pretension procedure must be monitored closely to ensure that the gasket is compressed enough to provide the tightness that is necessary. Gaskets are normally compressed so much that yielding occurs. This ensures that the gasket fills up geometric deformities in the flanges. Too much pretension can, however, deform the gasket too much. Careful monitoring of the pretension process is therefore essential.

In high-temperature services, the flanges will heat up at a faster rate than the bolts and under steady-state conditions will continue to be hotter than the bolts as a result of the thermal gradient. This results in a higher thermal expansion of the flanges with respect to the bolts, increasing the bolt load and concurrently the gasket stress. The gasket will then deform under the higher applied load during this cycle. Most gaskets will deform permanently and will not rebound when the load cycle goes away with varying conditions. The permanent set or plastic deformation that occurred during operation will cause loss of bolt load and concurrently loss of gasket stress. As gasket stress decreases leak rate increases. This can be controlled to a certain extent with close monitoring of the pretension load used to bolt the flange together, as well as choosing materials that are strong and resilient, especially for the gaskets. [11]

The analysis of flange connections is difficult with conventional methods, and it can therefore be of valuable assistance to be able to simulate the behavior of the wellhead under service conditions with a well constructed wellhead model. Further discussion of flange analysis and the modeling of flange connections can be found in [12], [13] and [14].

Another potential leakage problem that can arise is leakage between the casing steering and the surface casing, which can cause high stresses at the surface casing connection to the ground [15]. Recent wellhead design in Iceland has addressed this by providing a seal between the production casing and the casing steering. [16]

Corrosion

Wellhead equipment has to withstand highly corrosive chemicals found in geothermal fluids. Known problems due to this are for example sulphide induced stress corrosion cracking and hydrogen induced cracking. The high temperatures encountered in geothermal wells make the chemicals highly volatile and the high pressure inside the wellhead combined with the high speed of the fluid flow make this a serious problem to be accounted for in the design of geothermal wellheads [17]. Corrosion resistant materials and coating methods can limit the problem, and with good maintenance it can be controlled. Since corrosion is a time-dependent problem it cannot be accounted for in the analysis in this project.

2.2.5 Wellhead Analysis

From the above it can be seen that an effective analysis model of a geothermal wellhead has to take into account pressure and temperature loads, heat transfer and temperature distribution, thermal expansion and material property temperature dependency. The model must also be able to simulate bolt pretension and the subsequent yielding in gasket material.

This is taken into account in the model constructed in this project. It is made with the finite element analysis program ANSYS, using wellhead HE-46, which is introduced in this chapter, as a reference. In the following chapters the finite element method and the construction of the model is addressed. The final model is then subjected to several case studies using the service conditions addressed in this chapter as load cases.

3 The Finite Element Method

The finite element method is a method for numerical solution of field problems described by differential equations or by integral expressions. With the method, field variables are approximated by connecting interpolation functions, each defined over a small region called a finite element. Finite elements can be connected at nodes, where they share values of the field quantity, and the connected elements can therefore represent large fields, or structures.

The finite element method is very suitable for stress analysis of complex objects and structures. Due to the complexity of geothermal wellheads and their loading conditions, the method can be of great help in analyzing such structures.

3.1 Linear Finite Element Formulation

The state of stress throughout an element is, from Hooke‘s Law:

$$\{\boldsymbol{\sigma}\} = [\mathbf{D}]\{\boldsymbol{\varepsilon}\} \tag{3.1-1}$$

where [**D**] is called an elasticity matrix, and contains material properties.

For any quasistatic and admissible displacement the increment of strain energy stored is equal to the increment of work done by body forces {**F**} in volume V and surface tractions {**Φ**} on surface S. [19] This can be described with the following equation:

$$\int\{\delta\boldsymbol{\varepsilon}\}^{\mathbf{T}}\{\boldsymbol{\sigma}\}dV = \int\{\delta\mathbf{u}\}^{\mathbf{T}}\{\mathbf{F}\}dV + \int\{\delta\mathbf{u}\}^{\mathbf{T}}\{\Phi\}dS \tag{3.1-2}$$

The nodal displacements are related to the internal displacements throughout the entire element by means of a displacement function. The displacement function defining the displacement at any point within the element is:

$$\{\mathbf{u}\} = [\mathbf{N}]\{\mathbf{d}\} \tag{3.1-3}$$

where {**u**} is an array of displacements defined as:

$$\{\mathbf{u}\} = [\mathrm{u} \quad \mathrm{v} \quad \mathrm{w}]^{\mathrm{T}} \tag{3.1-4}$$

and {**d**} lists the nodal displacement d.o.f. of an element. Hence

$$\{\boldsymbol{\varepsilon}\} = [\mathbf{B}]\{\mathbf{d}\} \tag{3.1-5}$$

where

$$[\mathbf{B}] = \begin{bmatrix} \delta_x & 0 & 0 \\ 0 & \delta_y & 0 \\ 0 & 0 & \delta_z \\ \delta_y & \delta_x & 0 \\ \delta_z & 0 & \delta_x \\ 0 & \delta_z & \delta_y \end{bmatrix}$$

or

$$[\mathbf{B}] = [\boldsymbol{\partial}][\mathbf{N}] \tag{3.1-6}$$

Matrix [**B**] is called the strain-displacement matrix. From equations 3.1-3 and 3.1-5 we obtain

$$\{\boldsymbol{\delta u}\}^{\mathrm{T}} = \{\boldsymbol{\delta d}\}^{\mathrm{T}}[\mathbf{N}]^{\mathrm{T}} \tag{3.1-7}$$

and

$$\{\boldsymbol{\delta \varepsilon}\}^{\mathrm{T}} = \{\boldsymbol{\delta d}\}^{\mathrm{T}}[\mathbf{B}]^{\mathrm{T}} \tag{3.1-8}$$

From the stress-strain relations with initial strain and initial stress included we obtain [19]

$$\{\boldsymbol{\delta d}\}^{\mathbf{T}}\left(\int [\mathbf{B}]^{\mathbf{T}}[\mathbf{E}][\mathbf{B}] - \int [\mathbf{B}]^{\mathbf{T}}[\mathbf{E}]\{\boldsymbol{\varepsilon_0}\}\,\mathbf{dV} + \int [\mathbf{B}]^{\mathbf{T}}\{\boldsymbol{\sigma_0}\}\,\mathbf{dV} - \int [\mathbf{N}]^{\mathbf{T}}\{\mathbf{F}\}\,\mathbf{dV} - \int [\mathbf{N}]^{\mathbf{T}}\{\Phi\}\,\mathbf{dS}\right) = \mathbf{0} \tag{3.1-9}$$

The above equation must be true for any admissable virtual displacement $\{\boldsymbol{\delta d}\}$ from the equilibrium configuration. Therefore, equation 3.1-9 yields

$$[\mathbf{k}]\{\mathbf{d}\} = \{\mathbf{r_e}\} \tag{3.1-10}$$

where the element stiffness matrix is

$$[\mathbf{k}] = \int [\mathbf{B}]^{\mathbf{T}}[\mathbf{E}][\mathbf{B}]\ \mathrm{dV} \tag{3.1-11}$$

and the load vector applied to structure nodes by elements is [19]

$$\{\mathbf{r_e}\} = \int [\mathbf{N}]^{\mathbf{T}}\{\mathbf{F}\}\ \mathrm{dV} + \int [\mathbf{N}]^{\mathbf{T}}\{\Phi\}\ \mathrm{dS} + \int [\mathbf{B}]^{\mathbf{T}}[\mathbf{E}]\{\boldsymbol{\varepsilon_0}\}\ \mathrm{dV} - \int [\mathbf{B}]^{\mathbf{T}}\{\boldsymbol{\sigma_0}\}\ \mathrm{dV} \tag{3.1-12}$$

Assembly of elements to form a finite element structure result in structure equations

$$[\mathbf{K}]\{\mathbf{D}\} = \{\mathbf{R}\} \tag{3.1-13}$$

3.2 Nonlinearities

In structural mechanics the most common cases of nonlinearity are material nonlinearity, in which material properties are functions of stress or strain, geometric nonlinearity, in which deformation is large enough that equilibrium equations must be written with respect to the deformed structural geometry, and contact nonlinearity, in which a gap between adjacent parts may open or close, the contact area between parts changes as the contact force changes, or there is sliding contact with frictional forces. [19]

Problems in these catagories are nonlinear because stiffness, and sometimes loads as well, become functions of displacement or deformation. Thus, in equation 3.1-13, [**K**]{**D**} = {**R**}, coefficient matrix [**K**] and perhaps load vector {**R**} become functions of {**D**}. It is therefore not possible to solve immediately for {**D**} because information needed to construct [**K**] and {**R**} is not known in advance. An iterative process is required to obtain {**D**} and its associated [**K**] and {**R**} such that the product [**K**]{**D**} is in equilibrium with {**R**}. [19]

3.2.1 Material Nonlinearity

The relationship between stress and strain is linear in the elastic region of most materials, but becomes nonlinear when the material is subjected to a force that deforms it plastically. Elastic behavior is characterized by recoverable strain, whereas above the yield point plastic behavior is characterized by nonrecoverable strain where the material sustains permanent plastic deformation. The well known equations of equilibrium, the strain-displacement relationships, and the conditions of compatibility are all valid in plastic theory. New relationships must, however, be derived to connect stress and strain. [19]

Let σ be a uniaxial stress, such as the axial stress in a tensile test specimen, and ε the corresponding axial strain. As σ increases from zero, yielding begins at stress σ_Y, and the corresponding strain ε_Y. For strains larger than ε_Y, a strain increment dϵ can be regarded as composed of an elastic contribution dε_e and a plastic contribution dε_p. When $\varepsilon > \varepsilon_Y$, increment d$\varepsilon_e$ exists only when $E_t \neq 0$, and is associated with an increment of stress dσ which can be written in various ways. For strain in the plastic range, with dε = dε_e + dε_p,

$$d\sigma = E d\varepsilon^e \tag{3.2-1}$$

$$d\sigma = E(d\varepsilon - d\varepsilon^p) \tag{3.2-2}$$

$$d\sigma = E_t d\varepsilon \tag{3.2-3}$$

$$d\sigma = H_p d\varepsilon^p \tag{3.2-4}$$

where H_p is called the strain-hardening parameter, or the plastic modulus. [19] Substituting (3.2-2) and (3.2-4) into (3.2-3) leads to

$$H_p = \frac{E_t}{1 - (\frac{E_t}{E})}$$

or

$$E_t = E\left(1 - \frac{E}{E + H_p}\right) \tag{3.2-5}$$

If $H_p = 0$, for which $E_t = 0$, the material is called elastic-perfectly plastic. [19]

In three dimensions, strain increments are regarded to be composed of elastic and plastic components so that

$$\{\mathrm{d}\boldsymbol{\epsilon}\} = \{\mathrm{d}\boldsymbol{\varepsilon}^{\mathbf{e}}\} + \{\mathrm{d}\boldsymbol{\varepsilon}^{\mathbf{p}}\} \tag{3.2-6}$$

Where the superscripts e and p denote elastic and plastic. [19] Stress increments are associated with only the elastic component, that is

$$\{\mathrm{d}\boldsymbol{\sigma}\} = [\mathbf{E}]\{\mathrm{d}\boldsymbol{\varepsilon}^{\mathbf{e}}\} \tag{3.2-7}$$

or

$$\{\mathrm{d}\boldsymbol{\sigma}\} = [\mathbf{E}](\{\mathrm{d}\boldsymbol{\varepsilon}\} - \{\mathrm{d}\boldsymbol{\varepsilon}^{\mathbf{p}}\}) \tag{3.2-8}$$

Where [**E**] is the elastic material property matrix.

The three ingredients of elastic-plastic analysis are a yield criterion, a flow rule, and a hardening rule. [19] The yield criterion relates the state of stress to the onset of yielding. The flow rule relates the state of stress to the corresponding six increments of plastic strain, when an increment of plastic flow occurs. The hardening rule describes how the yield criterion is modified by straining beyond initial yield. The yield function can be written as

$$\mathrm{F} = \mathrm{F}\left(\{\boldsymbol{\sigma}\}, \{\boldsymbol{\alpha}\}, \mathrm{W_p}\right) \tag{3.2-9}$$

where $\{\alpha\}$ and W_p account for hardening. The flow rule is stated in terms of a function Q, which has units of stress and is called a plastic potential. With dλ, a scalar that is called the plastic multiplier, plastic strain increments are given by

$$\{\mathrm{d}\boldsymbol{\varepsilon}^{\mathbf{p}}\} = \left\{\frac{\partial \mathrm{Q}}{\partial \boldsymbol{\sigma}}\right\} \mathrm{d}\lambda \tag{3.2-10}$$

Hardening can be modeled as isotropic or as kinematic, either seperately or in combination. [19] Isotropic hardening can be represented by plastic work per unit volume W_p, which describes growth of the yield surface:

$$\mathrm{W_p} = \int \{\boldsymbol{\sigma}\}^{\mathrm{T}} \{\mathrm{d}\boldsymbol{\varepsilon}^{\mathbf{p}}\} \tag{3.2-11}$$

Kinematic hardening can be represented by a vector $\{\alpha\}$, which accounts for translation of the yield surface in stress space:

$$\{\boldsymbol{\alpha}\} = \int [\mathbf{C}] \{\mathrm{d}\boldsymbol{\varepsilon}^{\mathbf{p}}\} \tag{3.2-12}$$

The above equation follows from integration of

$$\{d\boldsymbol{\alpha}\} = [\mathbf{C}]\{d\boldsymbol{\varepsilon}^{\mathbf{p}}\} \tag{3.2-13}$$

where

$$[\mathbf{C}] = \frac{2}{3}H_p[1\ 1\ 1\ \tfrac{1}{2}\ \tfrac{1}{2}\ \tfrac{1}{2}] \tag{3.2-14}$$

and H_p is the plastic modulus defined with equation 3.2.-5. [19]

During an increment of plastic straining dF = 0, so from 3.2-9 we have

$$\left\{\frac{\partial F}{\partial \boldsymbol{\sigma}}\right\}^T \{d\boldsymbol{\sigma}\} + \left\{\frac{\partial F}{\partial \boldsymbol{\alpha}}\right\}^T \{d\boldsymbol{\alpha}\} + \left\{\frac{\partial F}{\partial W_p}\right\}^T dW_p = 0 \tag{3.2-15}$$

Substitution into 3.2-8 gives

$$\{d\boldsymbol{\sigma}\} = [\mathbf{E}]\left(\{d\boldsymbol{\varepsilon}\} - \left\{\frac{\partial Q}{\partial \boldsymbol{\sigma}}\right\} d\lambda\right) \tag{3.2-16}$$

$$dW_p = \{\boldsymbol{\sigma}\}^T \left\{\frac{\partial Q}{\partial \boldsymbol{\sigma}}\right\} d\lambda \tag{3.2-17}$$

and

$$\{d\boldsymbol{\alpha}\} = [\mathbf{C}]\left\{\frac{\partial Q}{\partial \boldsymbol{\alpha}}\right\} d\lambda \tag{3.2-18}$$

Substituting into 3.2-15, and solving for the plastic multiplier, we obtain

$$d\lambda = \lfloor \mathbf{P}_{\boldsymbol{\lambda}} \rfloor \{d\boldsymbol{\varepsilon}\} \tag{3.2-19}$$

where

$$\lfloor \mathbf{P}_{\boldsymbol{\lambda}} \rfloor = \frac{\left\{\frac{\partial F}{\partial \boldsymbol{\sigma}}\right\}^T [\mathbf{E}]}{\left\{\frac{\partial F}{\partial \boldsymbol{\sigma}}\right\}^T [\mathbf{E}]\left\{\frac{\partial Q}{\partial \boldsymbol{\sigma}}\right\} - \left\{\frac{\partial F}{\partial \boldsymbol{\alpha}}\right\}^T [\mathbf{C}]\left\{\frac{\partial Q}{\partial \boldsymbol{\alpha}}\right\} - \frac{\partial F}{\partial W_p}\{\boldsymbol{\sigma}\}^T \left\{\frac{\partial Q}{\partial \boldsymbol{\sigma}}\right\}} \tag{3.2-20}$$

Finally, from 3.2-16-19 we obtain

$$\{d\boldsymbol{\sigma}\} = \left[\mathbf{E}_{\mathbf{ep}}\right]\{d\boldsymbol{\varepsilon}\} \tag{3.2-21}$$

where

$$\left[\mathbf{E}_{\mathbf{ep}}\right] = [\mathbf{E}]\left([\mathbf{I}] - \left\{\frac{\partial Q}{\partial \boldsymbol{\sigma}}\right\} \lfloor \mathbf{P}_{\boldsymbol{\lambda}} \rfloor\right) \tag{3.2-22}$$

where [I] is a unit matrix. The elastic-plastic matrix [E_{ep}] can be regarded as a generalized form of the tangent modulus E_t. [19]

Element formulation using $\left[\mathbf{E_{ep}}\right]$ provides the tangent stiffness matrix

$$[\mathbf{k_t}] = \int [\mathbf{B}]^{\mathbf{T}} \left[\mathbf{E_{ep}}\right] [\mathbf{B}] \, dV \tag{3.2-23}$$

Assembly into a finite element structure provides

$$[\mathbf{K_t}]\{d\mathbf{D}\} = \{d\mathbf{R}\} \tag{3.2-24}$$

The above equation provides displacement increments produced by load increments when there is plastic straining. [19]

There are several plastic material models describing plastic behavior formulated above, that are used to represent the stress-strain curve above the yield limit. The Bilinear Kinematic Hardening is used in the model for the wellhead. That model assumes that the total stress range is equal to twice the yield stress. The stress-strain curve is represented with two lines. The plastic range is represented with a line with a slope of the tangent modulus, E_t.[20]

3.2.2 Geometric and Contact Nonlinearity

Geometric nonlinearity arises when deformations are large enough to alter the distribution or orientation of applied loads, or the orientation of internal resisting forces and moments. The essential difficulty of geometrically nonlinear analysis is that equilibrium equations must be written with respect to the deformed geometry, which is not known in advance. [19]

Contact nonlinearity is a kind of geometrically nonlinear problem that arises when different structures, or different surfaces of a single structure, either come into contact or separate, or slide on one another with friction. Contact forces must be determined in order to calculate structural behavior. The location and extent of contact may not be known in advance, and must also be determined. [19]

3.2.3 Solution Methods

A common solution method used to solve time-independent equations [**K**]{**D**} = {**R**}, when the stiffness matrix [**K**] and the load vector {**R**} can be functions of the displacements {**D**} is the Newton-Raphson method.

The Newton-Raphson method, more commonly known as Newton's method, is a method to follow a curve with small linear steps. This method is adopted to solve nonlinear finite element problems. With the method the load is divided into several load steps, and each load step is further divided into several substeps. Each substep has a local stiffness matrix [**K**], which can be found with regard to {**R**} and {**D**}. A global stiffness matrix is formed and solved for displacements.

The method evaluates the load vector which is the difference between restoring forces, due to element stresses, and the applied loads. Then a linear solution is performed and

convergence checked. If convergence is not obtained the load vector is reevaluated and the stiffness matrix is updated before a new solution is performed [20]. The Newton-Raphson method procedure can be seen on figure 3.1.

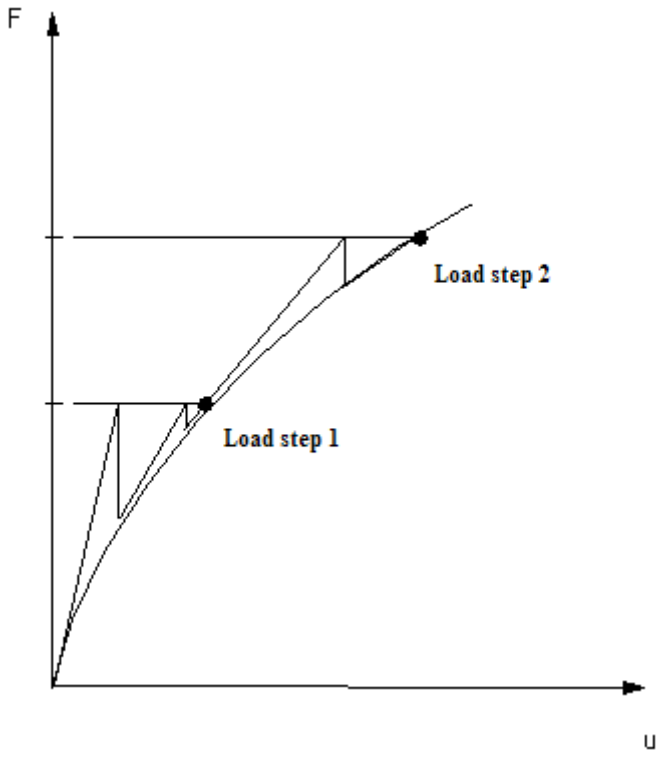

Figure 3.1 The Newton-Raphson solution method. F is the load and u is deflection

4 Finite Element Modeling of a Geothermal Wellhead

This chapter describes the modeling of the wellhead HE-46 with the finite element method using the commercial program ANSYS. Although the finite-element method can be used to analyze very complex problems, it is important to make the model as simple as possible, both to reduce modeling time and calculation time. The analyst must therefore understand the problem sufficiently well to be able to decide how detailed the model should be. An efficient model takes into account the most important physical aspects of the problem ahead, without making it too complex.

4.1 Geometry

As can be seen on figures 2.3-2.5 the wellhead is symmetrical around its middle axis up to the main valve. As the main focus of the analysis is the expansion spool and connected flanges, gaskets and casings, a model will only be made from the bottom of the wellhead basement floor and up to the main valve. Boundary conditions will be applied accordingly. Because of the bolts in the structure it is not possible to represent the wellhead sufficiently well with a two dimensional model. The model will therefore have to be three dimensional to be sufficiently accurate.

Due to the symmetry of the structure it is possible to divide it into parts and analyze each part seperately, thereby reducing the size of the model. This is important because the larger the finite element model, the longer the calculation time. It is sufficient to analyze a slice of the structure cut around each bolt. This can be seen on figure 4.1 (plan view).

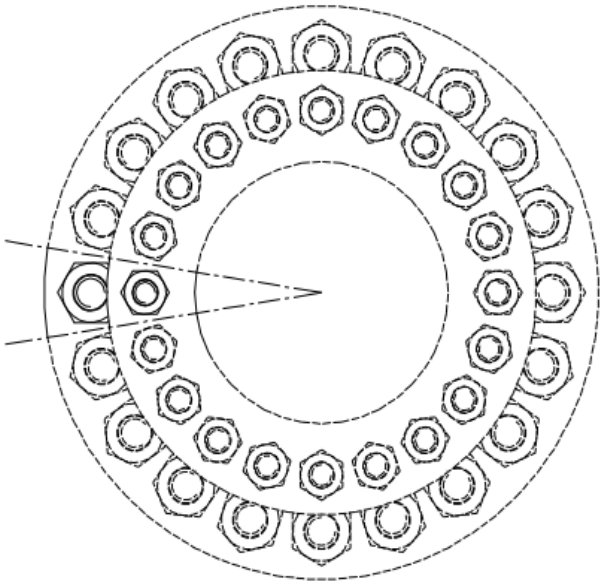

Figure 4.1 1/20 of the wellhead will be modeled

Referring to figure 2.5, table 4.1 provides the sizes of the wellhead parts that are used in the modeling process.

Table 4.1 Wellhead part materials and sizes

Wellhead part	Material	Size
Main valve flange	P265	12" x 900 RTJ
Upper expansion spool flange	P265	12" x 900 RTJ, ID = 320
Lower expansion spool flange	P265	18" x 900 RTJ, ID = 412.6
Surface casing flange	P265	18" x 900 RTJ, ID = 451
Expansion spool pipe	P265	ø457 x 22.2
Reduction pipe	P265	ø457-ø355.6 x 22.2
Upper bolts	A193	8UN, 1 3/8" x 12.75"
Lower bolts	A193	8UN, 1 7/8" x 10"
Upper gasket	316L	R57, octagonal
Lower gasket	316L	R70, octagonal
Surface casing	K55	18 5/8"
Production casing	K55	13 3/8"
Casing steering	S235	R235

The final 3D solid model (before meshing) can be seen on figure 4.2.

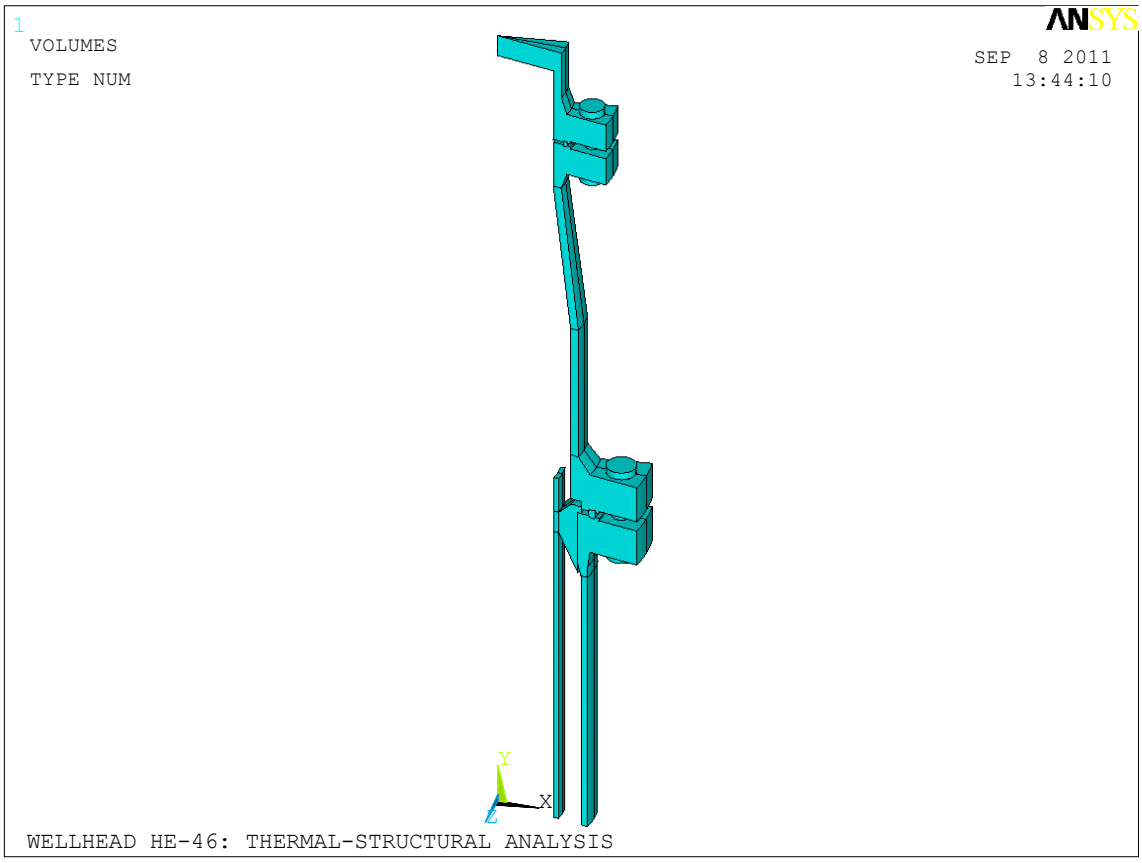

Figure 4.2 The 3D model of the wellhead

4.2 Material Properties

The material properties used in the model are the modulus of elasticity, E, the Poisson's ratio ν, and the yield strength f_y. Also, because the model will include thermal analysis, thermal material properties will have to be considered. The ones used here are the coefficient of thermal expansion, α, and the coefficient of thermal conductivity, k. Table 4.2 summarizes the materials used in the wellhead, and the corresponding material properties at 0°C. [17], [21], [22], [23]

Table 4.2 Wellhead part materials and the corresponding material properties at 0°C

Wellhead part	Material	ρ [kg/m^3]	E [GPa]	υ [-]	f_y [MPa]	k [W/m-K]	α[1/10^{-6} °C^{-1}]
Casings	K55	7850	207	0.3	380	55	10.7
Pipes/flanges	P265	7850	207	0.3	265	55	10.7
Bolts and nuts	A193	8000	193	0.3	720	16.2	14.1
Gasket rings	316L	8000	193	0.3	240	16.2	14.1
Casing steering	S235	7850	207	0.3	235	55	10.7

4.2.1 Carbon Steel Components

Table 4.2 provided material properties for the wellhead components at 0°C. Some of the properties, like the modulus of elasticity, and coefficients of thermal conductivity and thermal expansion are temperature dependent, and it is necessary to take this dependency into account in the construction of the model.

The casings, casing steering, pipes and flanges are all made of carbon steel. Figures 4.3-4.5 show the modulus of elasticity [17], coefficient of thermal conductivity [21] and coefficient of thermal expansion [21] for carbon steel plotted over the temperature range 0-300°C.

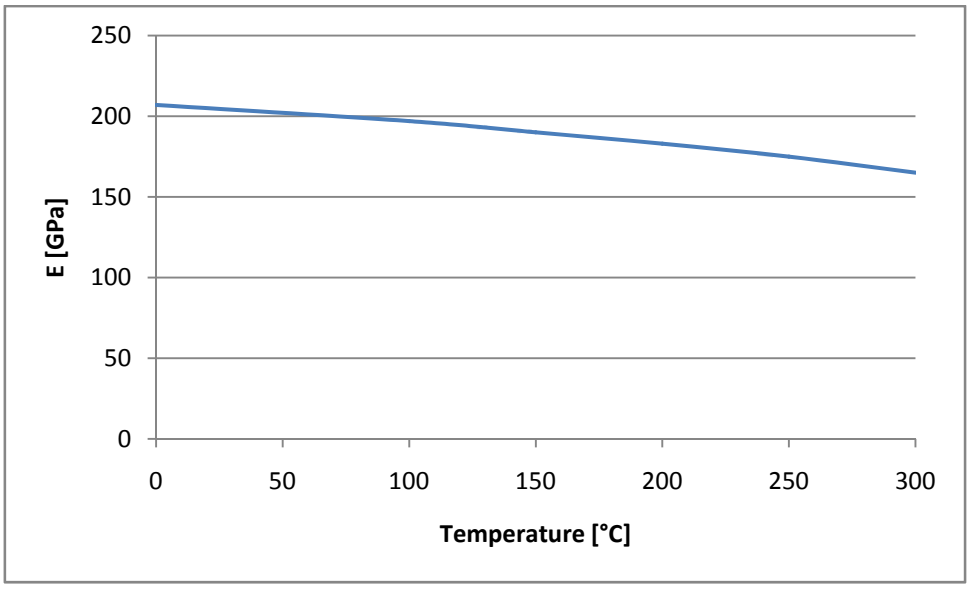

Figure 4.3 Modulus of elasticity for carbon steel from 0-300°C

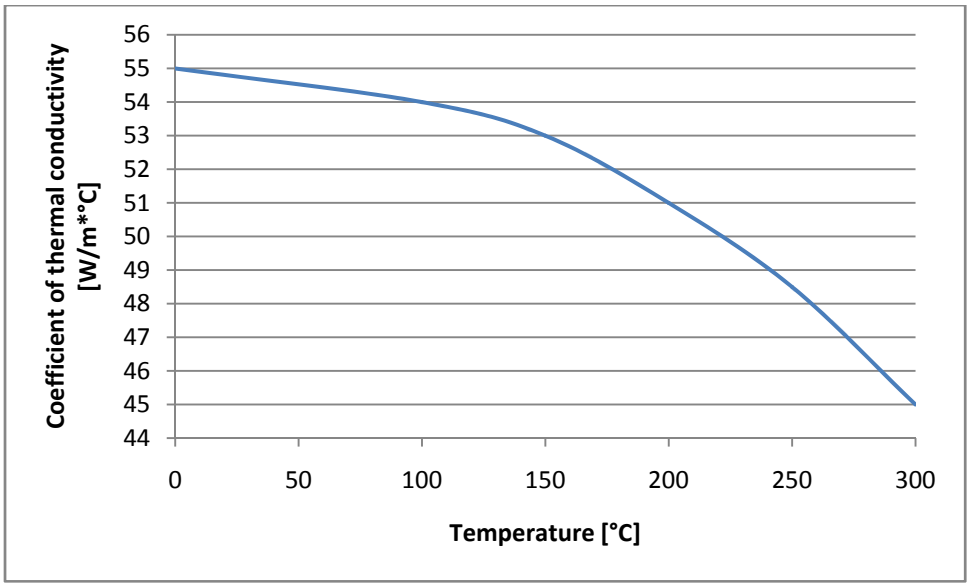

Figure 4.4 Coefficient of thermal conductivity for carbon steel from 0-300°C

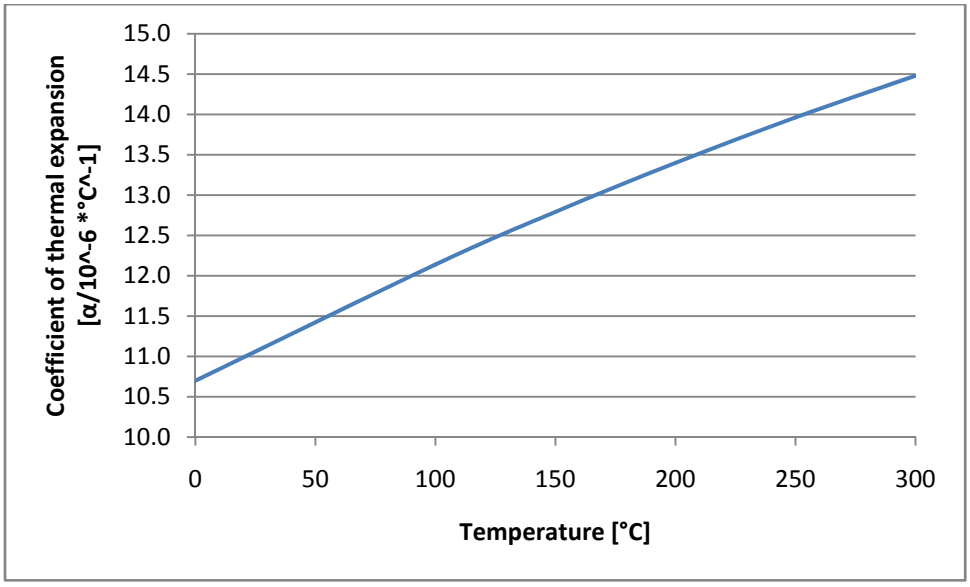

Figure 4.5 Coefficient of thermal expansion for carbon steel from 0-300°C

The above graphs are assumed to be valid for all carbon steel components of the wellhead, and are incorporated into the model by assigning the corresponding material property values at 0°C, 100°C, 150°C, 200°C, 250°C and 300°C.

Table 4.2 also provided the yield strength for the different materials at 0°C, and like the above properties it is temperature dependent. Figures 4.6-4.8 show the stress-strain curves for S235 [22], P265 [22] and K55 [22] at 0-300°C. Up to the yield strength of the material the relationship is linear but after the yield limit is reached the stress-strain curve is assumed to follow almost flat lines at the value of the yield strength [22]. The Bilinear Kinematic Hardening model is used to incorporate the behavior seen on the following figures into the finite element model.

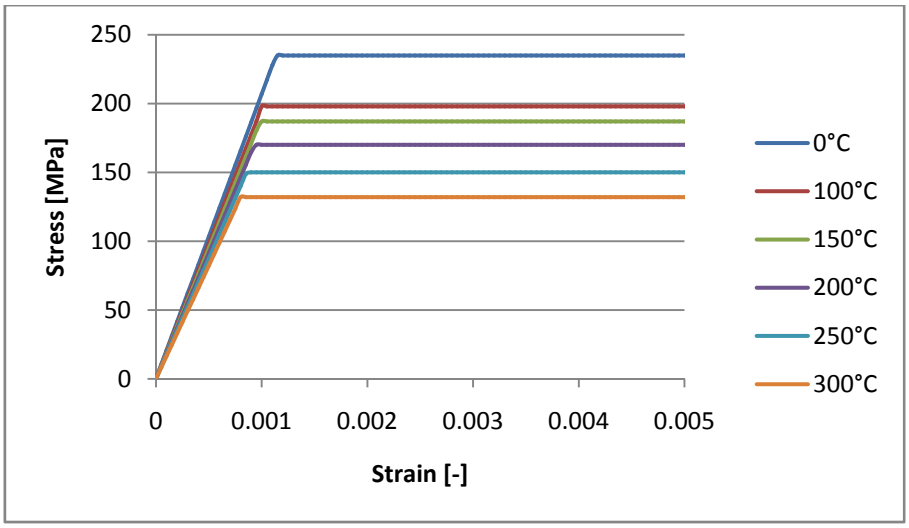

Figure 4.6 Stress-strain diagrams for S235 steel from 0-300°C

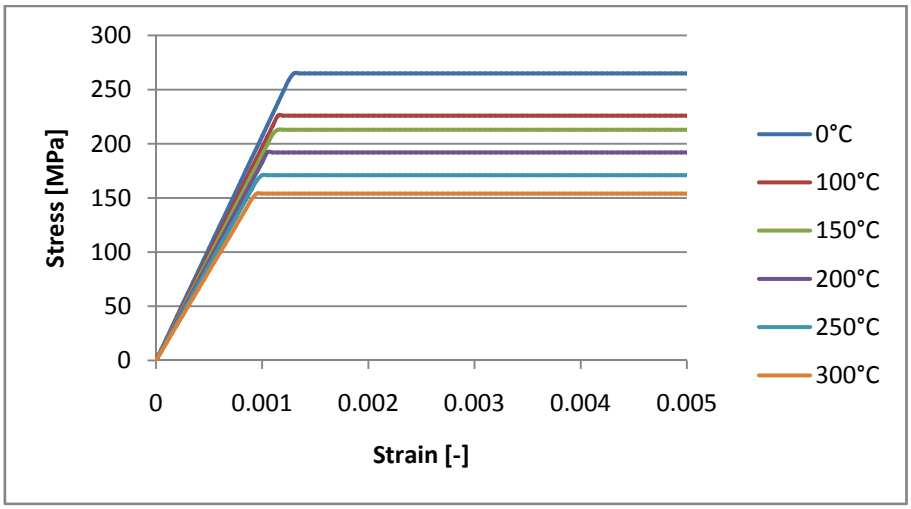

Figure 4.7 Stress-strain diagrams for P265 steel from 0-300°C

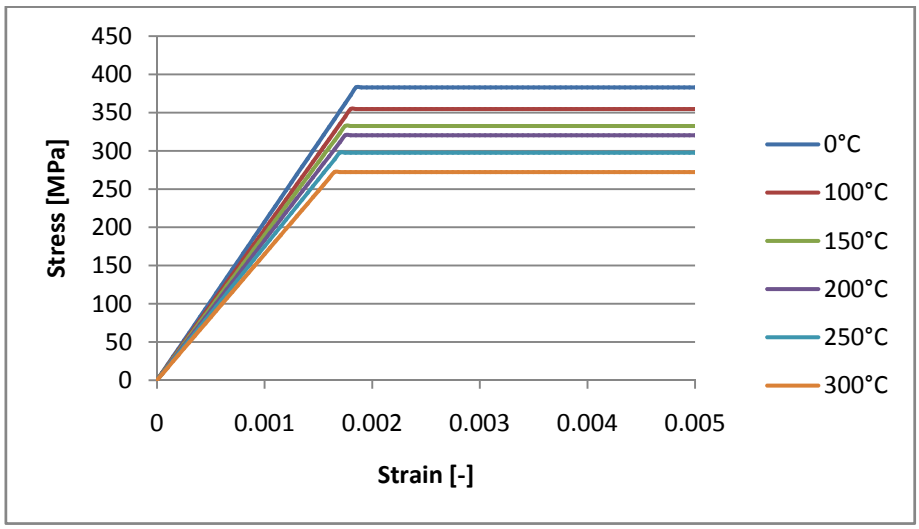

Figure 4.8 Stress-strain diagrams for K55 steel from 0-300°C

4.2.2 Stainless Steel Components

The gaskets, bolts and nuts are made of stainless steel; the gaskets are of steeltype 316L and the bolts and nuts are of steeltype A193. Figures 4.9-4.11 show the modulus of elasticity [17], coefficient of thermal conductivity [21] and coefficient of thermal expansion [21] for stainless steel plotted over the temperature range 0-300°C.

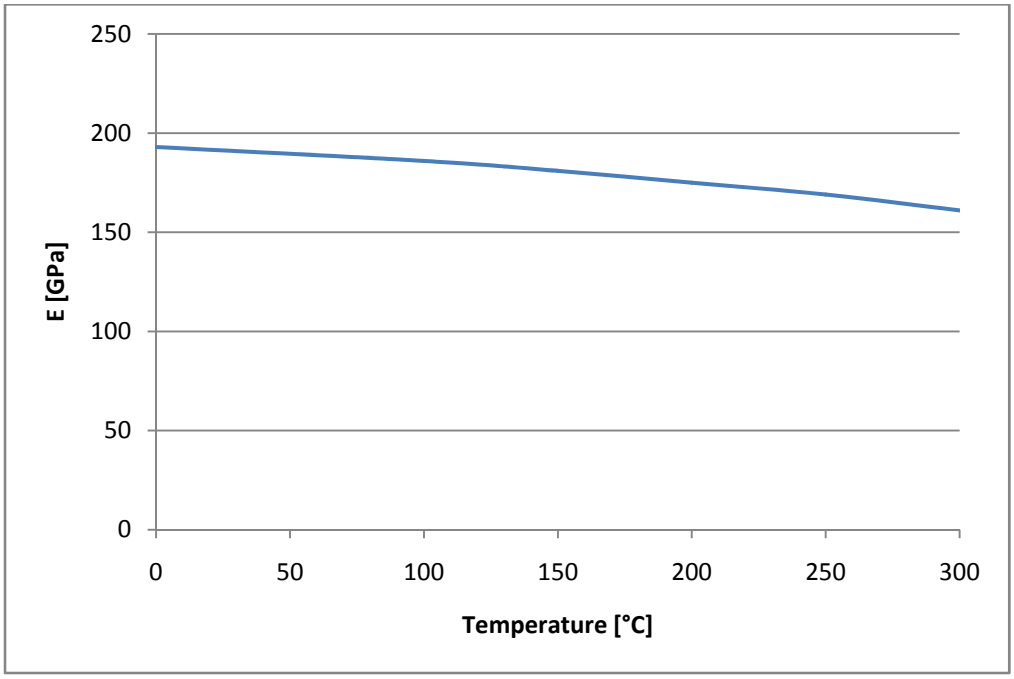

Figure 4.9 Modulus of elasticity for stainless steel from 0-300°C

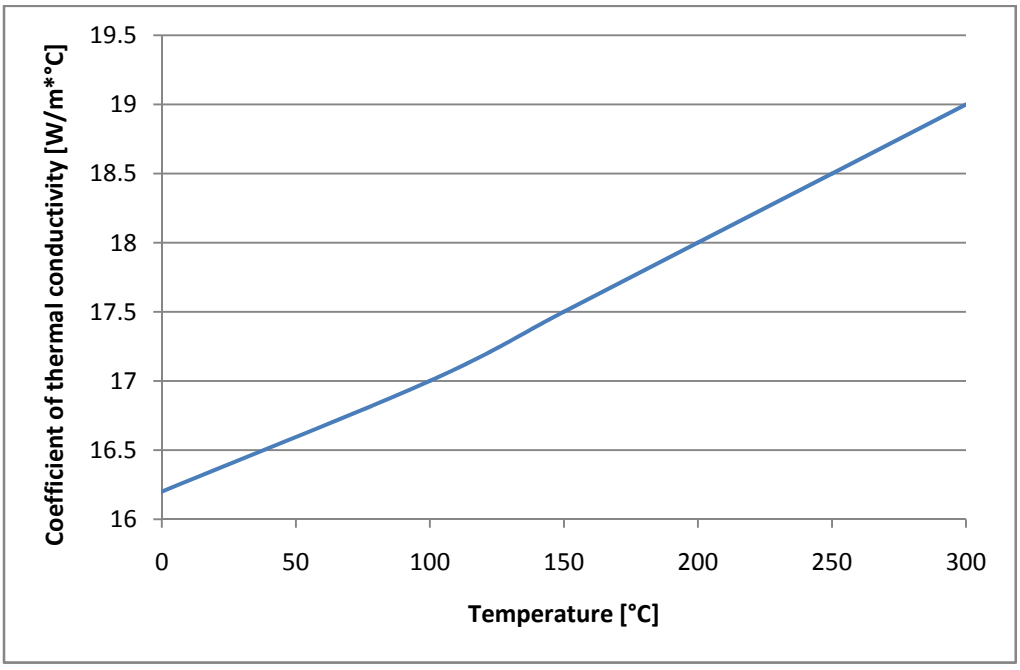

Figure 4.10 Coefficient of thermal conductivity for stainless steel from 0-300°C

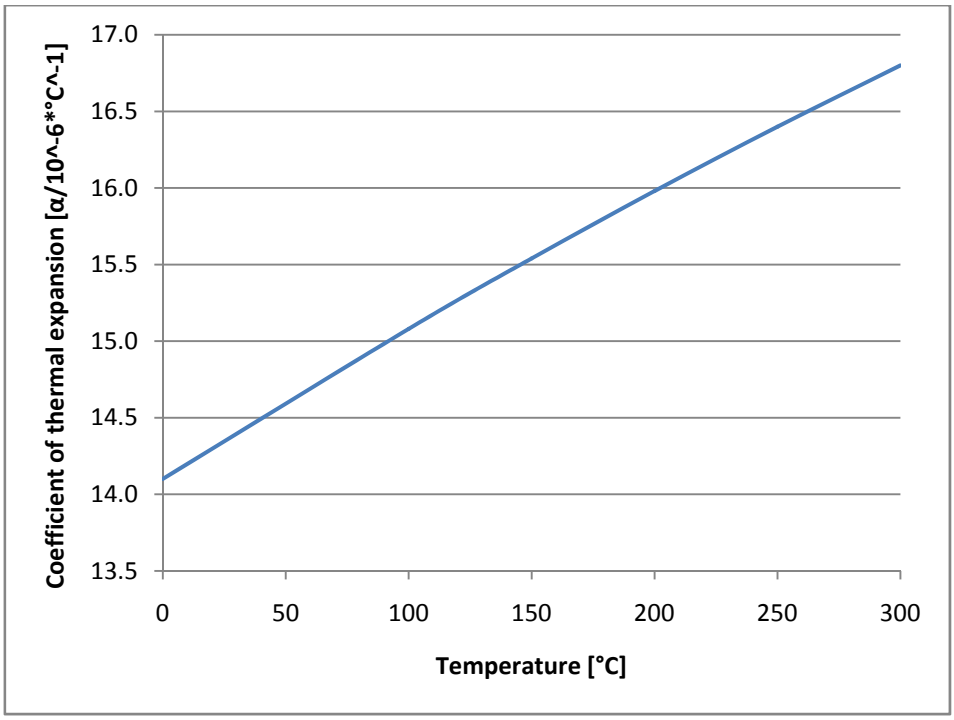

Figure 4.11 Coefficient of thermal expansion for stainless steel from 0-300°C

As for the carbon steels, idealized stress-strain curves for steel of material type 316L [23] and type A193 [23] are seen on figures 4.12 and 4.13. Stainless steel exhibits slightly different behavior than carbon steel; it is more ductile and has more strain-hardening abilities. [23]

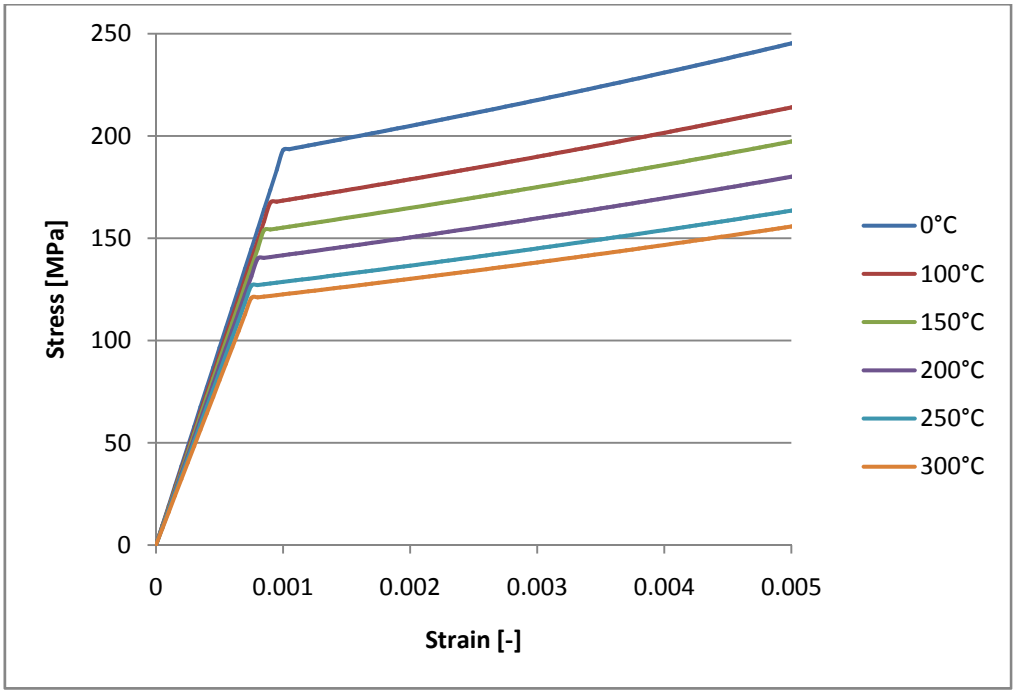

Figure 4.12 Stress-strain diagrams for 316L stainless steel from 0-300°C

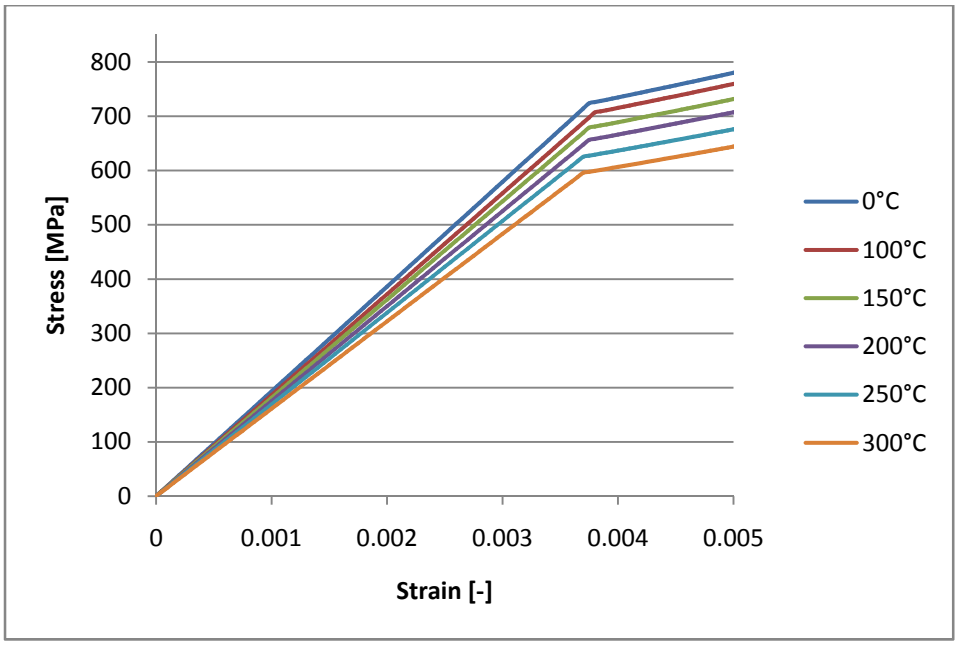

Figure 4.13 Stress-strain diagrams for A193 stainless steel from 0-300°C

4.3 Elements and Meshing

The solid model is meshed with solid elements. For the thermal analysis of the structure, SOLID87 [20] is used, and in the subsequent structural analysis, the corresponding structural element SOLID92 [20] is used. The elements are both 10-node, and utilize the same geometric structure, which can be seen on figure 4.14.

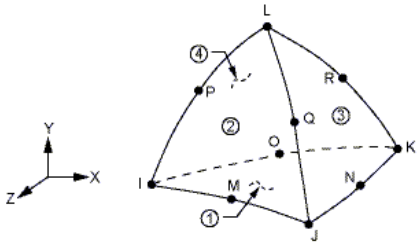

Figure 4.14 The SOLID87 and SOLID92 elements [20]

The elements have a quadratic displacement behavior and are well suited to model irregular meshes, as the case is for the model under consideration. The SOLID87 element has one degree of freedom at each node, temperature, and is applicable to a three-dimensional, steady-state thermal analysis. The SOLID92 element has three degrees of freedom at each node, translations in the nodal x, y and z directions. The element is capable of modeling plasticity, stress stiffening and large deflection. [20]

The 3D model of the flanges of the wellhead after being meshed with solid elements can be seen on figure 4.14.

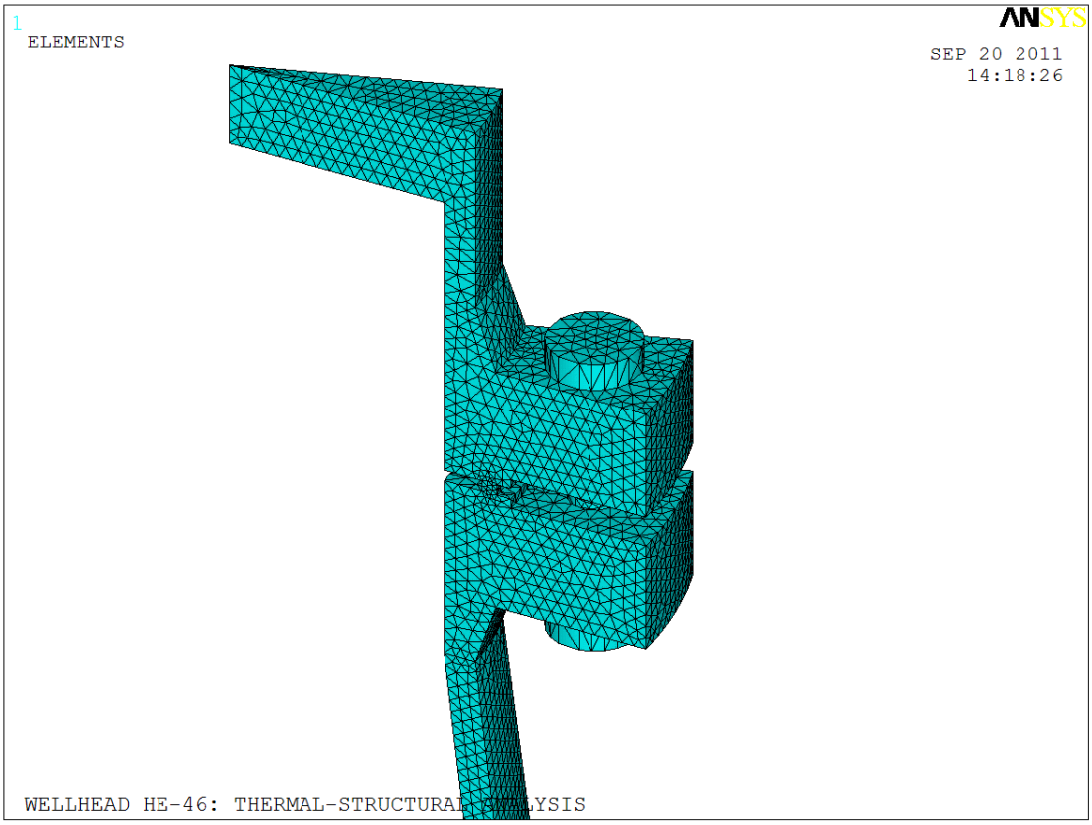

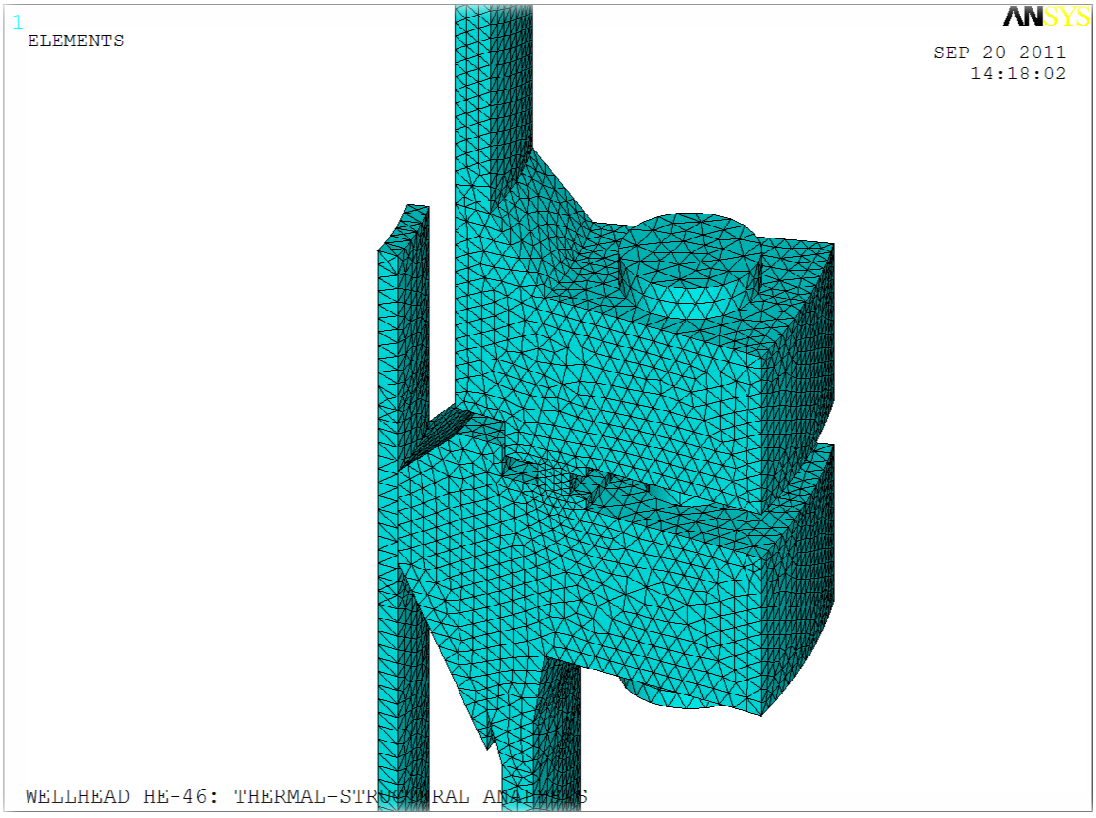

Figure 4.14 The meshed 3D model of the wellhead

To represent contact between the production casing and the casing steering, contact elements are utilized on the surfaces that come into contact. CONTA174 [20] is used on the surface of the production casing. It is an 8-node element that is intended for general rigid-flexible and flexible-flexible (as in this case) contact analysis. The contact element is constrained against penetration into the target surface. The target surface (here the surface of the casing steering) has to be covered with the corresponding target element, TARGE170. [20] The elements can be seen on figure 4.15.

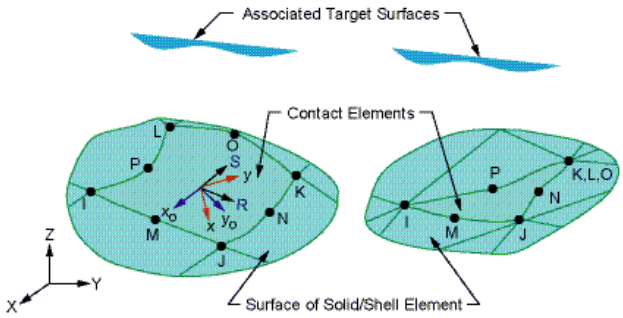

Figure 4.15 CONTA174 and TARGE170 elements [20]

Finally, to model the pretension in the bolts a special pretension element is used, PRETS179 [20]. It has one translation degree of freedom, which defines the pretension direction. The pretension elements are inserted in the middle of the solid meshed bolts, and the pretension force assigned. [20] The pretension element can be seen on figure 4.16.

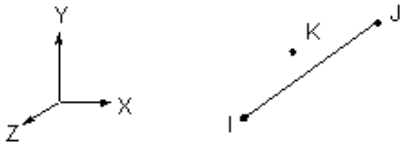

Figure 4.16 PRETS179 element [20]

When the model has been meshed with solid, contact and pretension elements there are about 110.000 elements that make up the model.

4.4 Boundary Conditions, Loads and Model Function

The model has fixed boundary conditions at the bottom of the wellhead, where the ground of the wellhead cellar is located. Symmetrical boundary conditions are used because the model consists of 1/20 of the three dimensional wellhead structure. At the boundaries between the 1/20 model and the “imaginary” other parts of the model, movement is restricted in the tangential directions, as can be seen on figure 4.17.

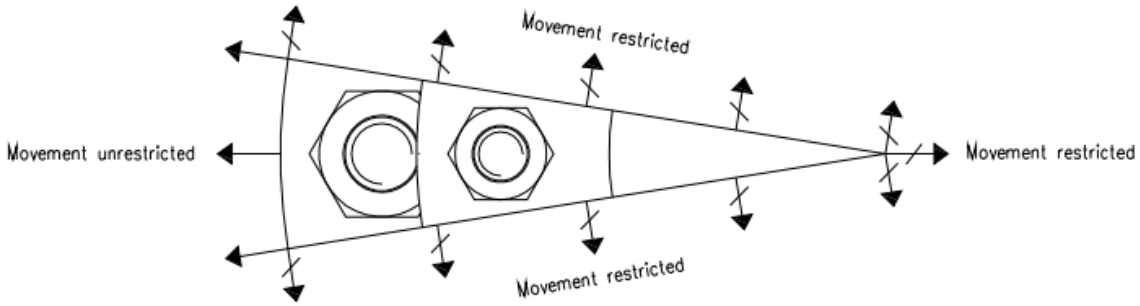

Figure 4.17 Symmetry boundary conditions

When the boundary conditions are defined the meshed model is ready to be subjected to analysis. The pretension elements are used to generate pretension in the bolts. Then, the inside of the wellhead model will be subjected to temperature loads, and the outside of the model subjected to fixed temperature boundary conditions, based on measurements during charging of an actual well. The temperature distribution can thus be calculated. The results from this heat transfer analysis are transferred to the structural analysis as temperature loads. Finally, the inside of the model is subjected to pressure loads.

Due to the high loading, and the nonlinearities incorporated in the model, the solution method will have to be nonlinear. The Bilinear Kinematic Hardening material rule discussed in chapter 3.2 will be used to model the plastic deformation expected in the gaskets and surrounding area. The Newton-Raphson method, also discussed in chapter 3.2, will be used to reach a solution, with several load steps and substeps within load steps used to make the solution converge.

5 Case Studies

The modeling of a high temperature geothermal wellhead with the finite element method was described in chapter 4, and in this chapter the finished model will be subjected to several load cases in order to examine how it performs. First, a pretension analysis will be performed. Then the model will be subjected to loads simulating the charging and subsequent operating conditions of a wellhead. Finally, the model will be subjected to an extreme pressure value that can be found inside closed wellheads, and an accompanying extreme temperature value.

The results will mainly be presented with figures showing the Von Mises stress distribution in the various parts of the wellhead. The Von Mises stress is found with the following equation:

$$\sigma_{Von\ Mises} = \sqrt{\frac{1}{2}[(\sigma_x - \sigma_y)^2 + (\sigma_y - \sigma_z)^2 + (\sigma_z - \sigma_x)^2] + 3\tau_{xy}{}^2 + 3\tau_{yz}{}^2 + 3\tau_{zx}{}^2} \qquad (5.1\text{-}1)$$

These will be compared to the yield strength of each material. Maximum values will be presented in tables following each load case, and then compared in a subsequent section.

5.1 Load Case 1: Pretension

As the discussion in section 2.2.4 indicated the pretension procedure of the wellhead needs to be carefully monitored. The bolts are pretensioned both to hold the wellhead flanges together, and to press the gasket over the yield limit to prevent leakage. It is standard practice to assign pre-established values for the required pretension torque. For a similar wellhead in the Reykjanes area in Iceland the recommended torque value is about 5900 Nm for the larger bolts in the wellhead connection, and about 1900 Nm for the smaller bolts [24]. These values are used as the normal pretension values in this project. As the pretension elements used in the bolts are loaded with force values, the force F_i in equation 2.1-1 has to be solved for the above values. For the lower bolts it is found to be about 410 kN and for the upper bolts about 181 kN.

The pretension load case setup can be seen on figure 5.1. The resulting Von Mises stress distribution in the model can be seen on figure 5.2. The bolts have been removed from the figure to show better how the stresses are distributed. Due to the high pretension load and the high yield strength of the bolt material (720 MPa at 0°C) the bolts experience much higher stresses than the rest of the wellhead equipment. They will therefore be excluded from the rest of the figures in the section. On figures 5.3 and 5.4 the Von Mises stress distribution as well as the yield stress of the flange connections can be seen more closely. Finally, figures 5.5 and 5.6 show the results for the gaskets alone. (The unit bar in the bottom of the figures shows the results in Pa].

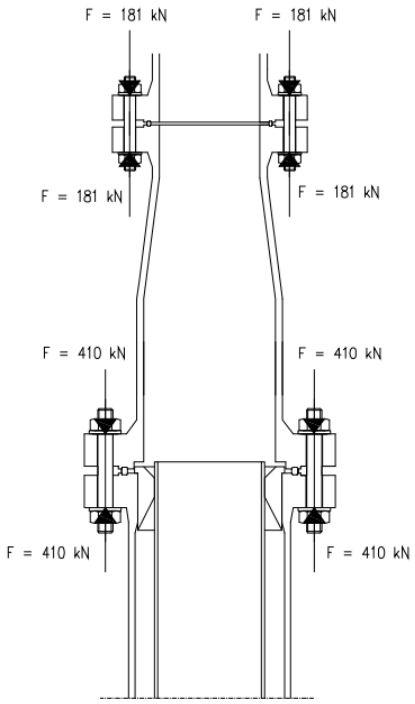

Figure 5.1 Load case 1

Figure 5.2 Von Mises stress distribution for load case 1

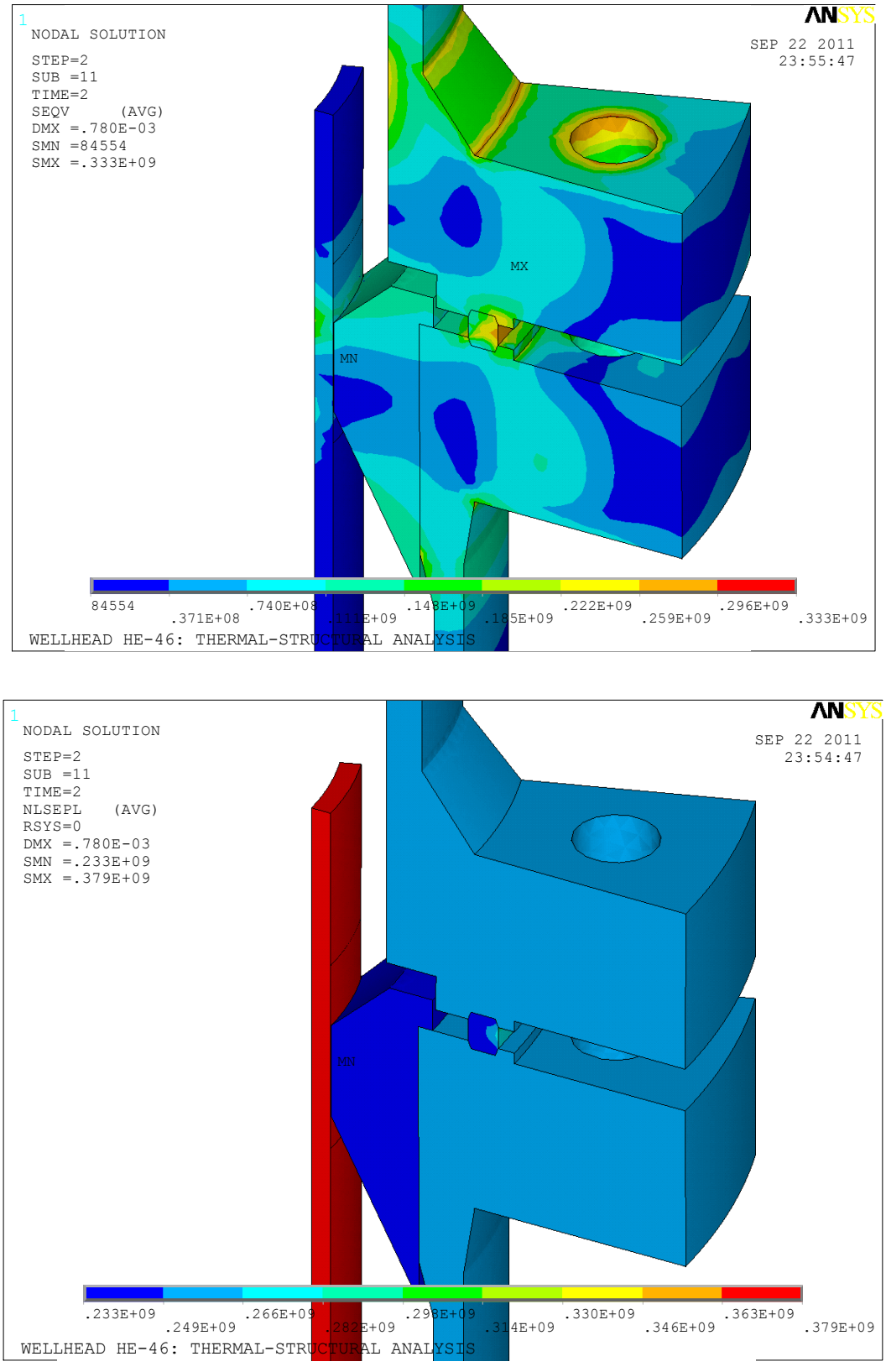

Figure 5.3 Load Case 1: Von Mises stress distribution (above) and the yield stress (below) in the lower flange connection

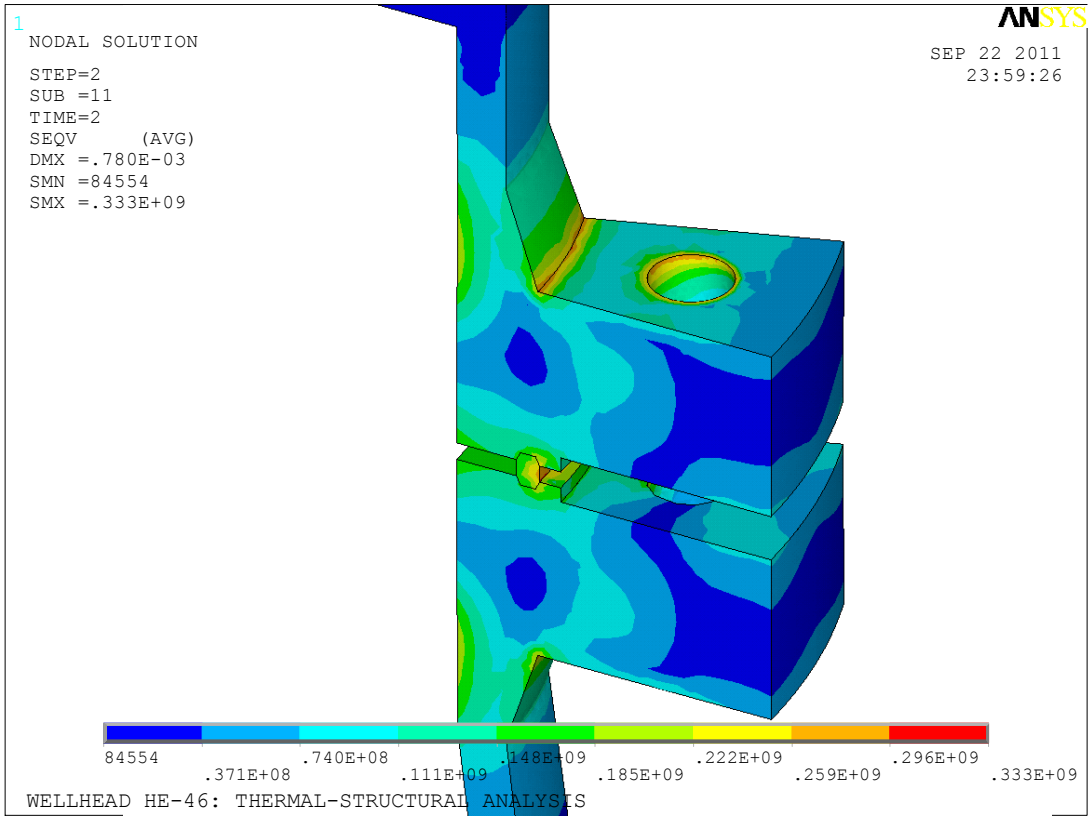

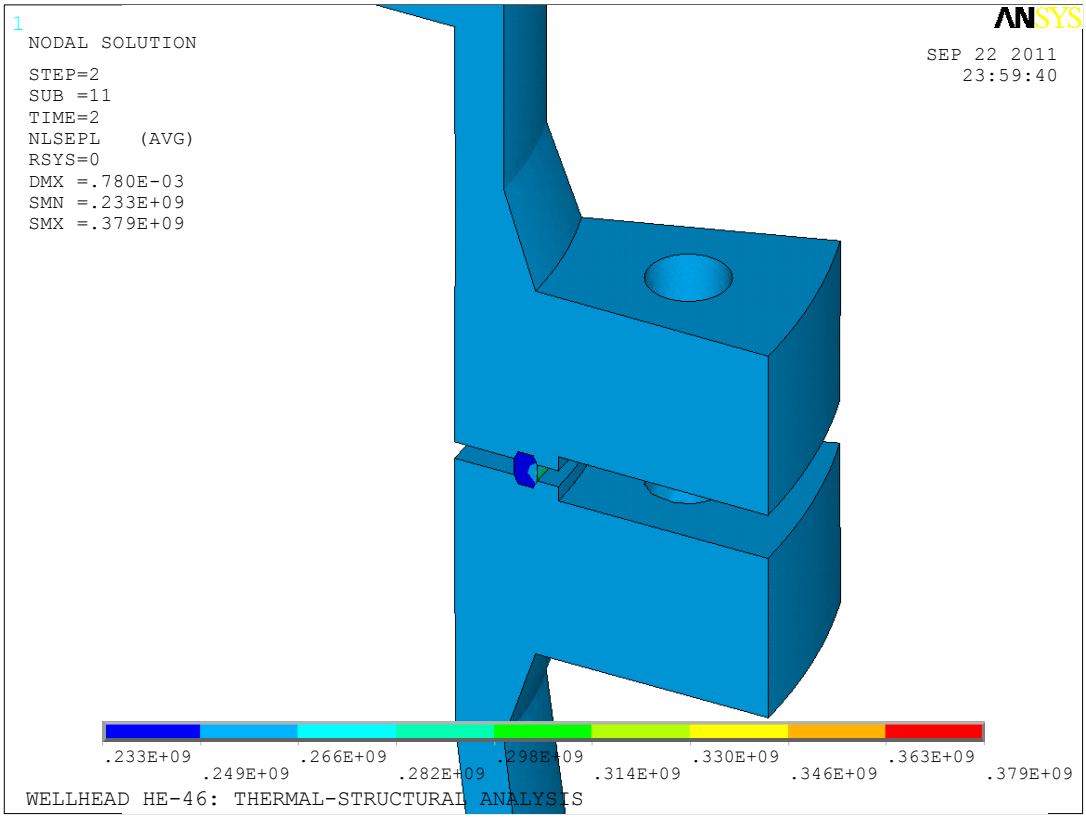

Figure 5.4 Load Case 1: Von Mises stress distribution (above) and the yield stress (below) in the upper flange connection

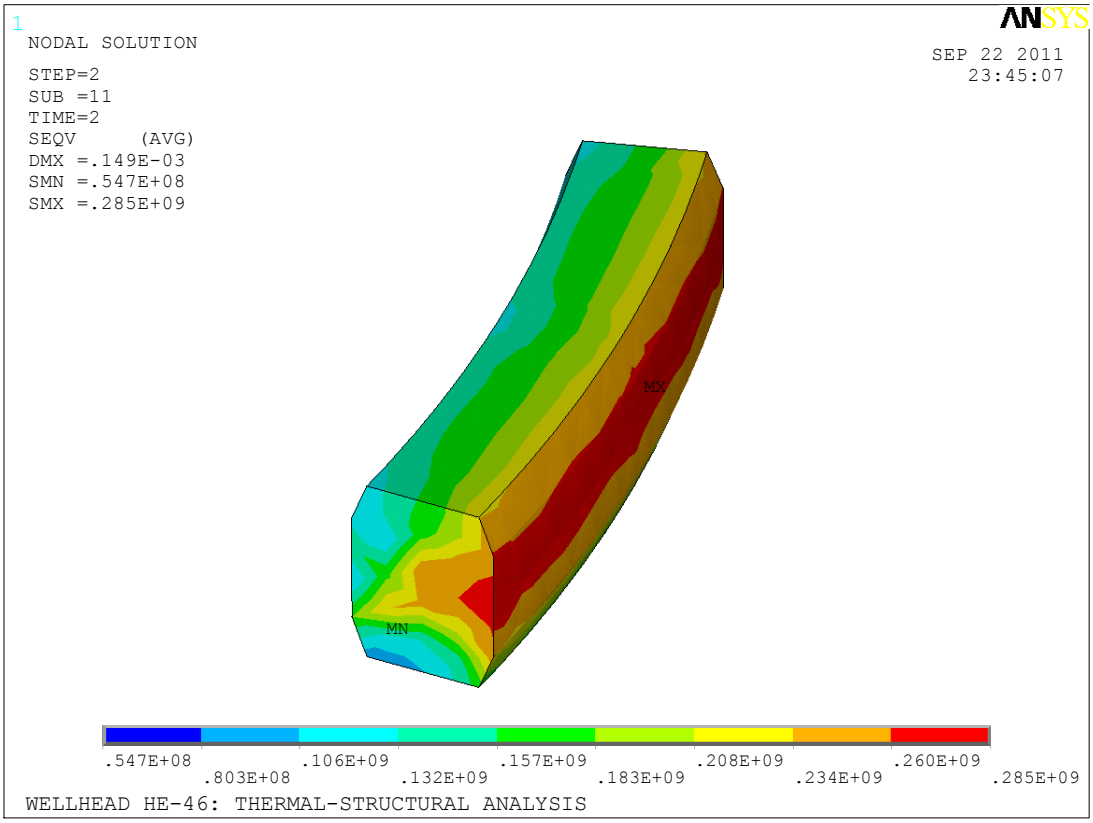

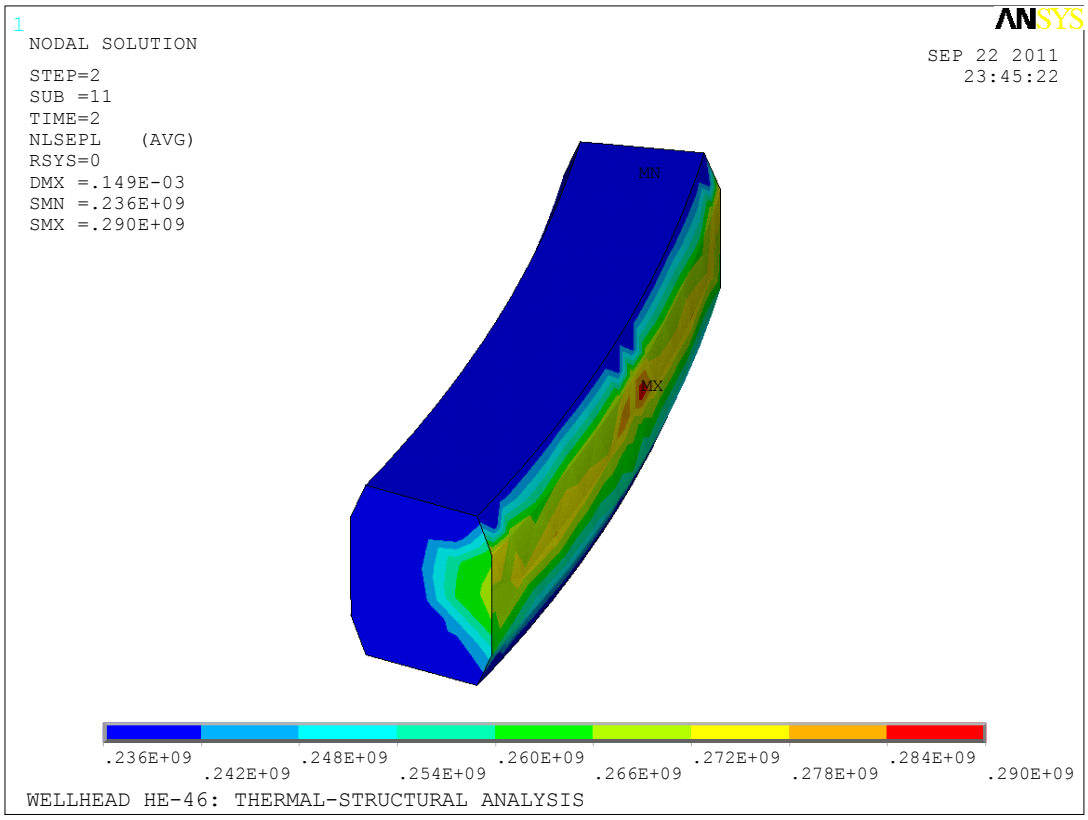

Figure 5.5 Load Case 1: Von Mises stress distribution (above) and the yield stress (below) in the lower gasket

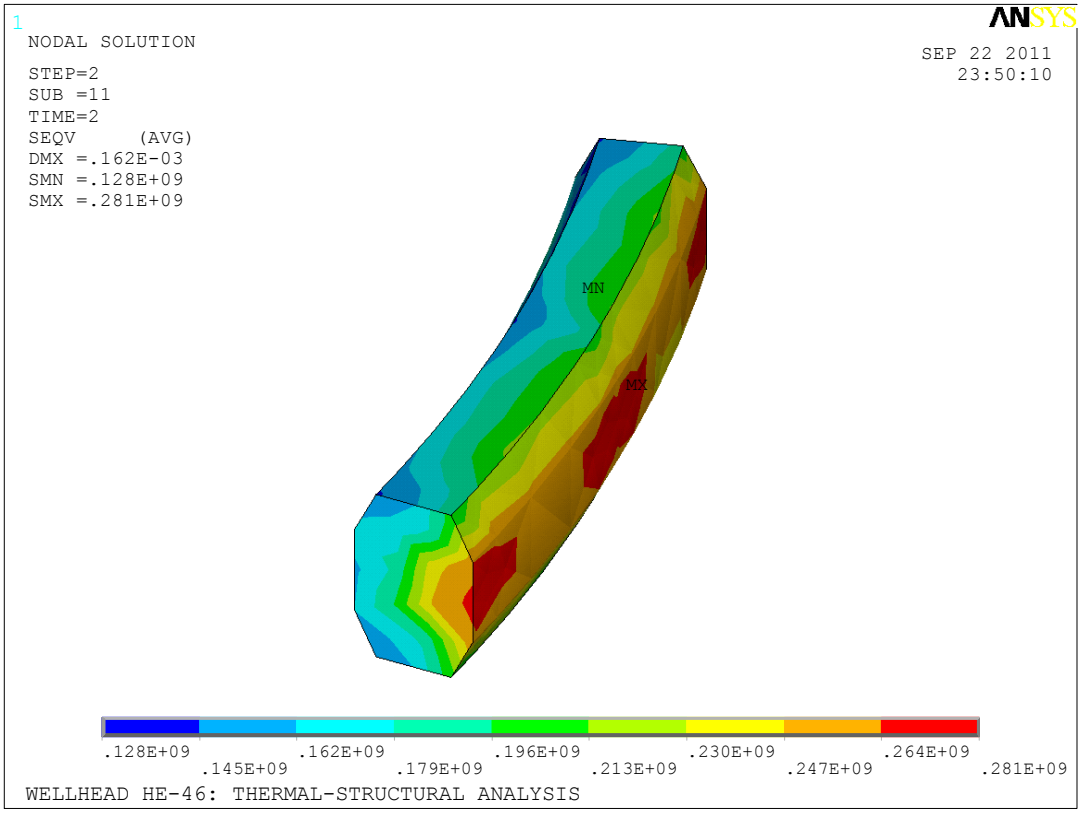

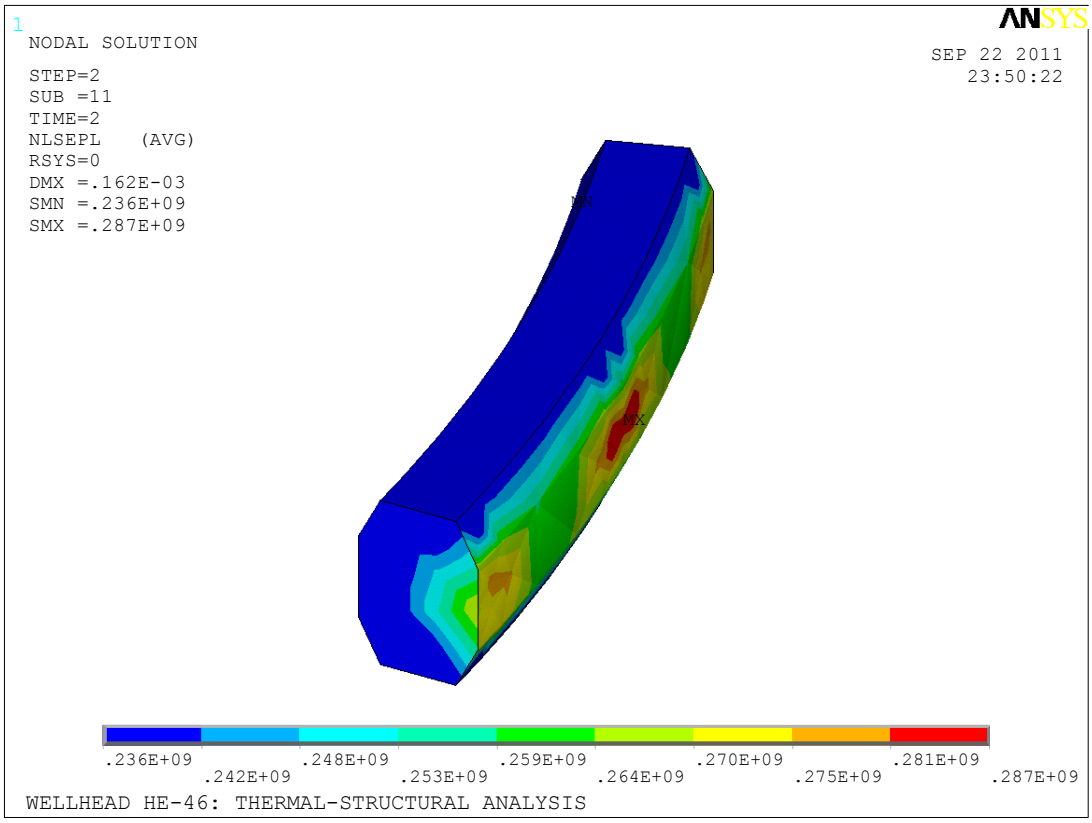

Figure 5.6 Load Case 1: Von Mises stress distribution (above) and the yield stress (below) in the upper gasket

It can be seen on the above figures how the maximum stresses in the flanges occur at stress concentration areas, at sharp corners and under the bolt nuts. The highest Von Mises stress in the lower flanges is 259 MPa, which is just under the yield stress, 263 MPa. The highest Von Mises stress in the upper flanges is 260 MPa, also just under the yield stress of 263 MPa. It is possible that the high stresses monitored at these stress concentration areas are due to too coarse mesh at these areas. The main parts of the flanges have stresses that are under 222 MPa.

The approximate yield strength of the gasket material is 240 MPa at 5°C. The orange and red areas on the above figures show areas where the Von Mises stress is between 234 and 285 MPa, thereby indicating how the gasket has started to deform plastically.

Table 5.1 summarizes the maximum Von Mises stresses compared to yield stress for load case 1. It can be seen in the table that only the gaskets stresses go above the yield stress. The stresses in the flanges go almost up to the yield limit, but only at areas of stress concentration.

Table 5.1 Load Case 1: Maximum Von Mises stresses compared to yield stress

Wellhead part	Von Mises stress [MPa]	Yield stress [MPa]	% of yield stress
Production casing	153	379	40%
Casing steering	148	233	64%
Lower flanges	259	263	98%
Upper flanges	260	263	99%
Lower gasket	285	236	121%
Upper gasket	281	236	119%

5.2 Load Case 2: Charging

When wells are opened temperature rise is sudden. This causes rapid thermal expansion, causing thermal stresses, and also affects the material properties in the wellhead equipment. As discussed in 2.4, the effect of the elevated temperature on flange connections can cause leakage.

Measurements of wellhead HE-46 were made in April 2011 (see Appendix). The temperatures measured on the outside of the wellhead are used here as boundary conditions. The temperature of the geothermal fluid is assumed to be 212°C, as was discussed in section 2.2.3, and the inner pressure is assumed to be 18 bar, which is the normal operating pressure of the wellhead, and was also measured during charging of the well. Of course the pretension load described in the previous section is maintained during this load case.

On figure 5.7 the setup for load case 2 can be seen.

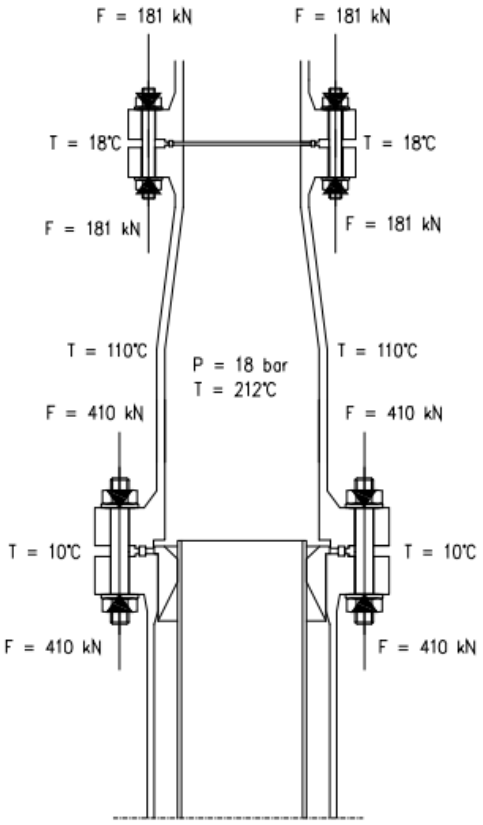

Figure 5.7 Load case 2

On figure 5.8 the temperature distribution (upper figure) and the Von Mises stress distribution (lower figure) during charging can be seen. Figures 5.9 and 5.10 show the stress distribution in the flanges, as well as the yield stress at this temperature. Figures 5.11 and 5.12 show the distribution in the gaskets.

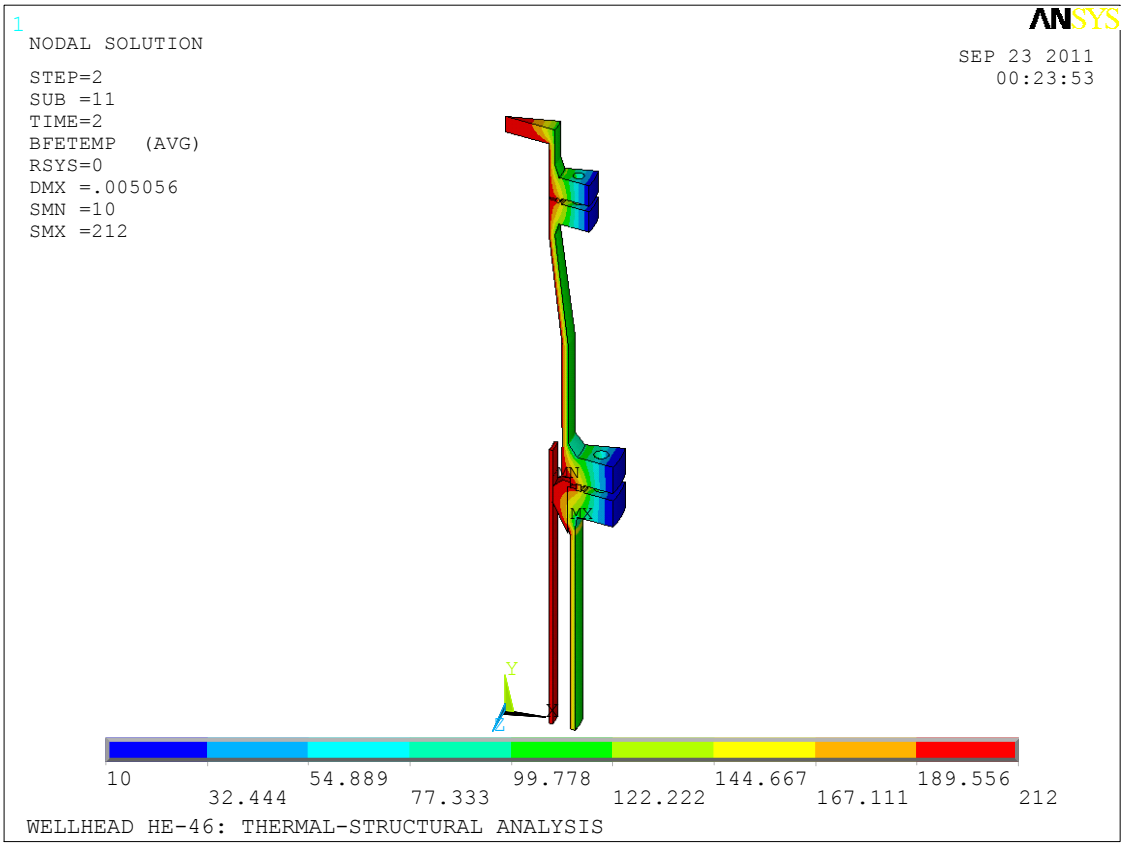

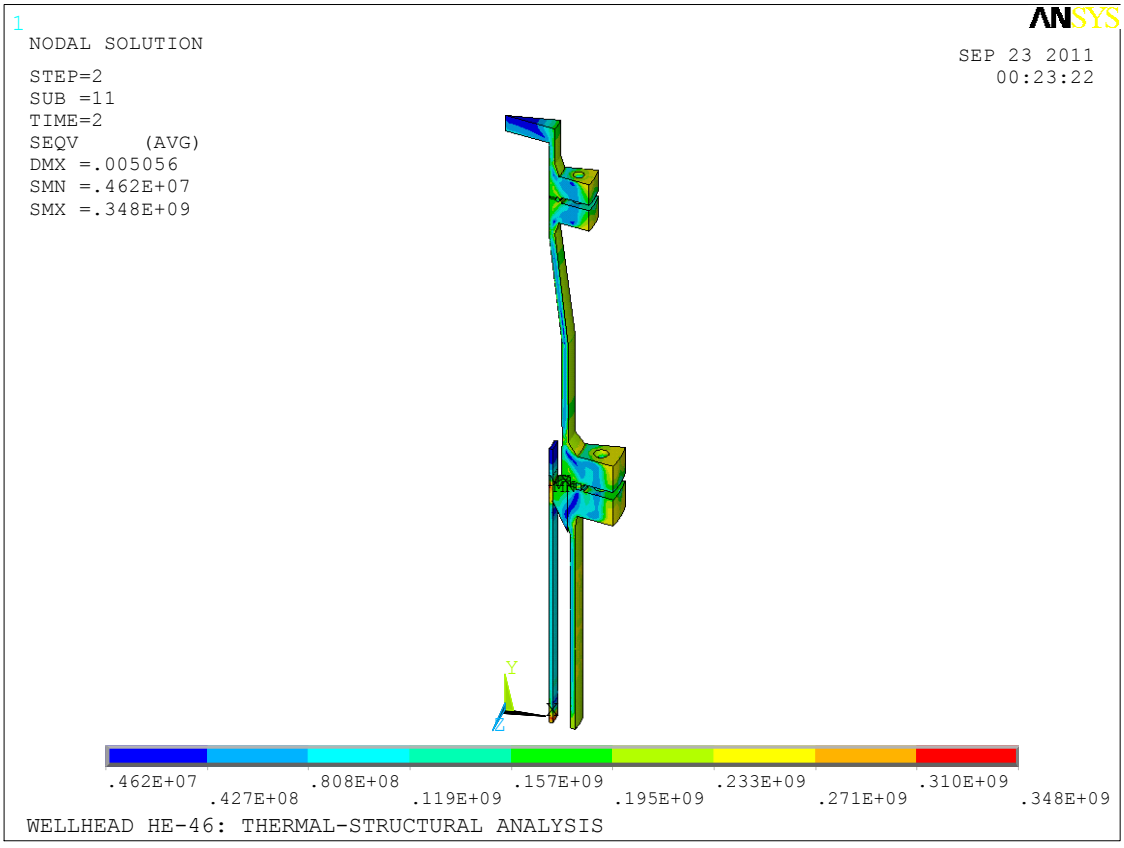

Figure 5.8 Temperature and Von Mises stress distribution for load case 2

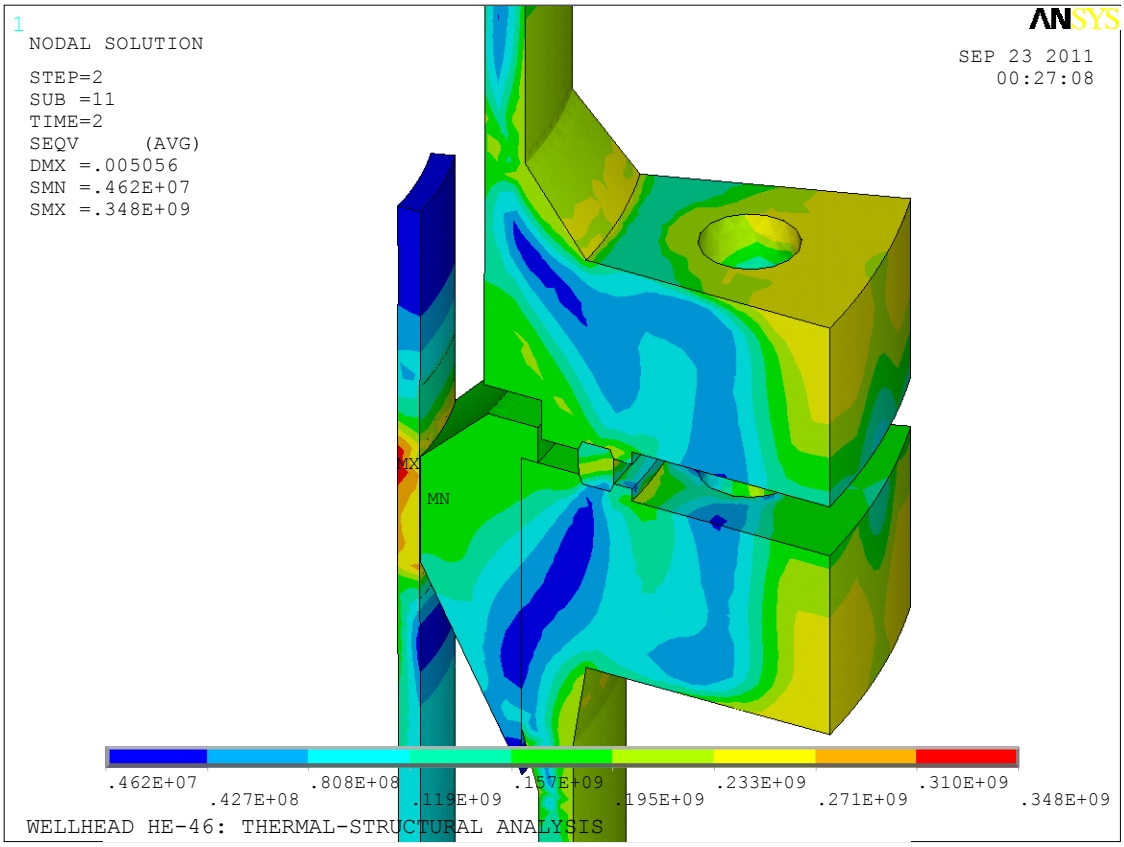

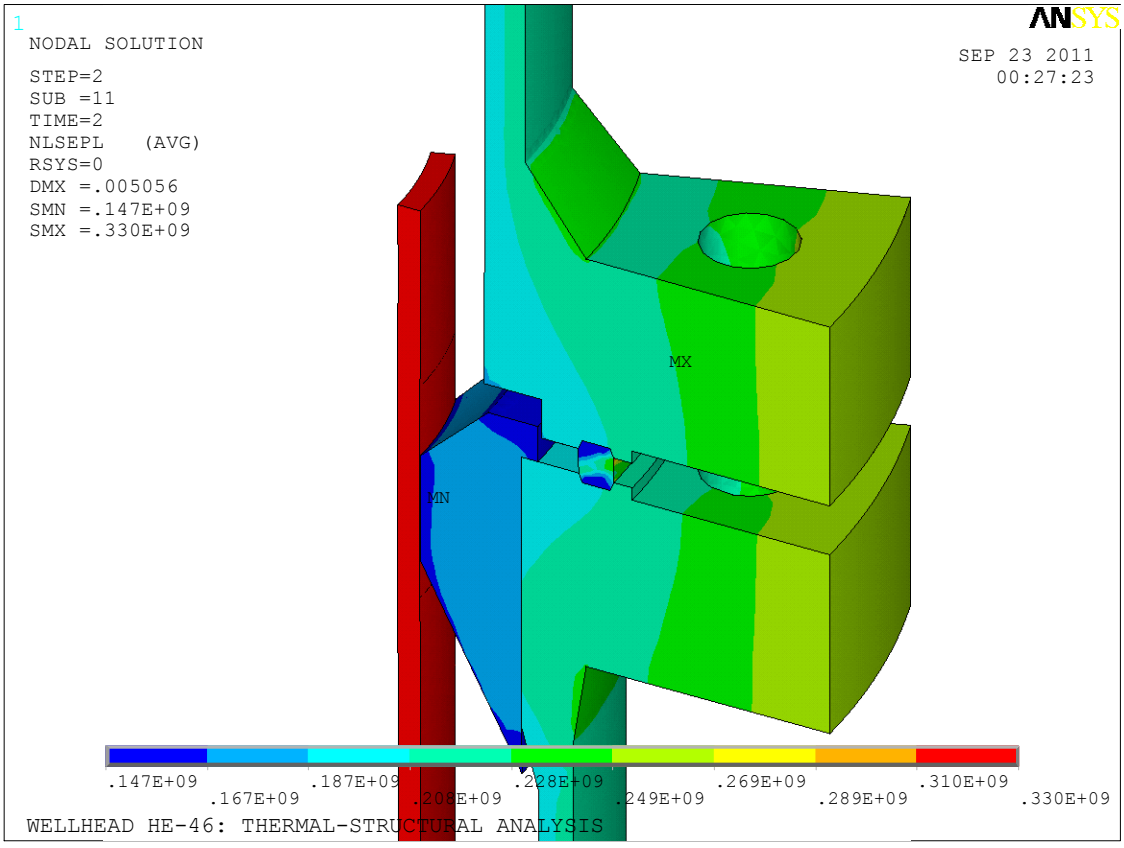

Figure 5.9 Load Case 2: Von Mises stress distribution (above) and the yield stress (below) in the lower flange connection

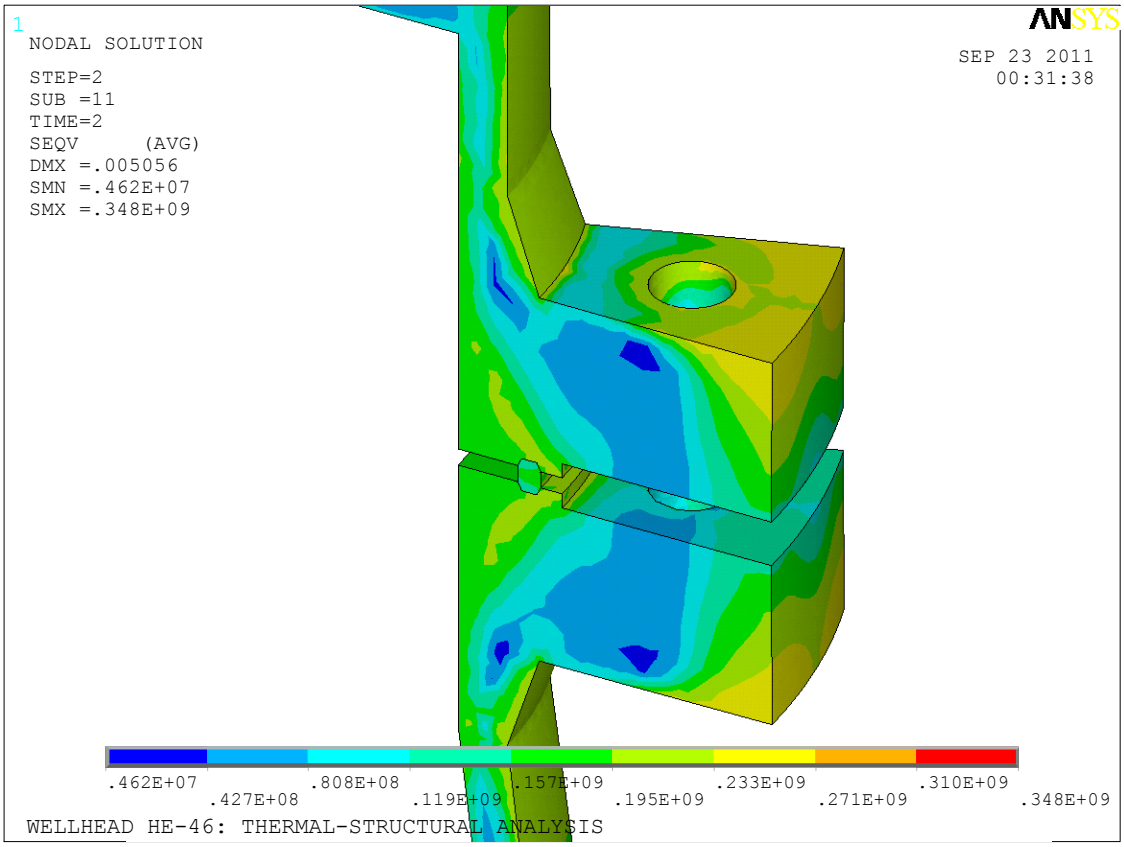

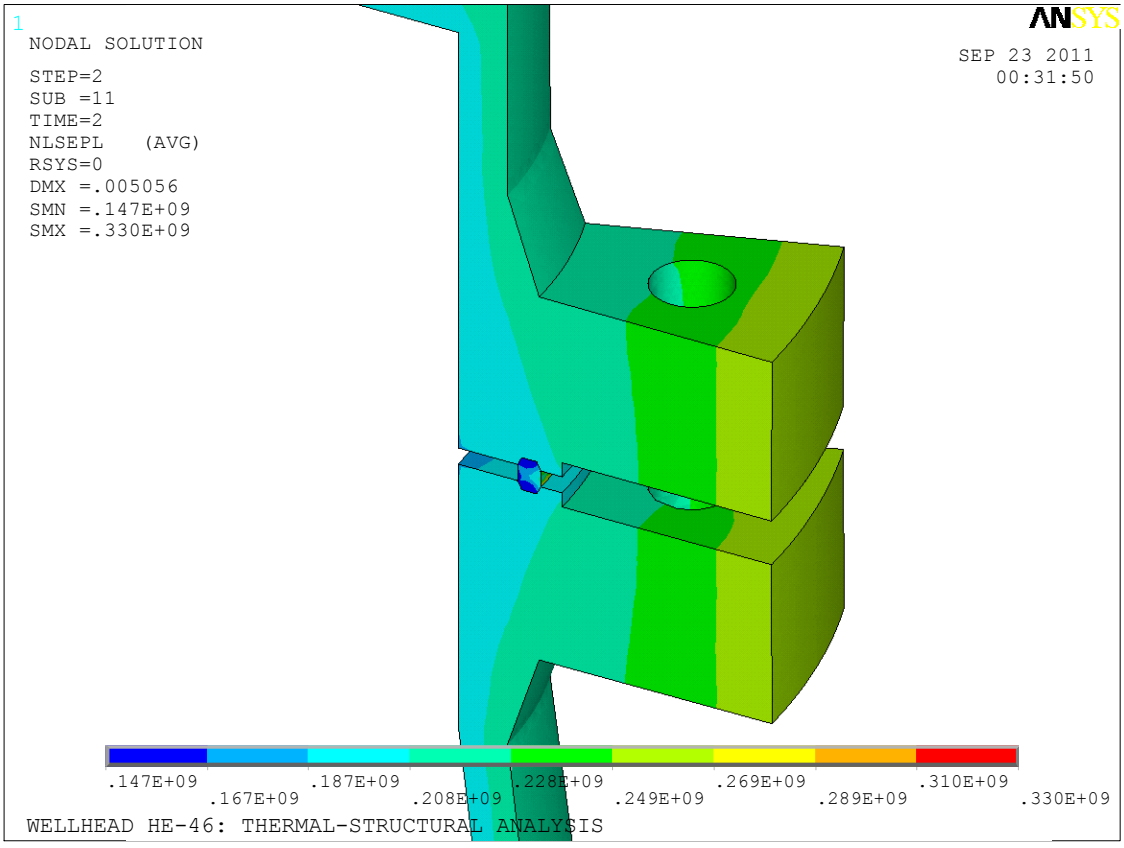

Figure 5.10 Load Case 2: Von Mises stress distribution (above) and the yield stress (below) in the upper flange connection

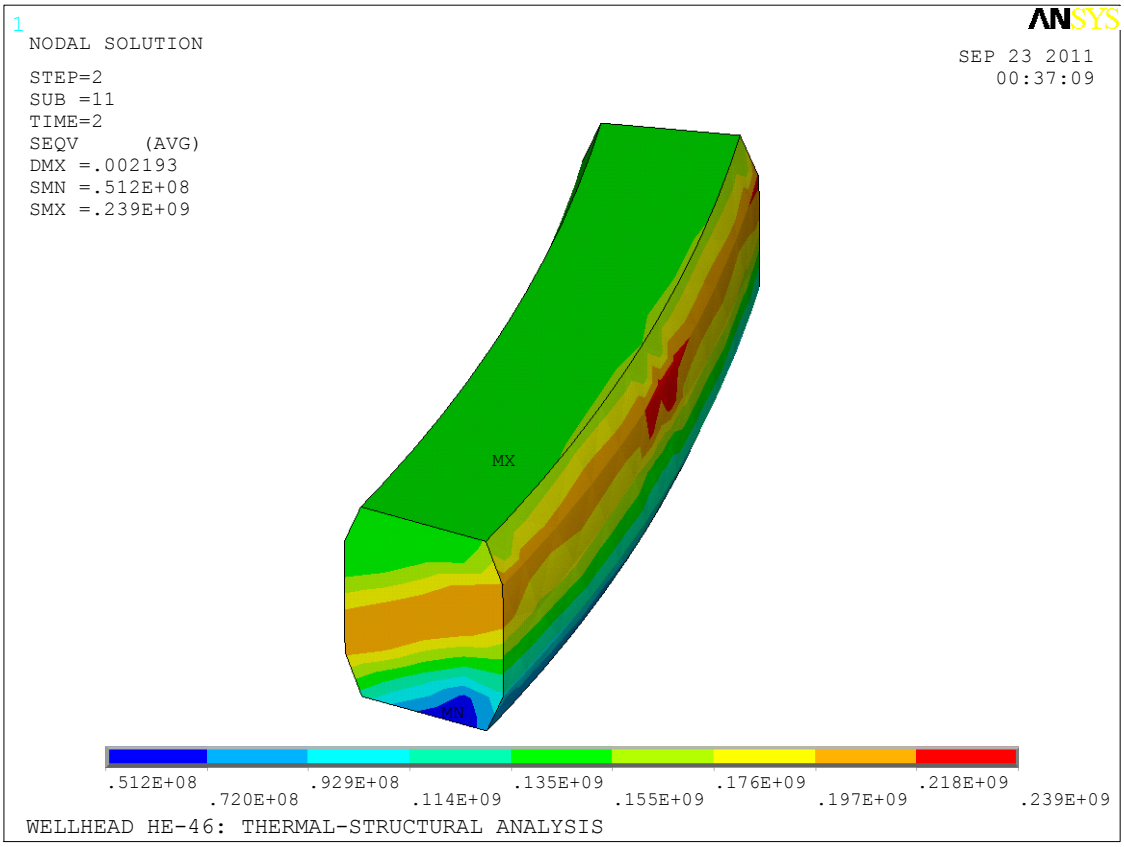

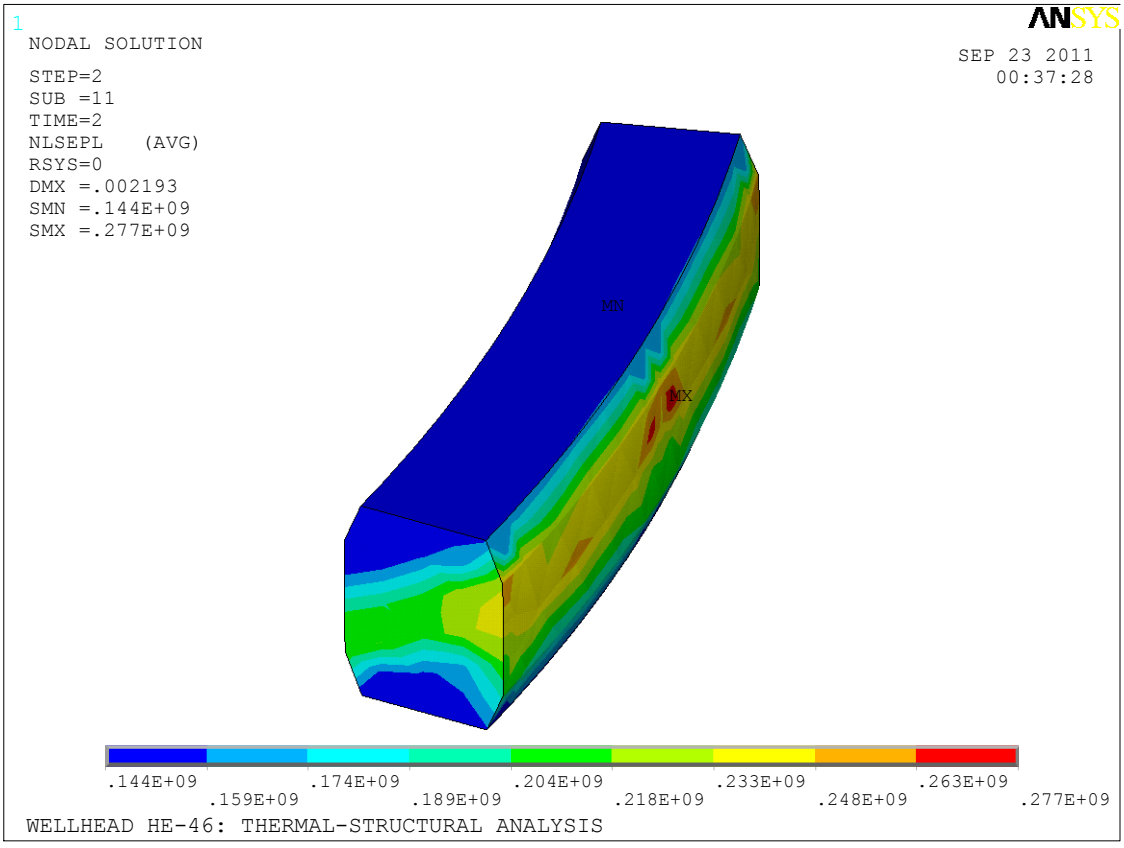

Figure 5.11 Load Case 2: Von Mises stress distribution (above) and the yield stress (below) in the lower gasket

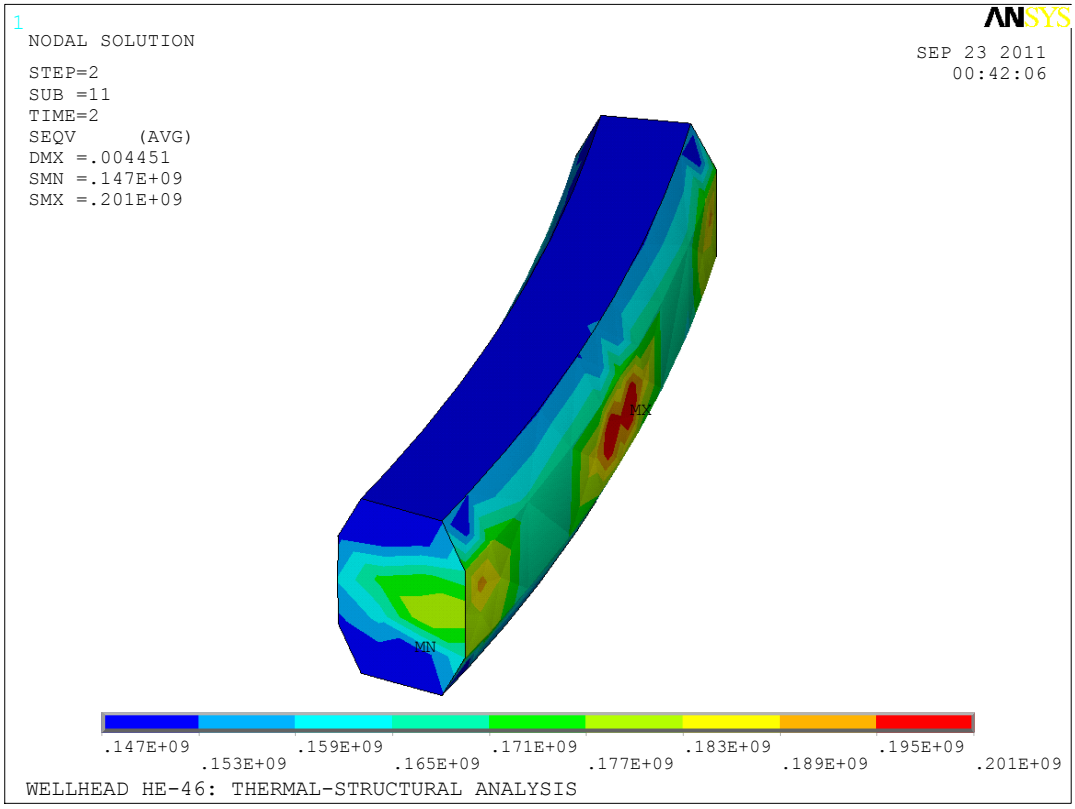

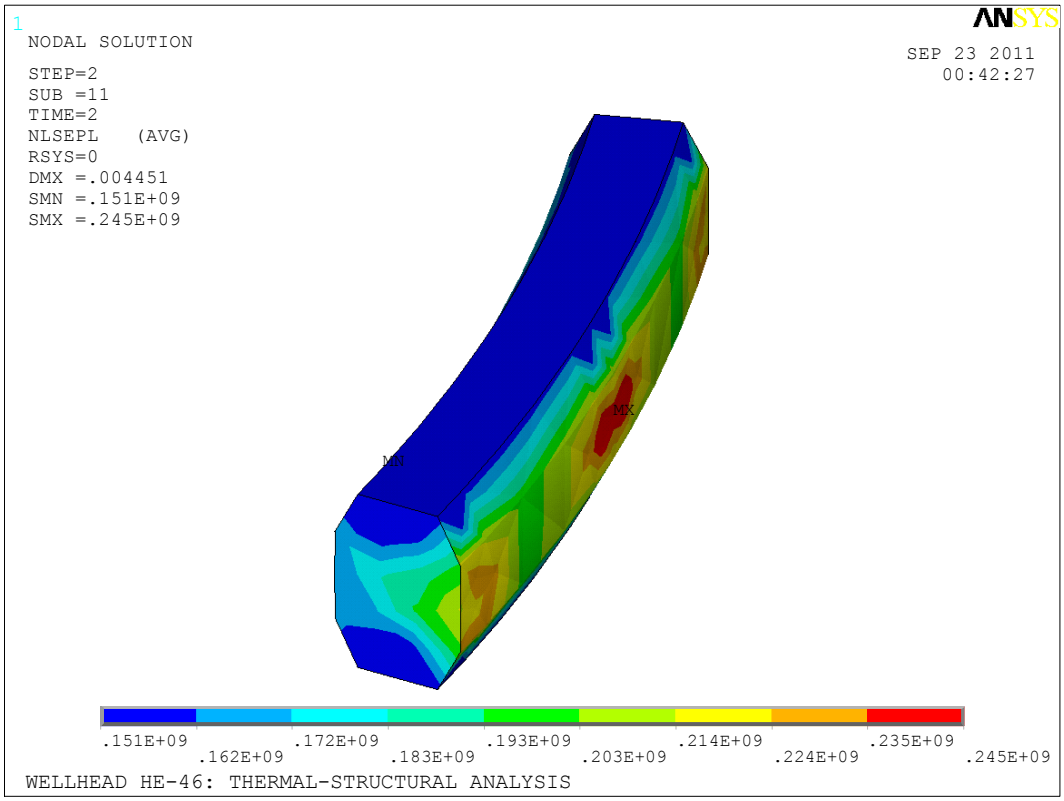

Figure 5.12 Load Case 2: Von Mises stress distribution (above) and the yield stress (below) in the upper gasket

On the above figures it can be seen how the stress distribution has changed considerably from the one seen for load case 1. The stresses in the flange ends have increased from just under 100 MPa up to about 240 MPa. This is mainly due to thermal stresses, produced by the thermal gradient. As can be seen on the upper figure 5.8 the temperature difference in the flanges is very high. Thermal expansion in the wellhead is also considerable; the maximum vertical displacement is over 5 mm at the top of the model. Also, the Von Mises stresses in the production casing go over the yield strength. The highest Von Mises stress in the production casing is 348 MPa, at the surface which comes into contact with the casing steering. There is also yielding at the contact surface of the casing steering itself.

Comparing figures 5.11 and 5.12 with 5.5 and 5.6 it can be seen how the stress distribution has changed considerably from the pretension load case. The stresses are lower, mainly because the yield strength of the gasket material is lower at the elevated temperature found inside the wellhead. This lower stress value can cause leakage trouble.

In table 5.2 the maximum Von Mises stresses and the yield stresses are summarized.

Table 5.2 Load Case 2: Maximum Von Mises stresses compared to yield stress

Wellhead part	Von Mises stress [MPa]	Yield stress [MPa]	% of yield stress
Production casing	348	330	105%
Casing steering	157	158	99%
Lower flanges	236	249	95%
Upper flanges	242	249	97%
Lower gasket	239	144	166%
Upper gasket	201	151	133%

5.3 Load Case 3: Normal Operating Conditions

After the flow in the well has stabilized the temperature distribution has evened more out. This was measured the day after the first measurements which were mentioned in the previous section, and the measured values were used as boundary conditions for the model. This load case setup can be seen on figure 5.13.

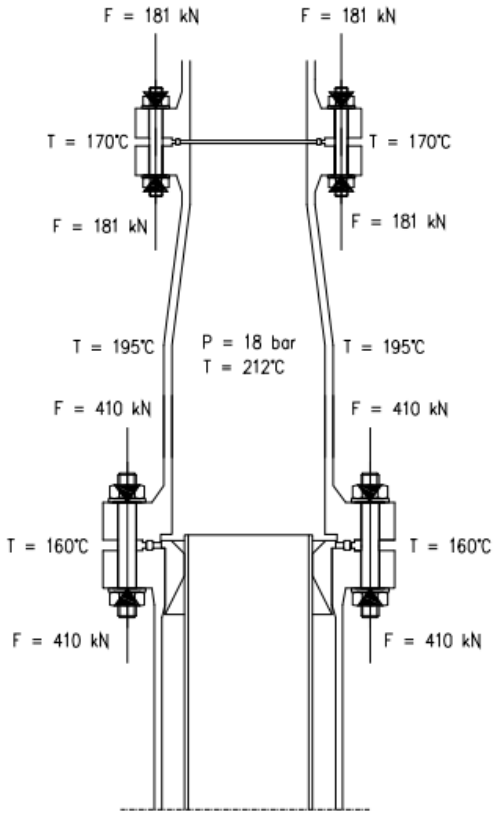

Figure 5.13 Load case 3

The temperature distribution, and the Von Mises stress distribution for this load case can be seen on figure 5.14. As before, figures 5.15 and 5.16 show the results for the flanges, and figures 5.17 and 5.18 for the gaskets.

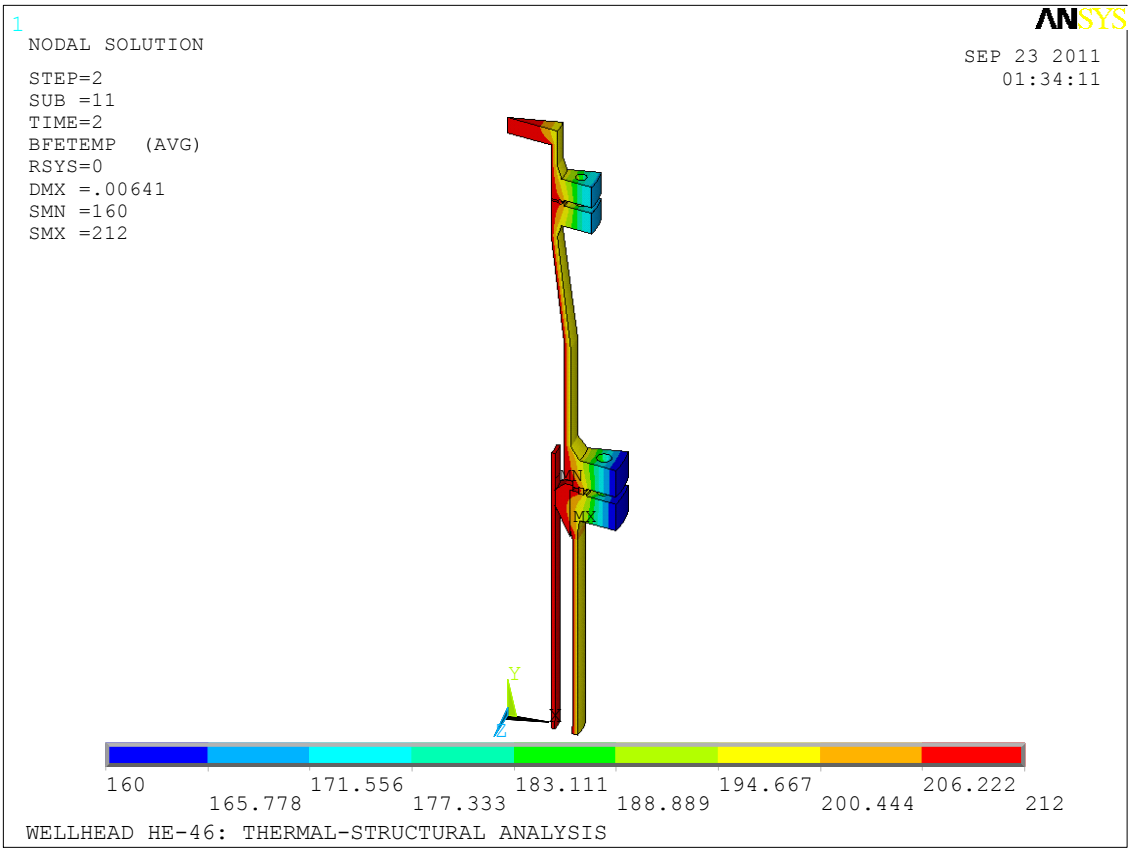

Figure 5.14 Temperature and Von Mises stress distribution for load case 3

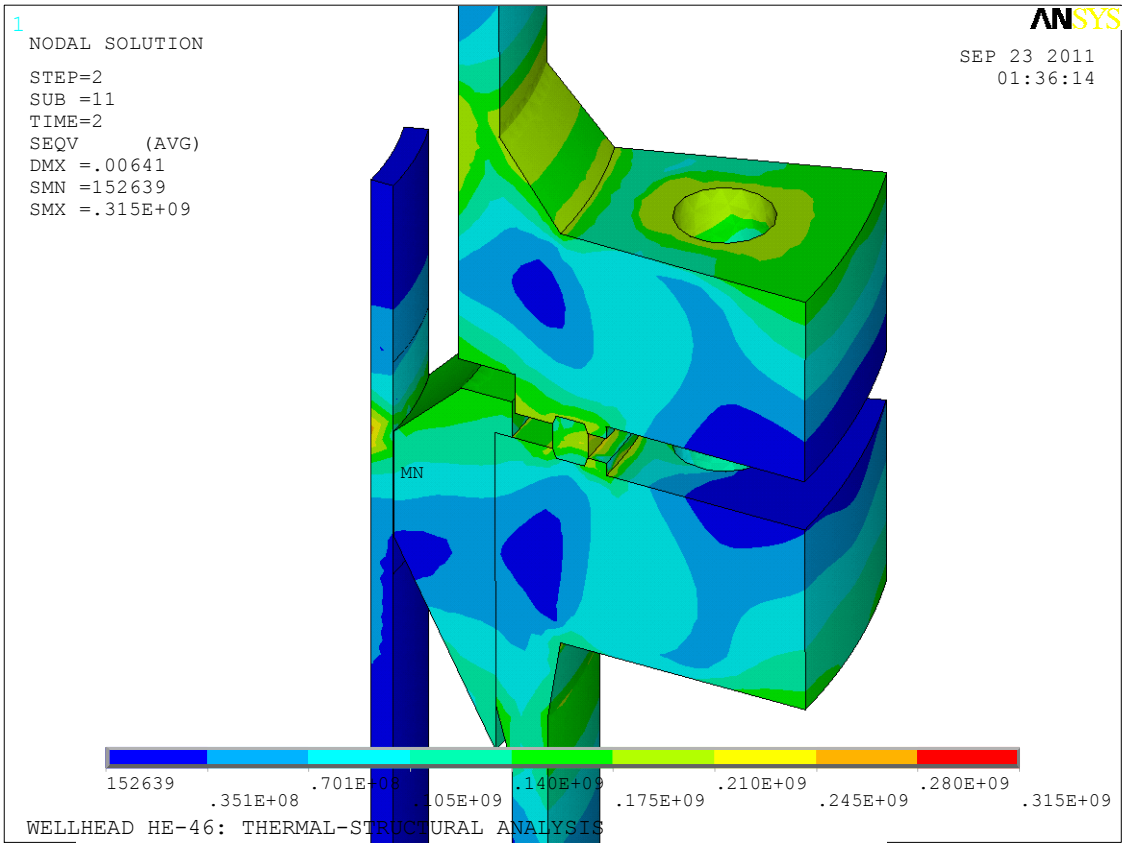

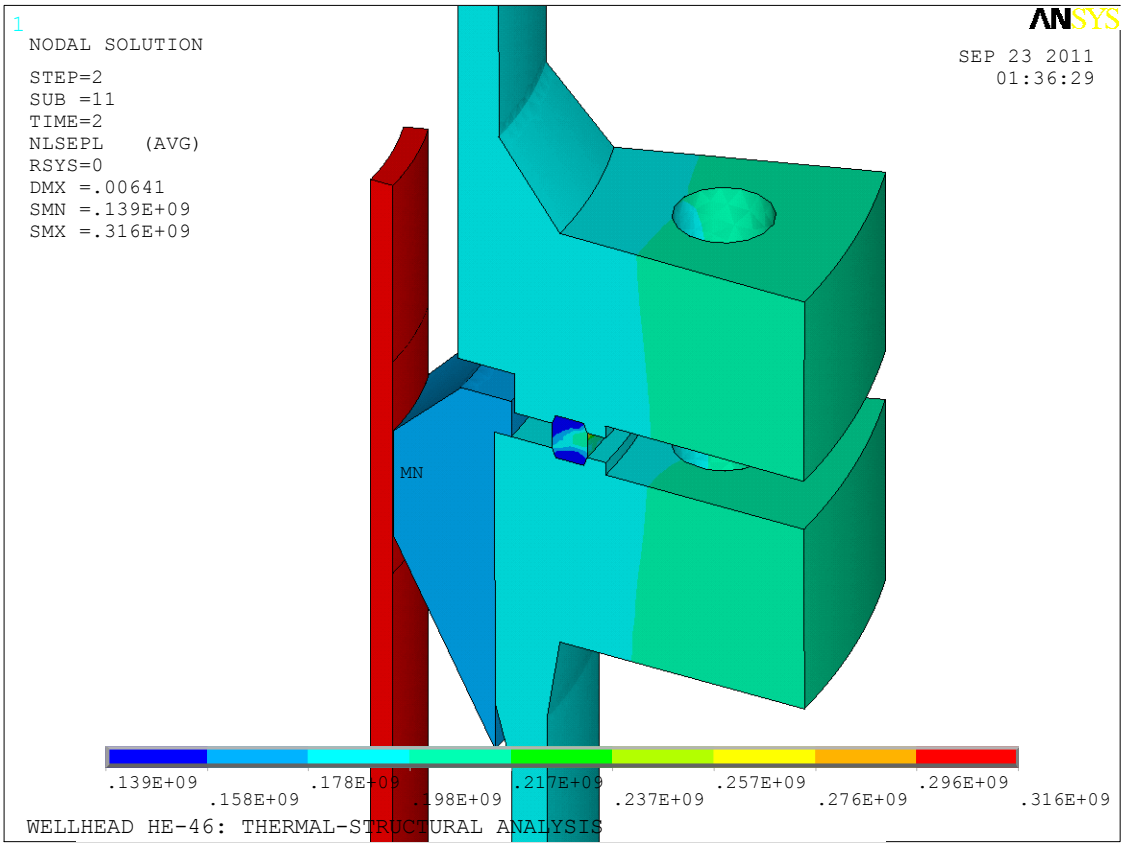

Figure 5.15 Load Case 3: Von Mises stress distribution (above) and the yield stress (below) in the lower flange connection

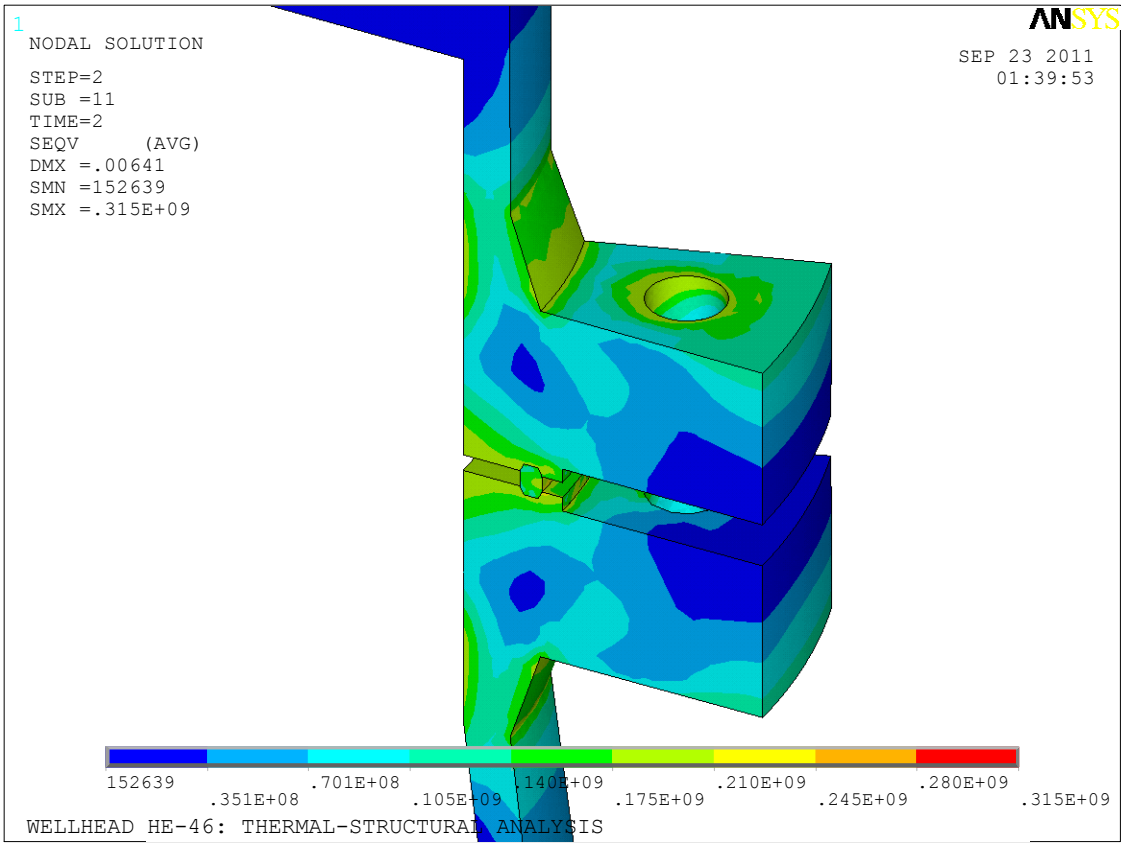

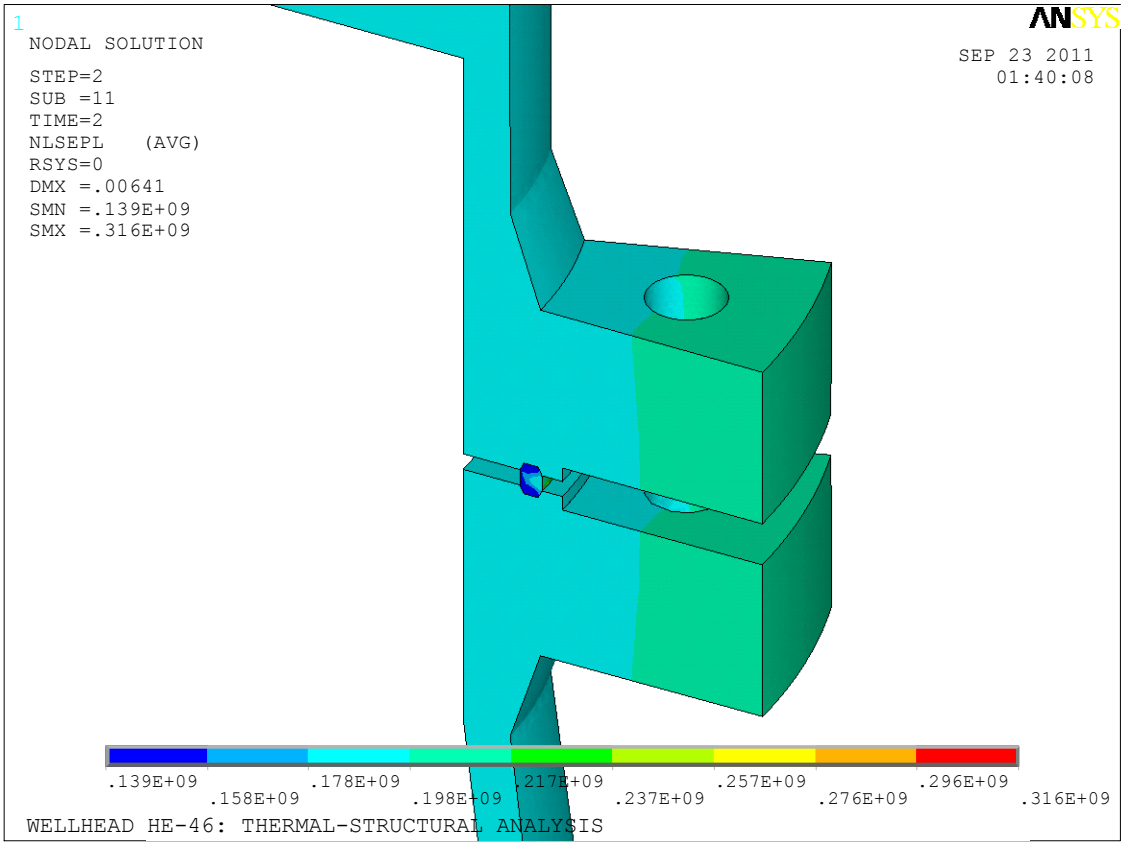

Figure 5.16 Load Case 3: Von Mises stress distribution (above) and the yield stress (below) in the upper flange connection

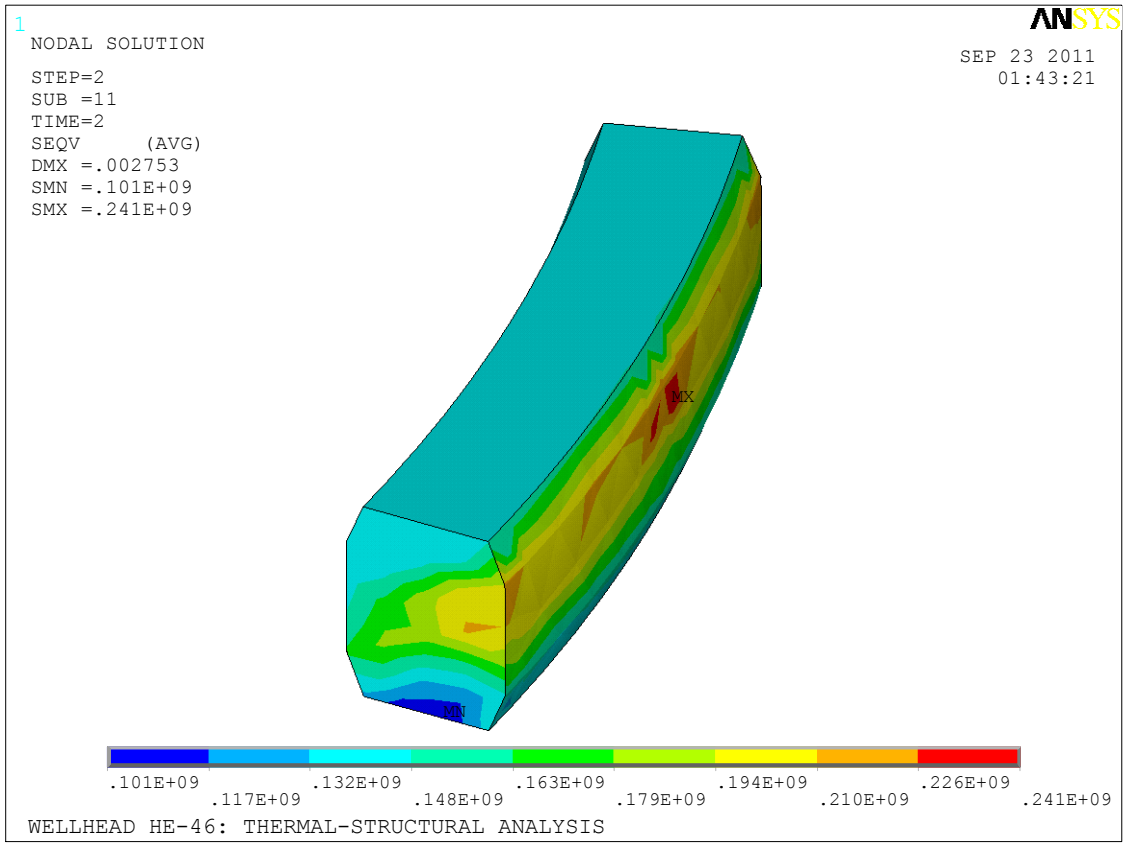

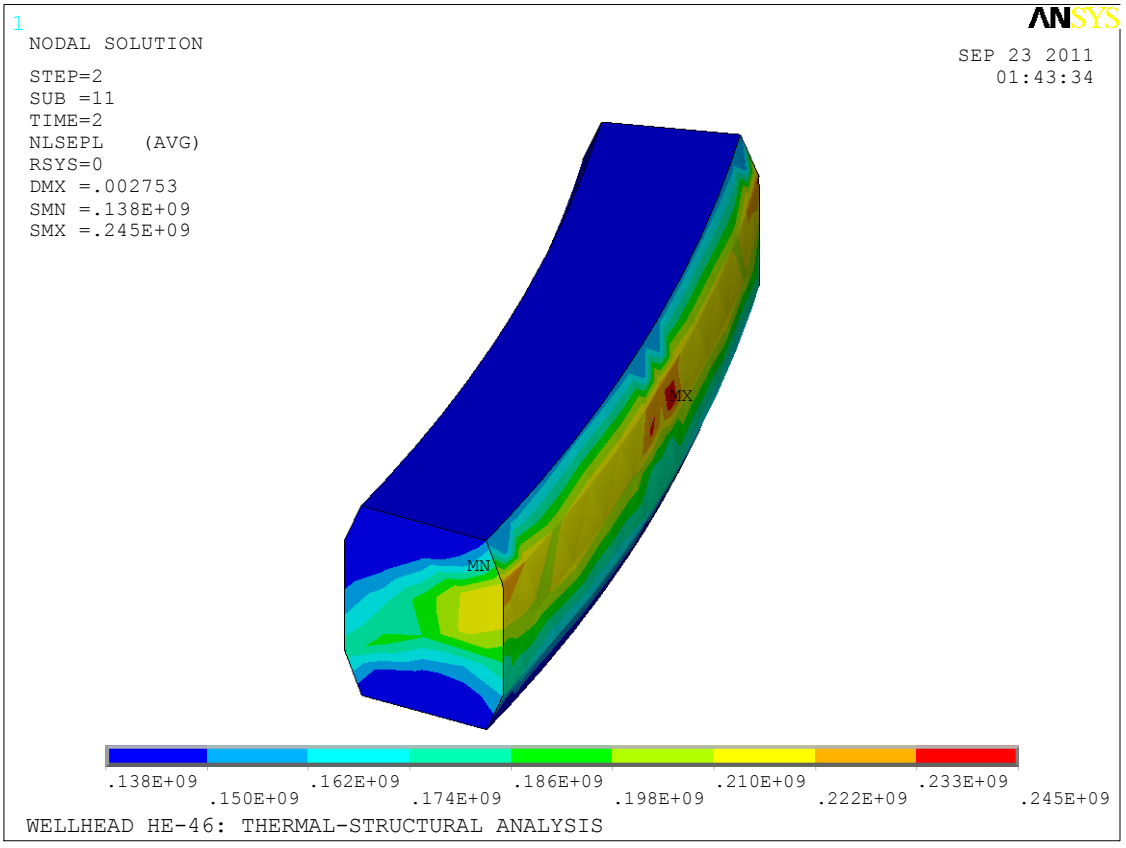

Figure 5.17 Load Case 3: Von Mises stress distribution (above) and the yield stress (below) in the lower gasket

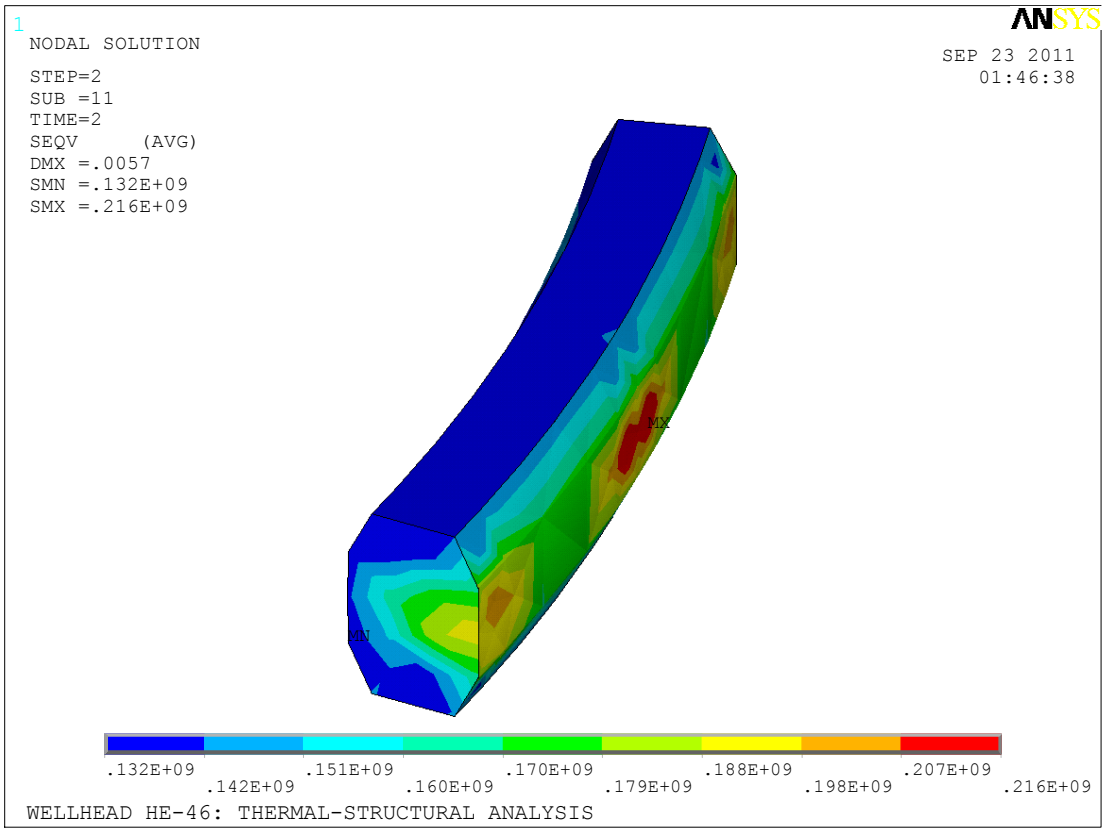

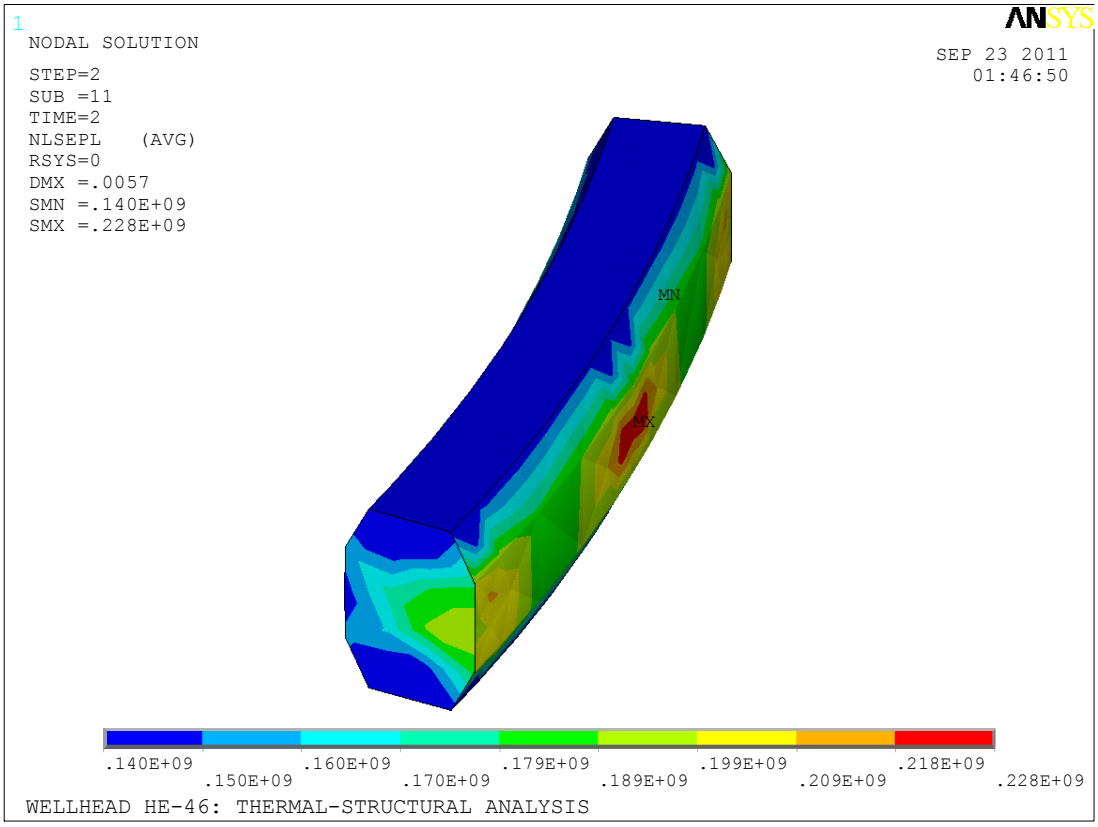

Figure 5.18 Load Case 3: Von Mises stress distribution (above) and the yield stress (below) in the upper gasket

Table 5.3 summarizes the maximum stresses found in the components during this load case. It is interesting to see how the stresses are considerably lower for this load case in most parts of the wellhead. This is mainly because the temperature gradient is much lower, because the temperature distribution has evened out. The maximum vertical thermal expansion for this case is about 6.5 mm at the top of the model. The gaskets show plastic deformation as before, and the maximum stresses are higher than before.

Table 5.3 Load Case 3: Maximum Von Mises stresses compared to yield stress

Wellhead part	Von Mises stress [MPa]	Yield stress [MPa]	% of yield stress
Production casing	280	316	89%
Casing steering	143	158	91%
Lower flanges	140	217	65%
Upper flanges	210	217	97%
Lower gasket	241	138	175%
Upper gasket	216	140	154%

5.4 Load Case 4: Maximum Design Loads

Finally, it is interesting to see what happens when the wellhead is subjected to an extreme load case. Referring to figure 2.6, it can be seen that the main valve of the wellhead is rated for a maximum load of 100 bar and 300°C. This extreme pressure can sometimes be reached inside wellheads when the well is closed, and gases build up on top of the geothermal fluid, and thereby pushing the fluid down into the well. This temperature value could never be reached in reality at this wellhead, because the reservoir temperature isn't high enough. However, since the main valve is designed to withstand this load, it will be subjected to the model.

The setup for load case 4 can be seen on figure 5.19.

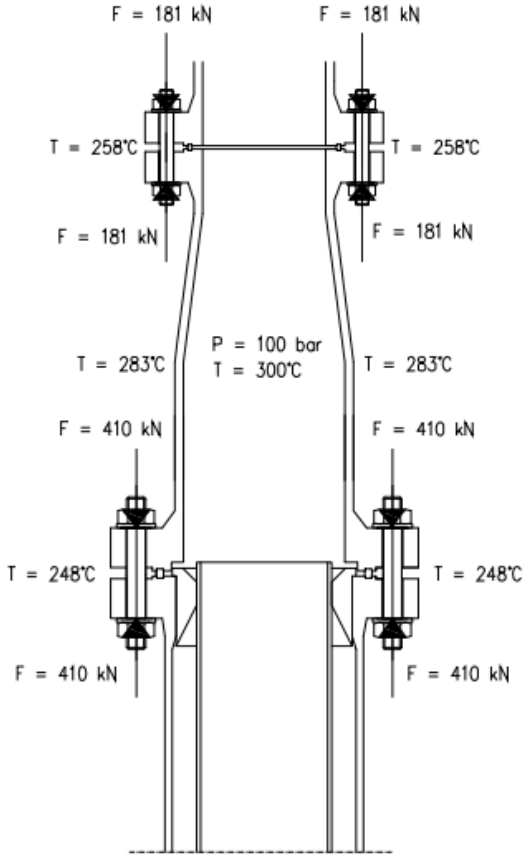

Figure 5.19 Load case 4

The temperature boundary conditions on the outside of the well are fixed as before, by assuming a similar temperature distribution as the measurements provided, scaling it up due to the higher inner temperature. On figures 5.20 the temperature distribution and the stress distribution for this case can be seen. Figures 5.21, 5.22, 5.23 and 5.24 show the results for the flanges and gaskets, as before.

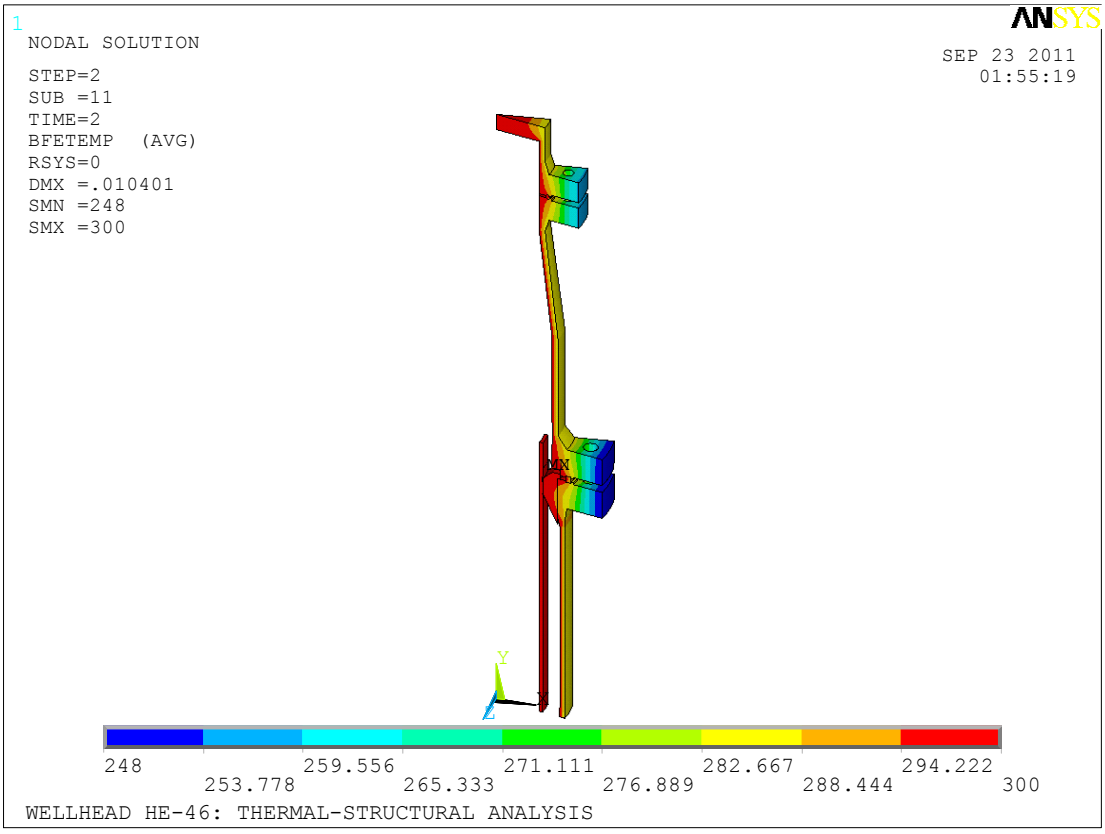

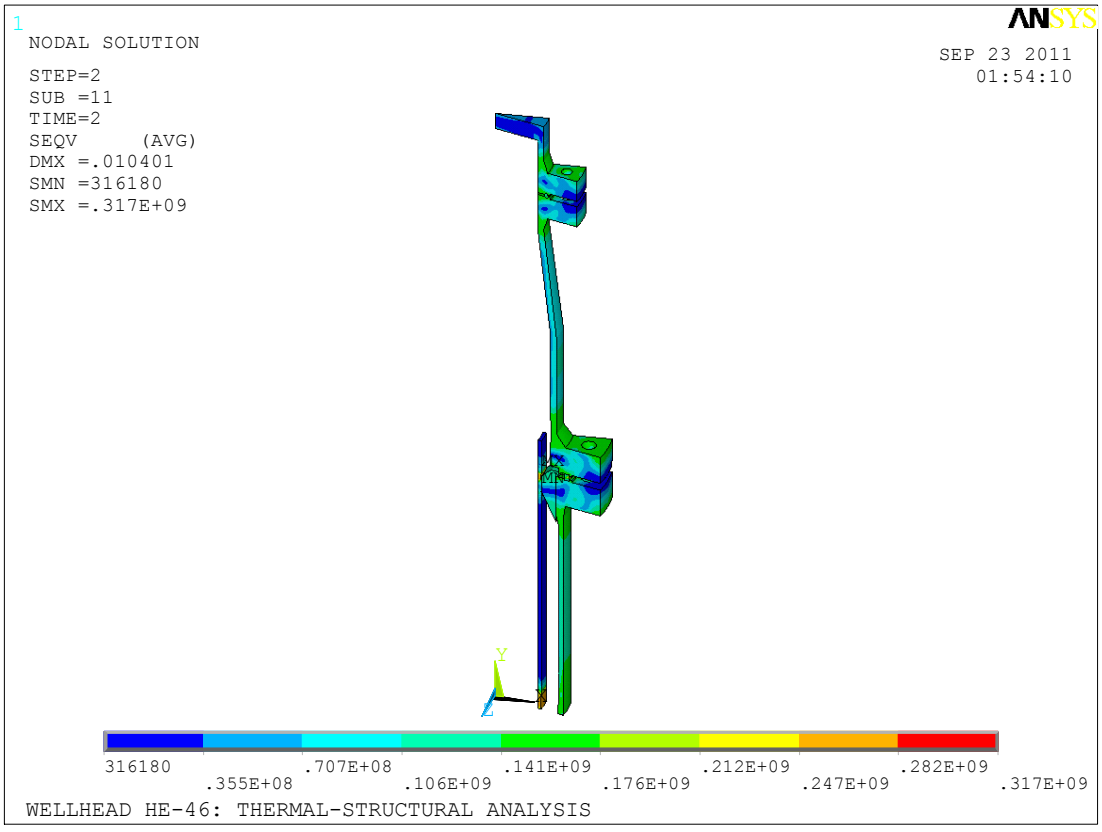

Figure 5.20 Temperature and Von Mises stress distribution for load case 4

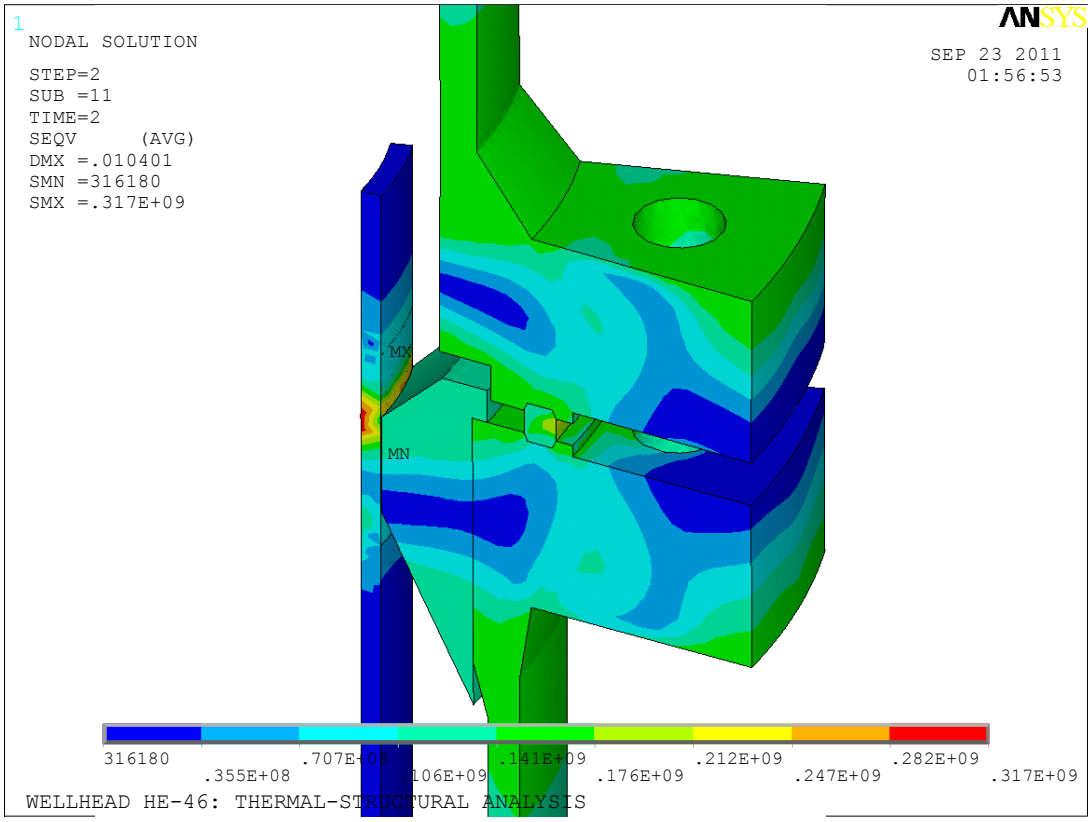

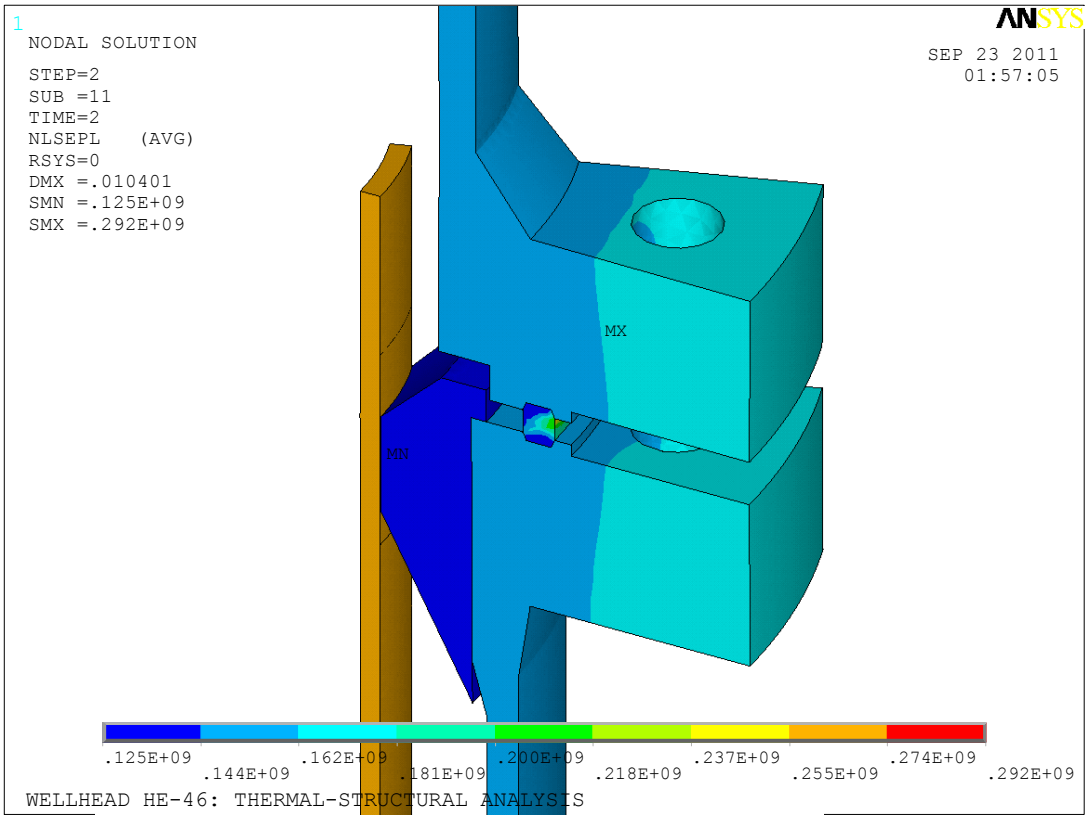

Figure 5.21 Load Case 4: Von Mises stress distribution (above) and the yield stress (below) in the lower flange connection

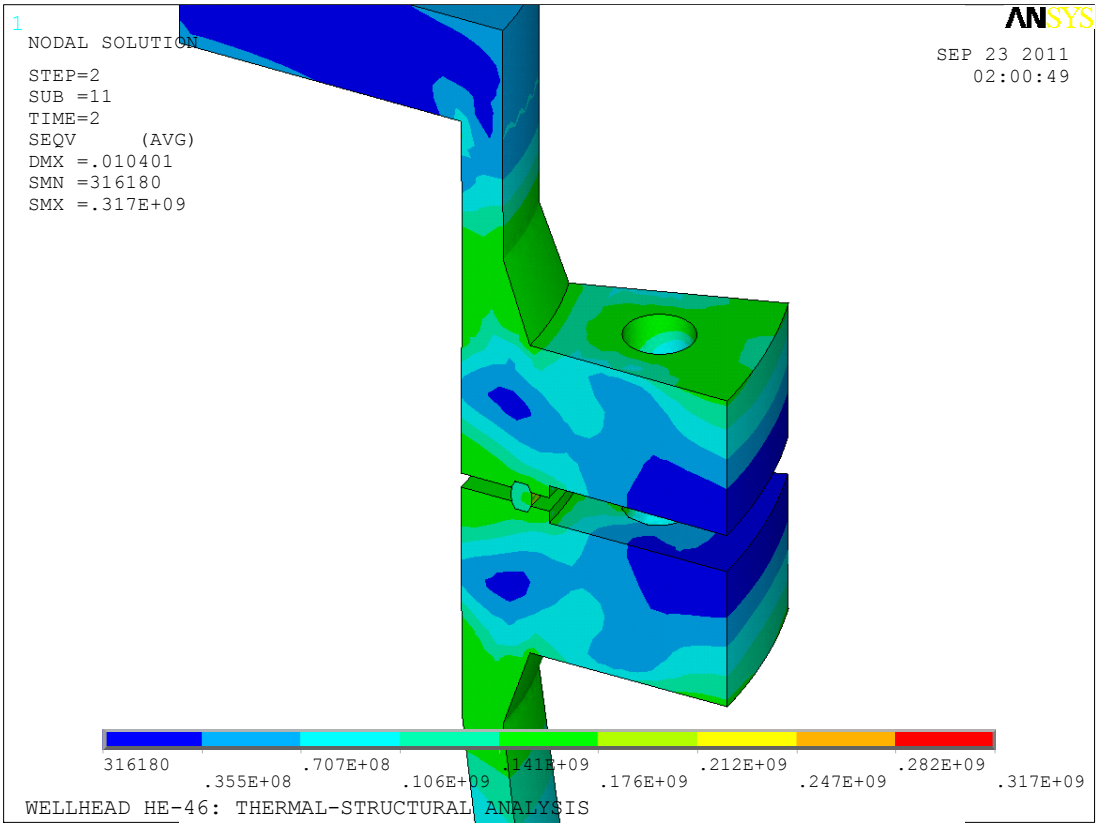

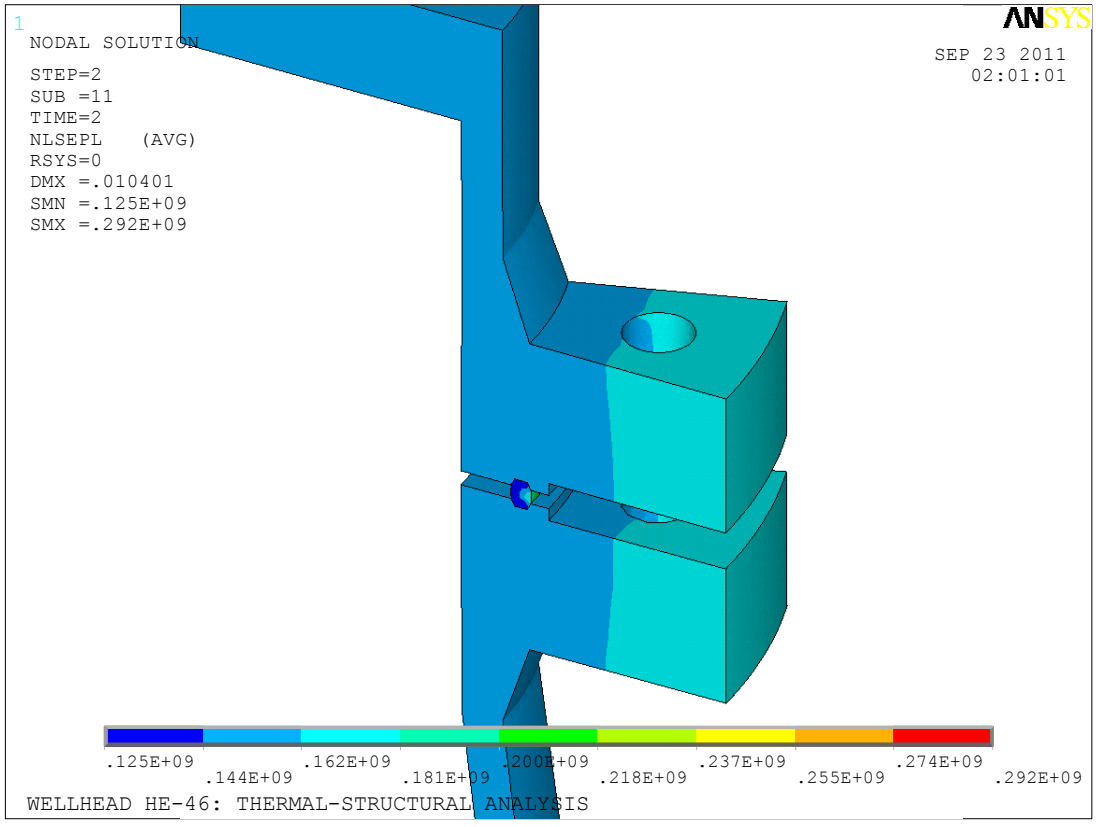

Figure 5.22 Load Case 4: Von Mises stress distribution (above) and the yield stress (below) in the upper flange connection

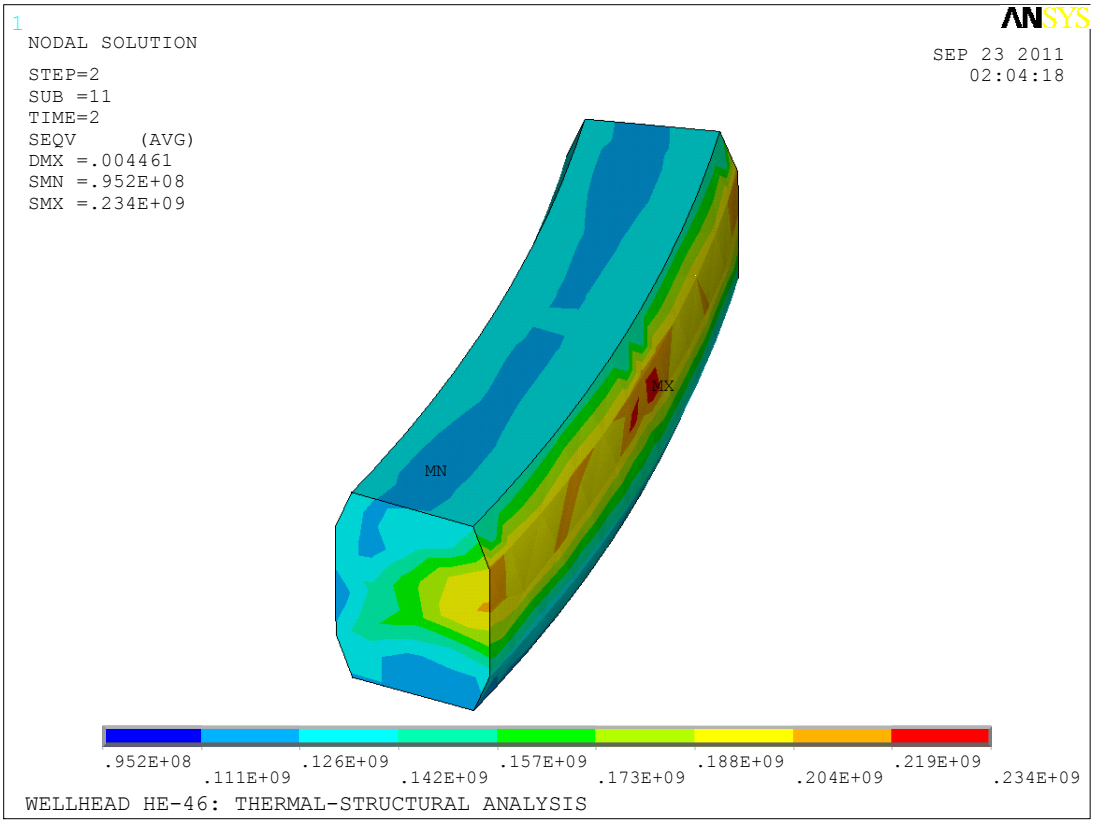

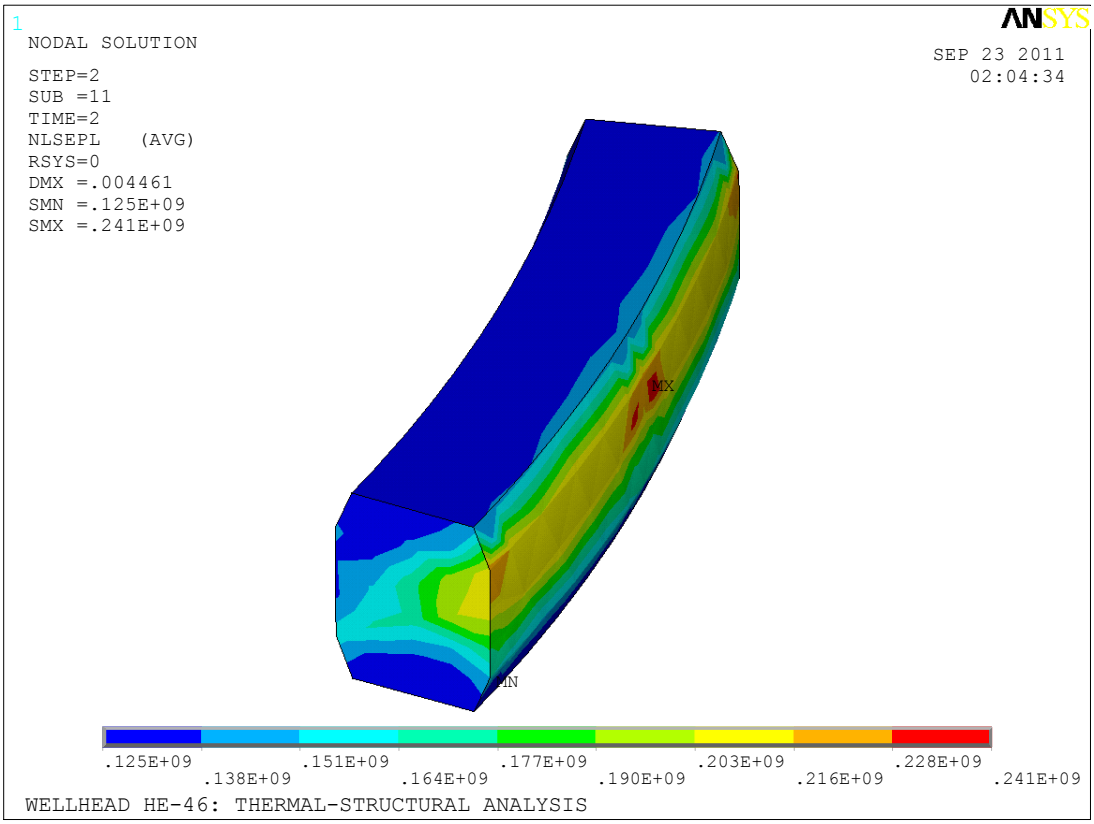

Figure 5.23 Load Case 4: Von Mises stress distribution (above) and the yield stress (below) in the lower gasket

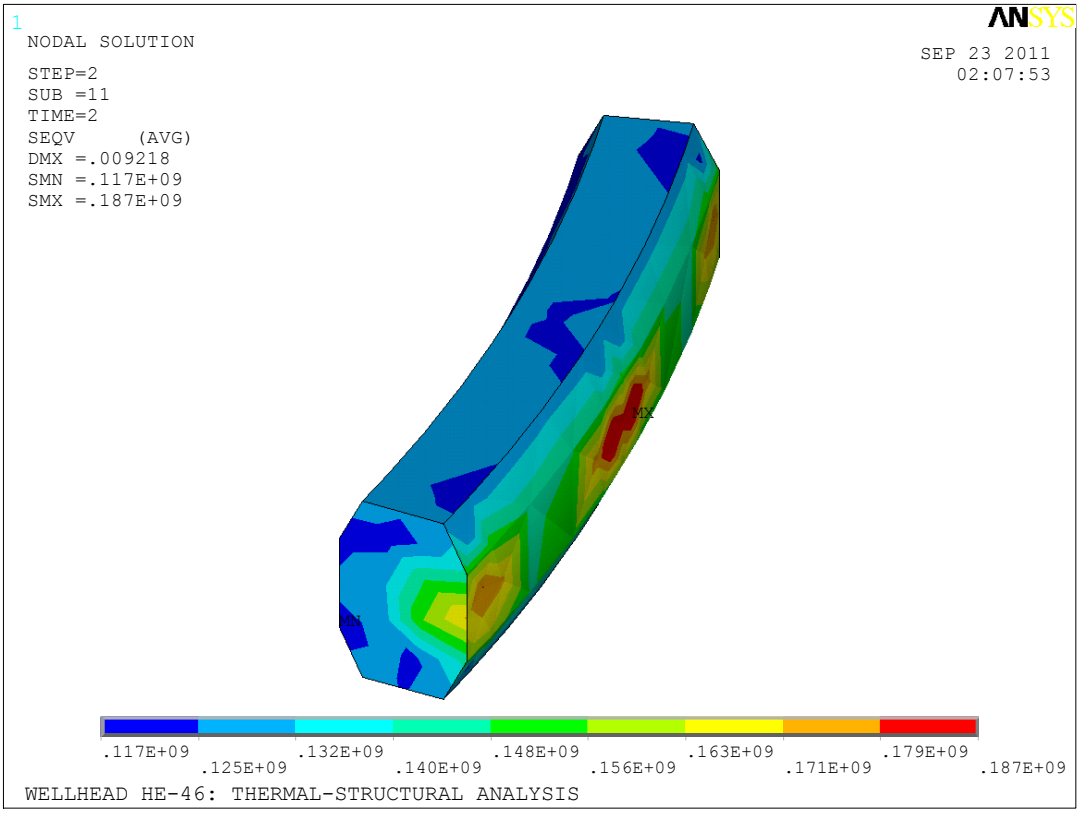

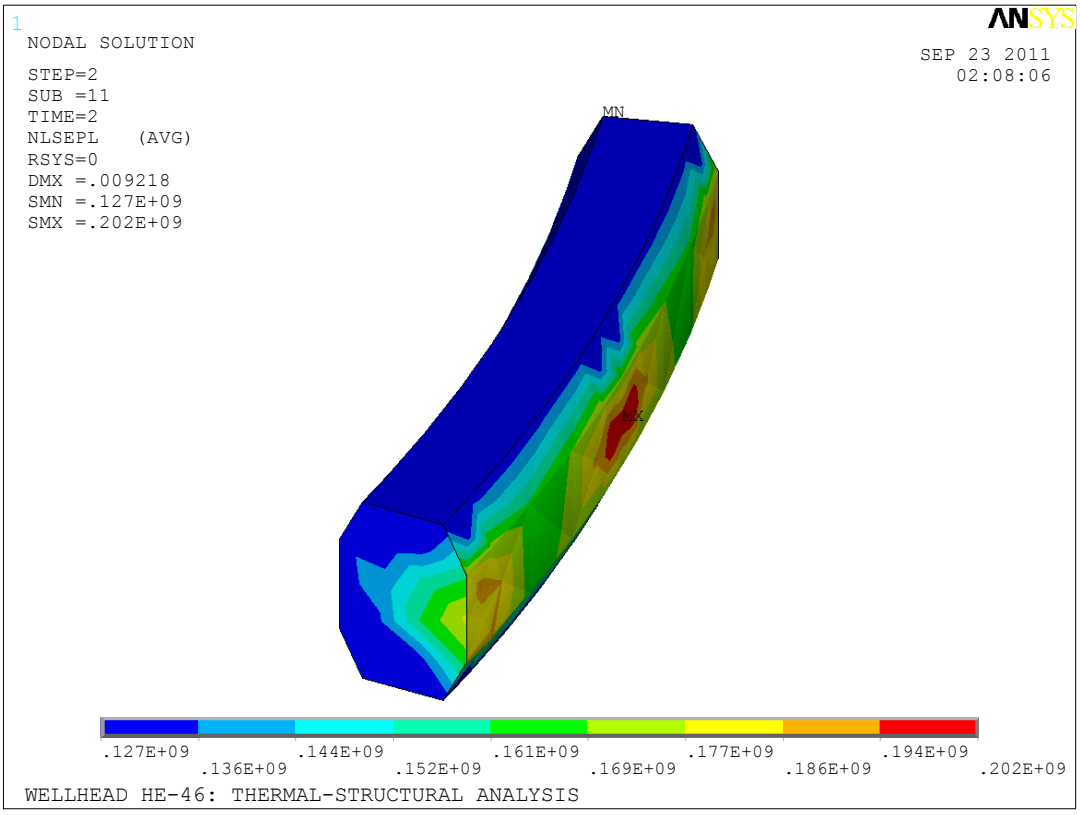

Figure 5.24 Load Case 4: Von Mises stress distribution (above) and the yield stress (below) in the upper gasket

For this extreme load case, the maximum Von Mises stresses in the production casing and the casing steering go over the yield limit. The flanges experience stresses just under the yield stress. Clearly, the wellhead is not designed to withstand this extreme load case, especially the temperature value, which reduces the strength of the steel considerably.

The maximum vertical displacement in the wellhead is just over 10 mm at the top of the model, which reflects the thermal expansion in the complete equipment.

Table 5.4 summarizes the results for load case 4.

Table 5.4 Load Case 4: Maximum Von Mises stresses compared to yield stress

Wellhead part	Von Mises stress [MPa]	Yield Stress [MPa]	% of yield stress
Production casing	317	255	124%
Casing steering	141	125	113%
Lower flanges	176	181	97%
Upper flanges	172	181	95%
Lower gasket	234	125	187%
Upper gasket	187	127	147%

5.5 Results Summary and Comparison

Examination of the results from load cases 1 to 4 revealed that the temperature is a high factor in the stress distribution in the wellhead equipment, especially during the first seconds of charging when there exists a steep temperature gradient in the wellhead. The effect of reduced strength of steel with higher temperatures is also a critical factor. Clearly, temperature effects should not be underestimated in the design of wellhead equipment. Figures 5.25 to 5.30 summarize the maximum Von Mises stresses and the reduction in yield strength for the production casing, the casing steering, the flanges and the gaskets for all the load cases. The figures show that the production casing and the casing steering experience yielding for the extreme load case. As was expected, the gaskets experience yielding during all the load cases.

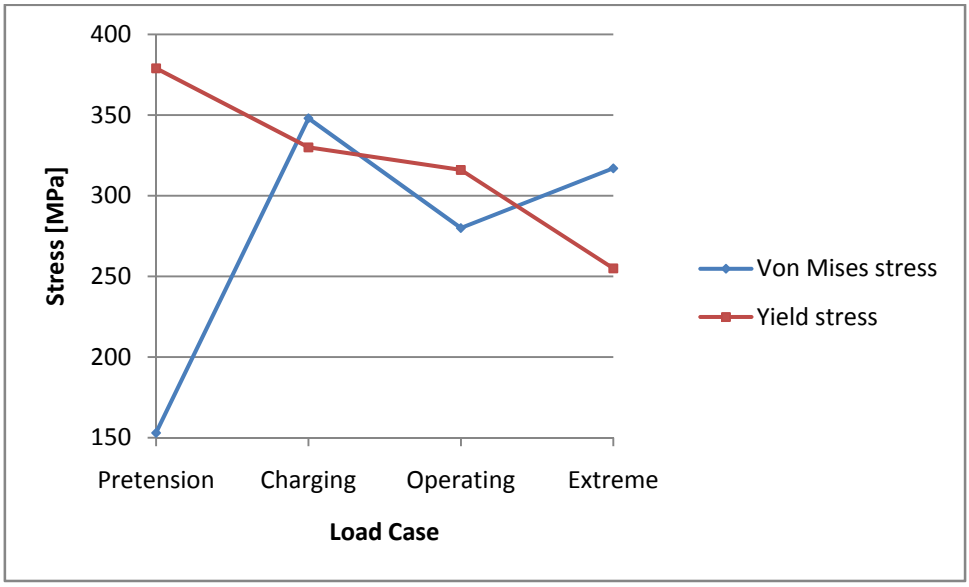

Figure 5.25 Maximum Von Mises stresses and yield stresses for the production casing

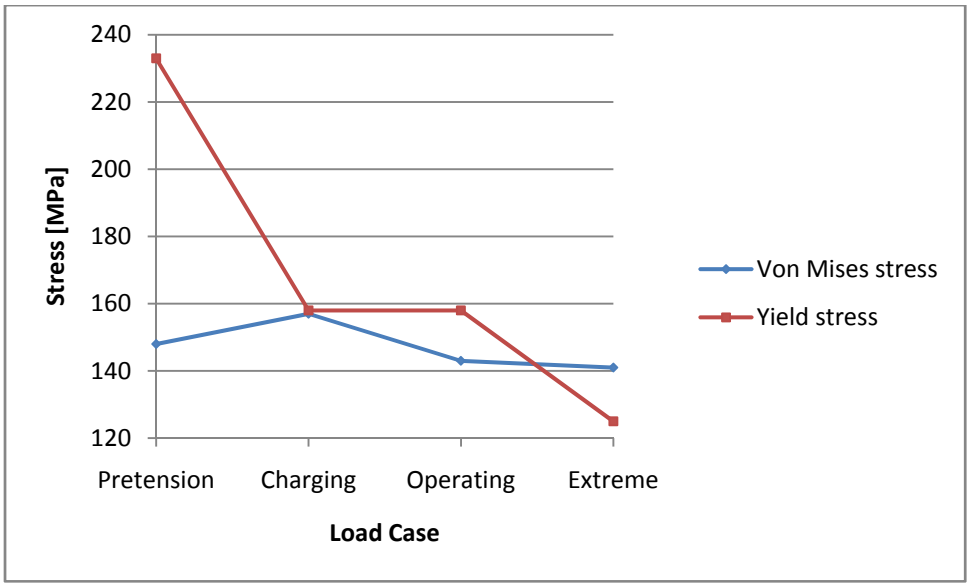

Figure 5.26 Maximum Von Mises stresses and yield stresses for the casing steering

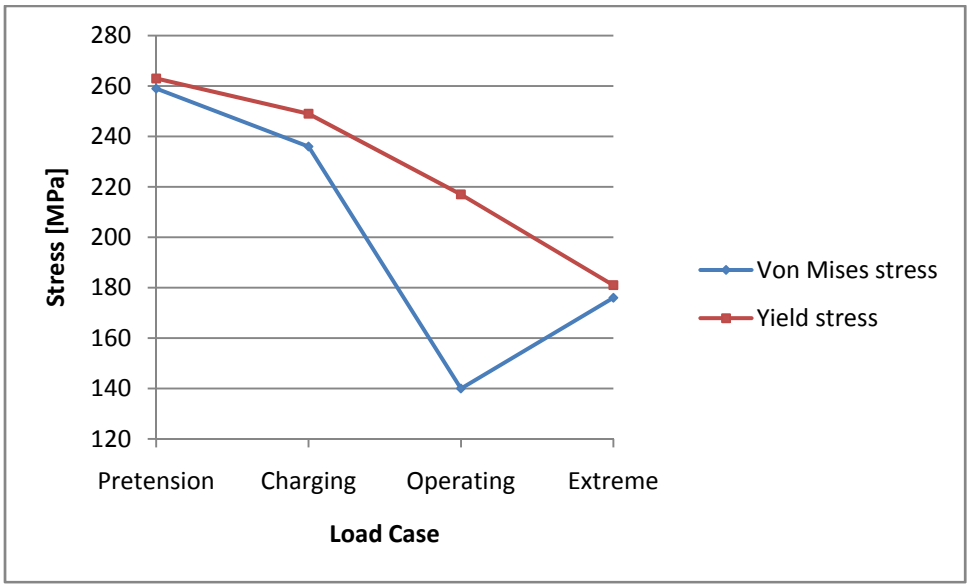

Figure 5.27 Maximum Von Mises stresses and yield stresses for the lower flanges

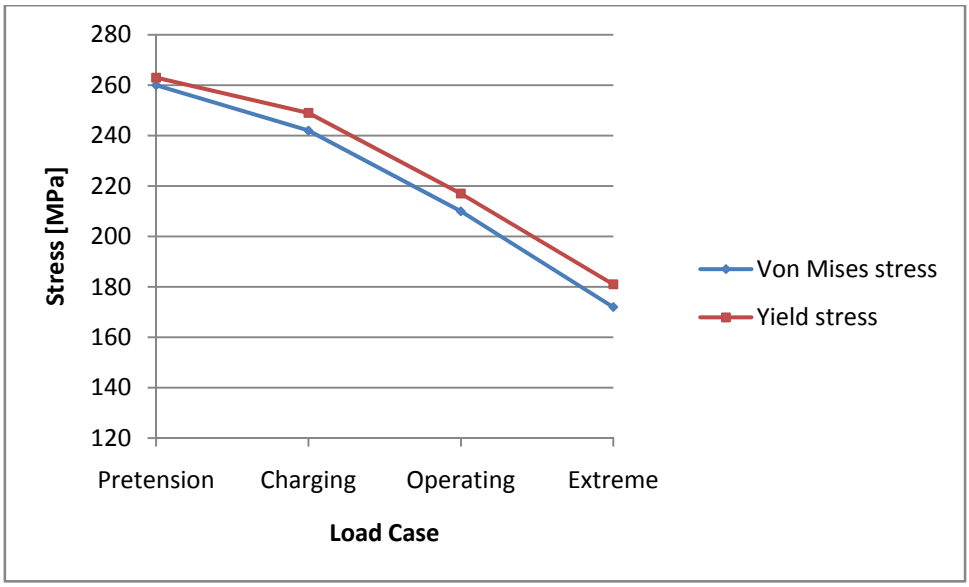

Figure 5.28 Maximum Von Mises stresses and yield stresses for the upper flanges

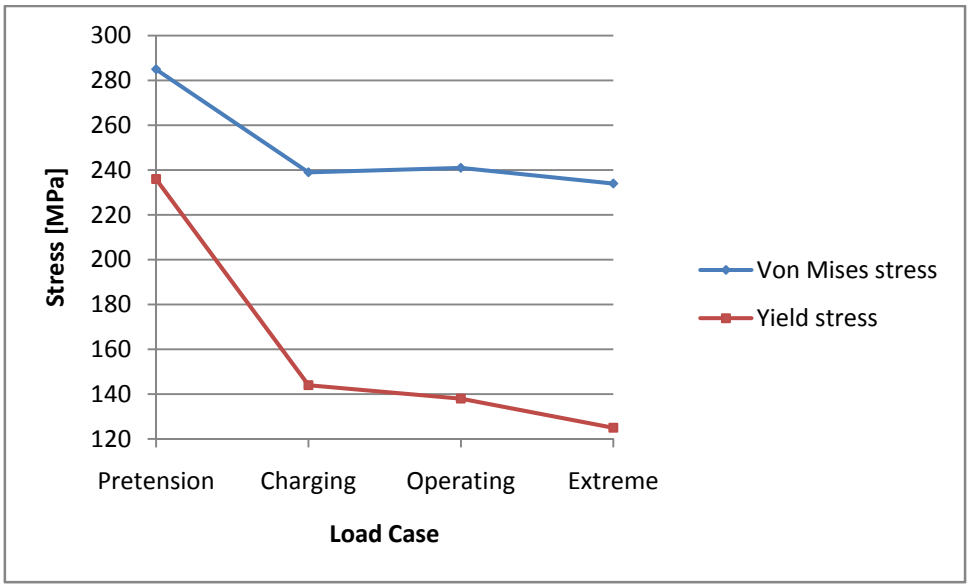

Figure 5.29 Maximum Von Mises stresses and yield stresses for the lower gasket

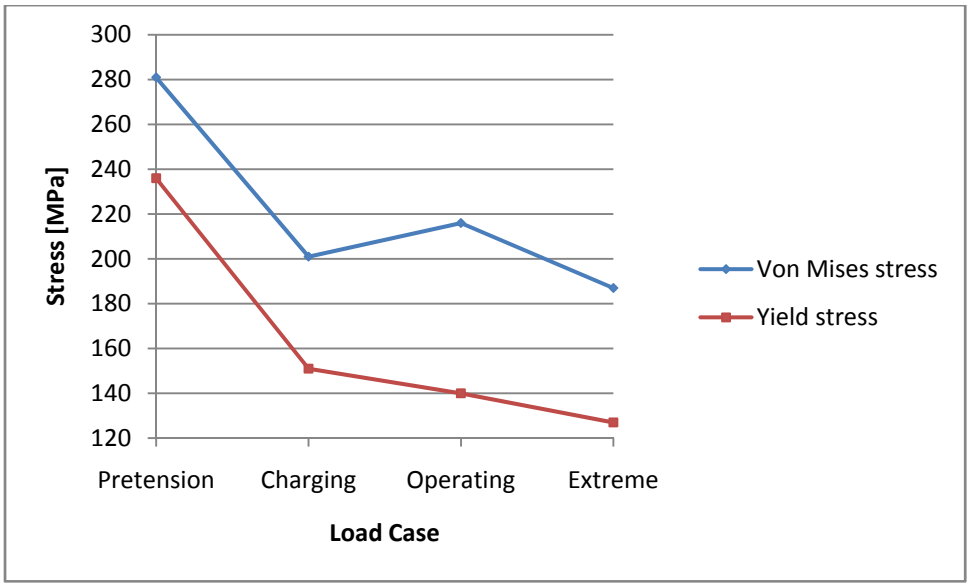

Figure 5.30 Maximum Von Mises stresses and yield stresses for the upper gasket

It is also clear from the above figures that the stresses in the gaskets are much lower during operation of the wellhead, than they are during initial pretension. This can cause leakage problems if not carefully monitored.

Finally, figure 5.31 shows the maximum displacement in the wellhead during the load cases, from 1 to 4. When the wellhead is cold in case 1 there is no expansion and then the expansion gradually increases. The final displacement value was about 10 mm.

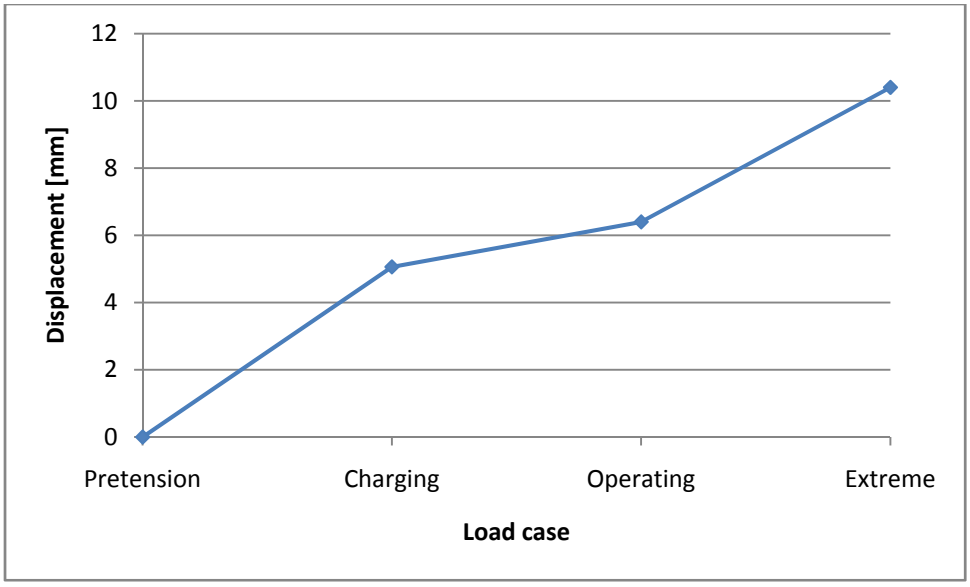

Figure 5.31 Maximum displacements in the wellhead

6 Conclusions

The analysis performed showed how the high temperatures encountered during operation of geothermal wellheads can have considerable effect on the stresses in the wellhead. When the temperature gradient is high, the resulting stresses are high. This can have effect on gasket stresses, which effects how well leakage in the flanged connection is controlled.

Thermal stresses are not the only effect of high temperatures. The material properties in the wellhead are dependent on temperature, with the strength of steel being reduced with higher temperature. This combined with high pretension loads and high pressure make wellhead equipment vulnerable to damage if this is not accounted for in the design process.

The model constructed in this project was able to simulate bolt pretension, thermal expansion, heat transfer, pressure loading, and nonlinear material behavior, all of which are of great importance in analysis of wellheads. The model can therefore be of great help for designers of wellhead equipment, as well as in the maintenance of it. Complex gasket behavior during pretensioning and production can be more closely analyzed with the model than conventional methods provide.

The wellhead model can also be used to analyze the effect of using different materials in the construction of wellheads, making experimentation in the design phase easier. This can make designs more economical and more safe.

Further improvements can be made to the model, however. As was mentioned in chapter 2 no account of vibration and corrosion is taken in the model. This could be an interesting continuation of the project.

Appendix A

A.1 Drawings of Wellhead HE-46

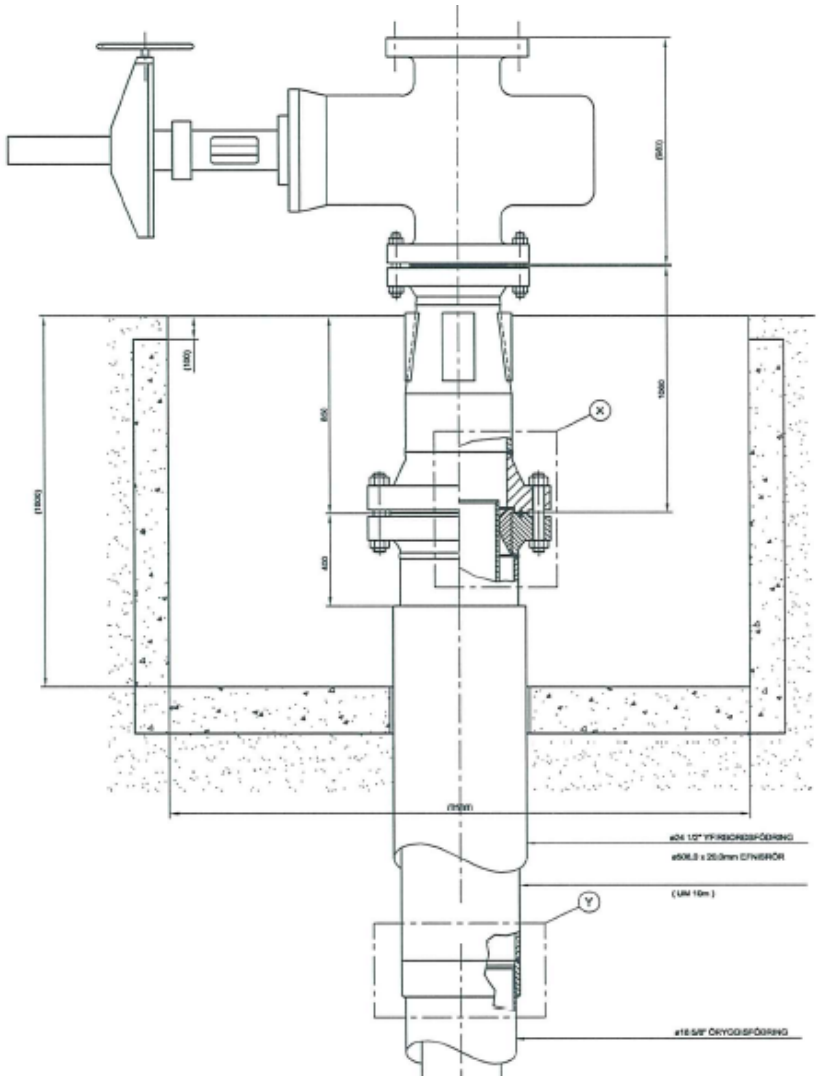

Figure A.1 Wellhead with a 12" Class 900 main valve and an expansion spool[2]

[2] Drawings provided by Mannvit, with kind permission to use in this project

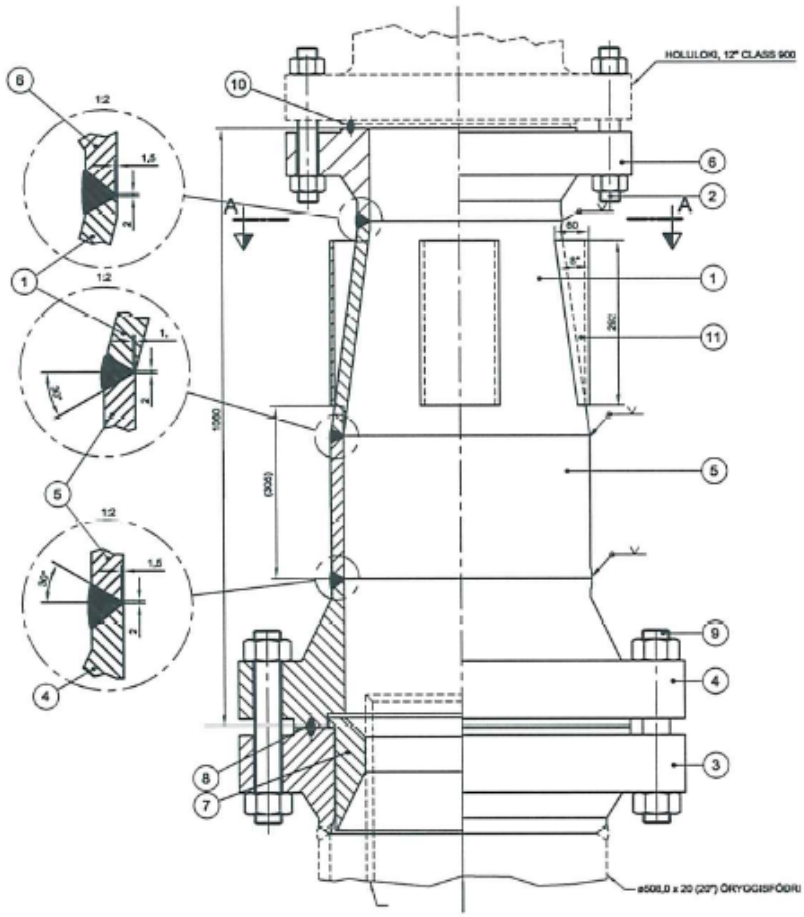

Figure A.2 Expansion spool and bolted flanges[1]

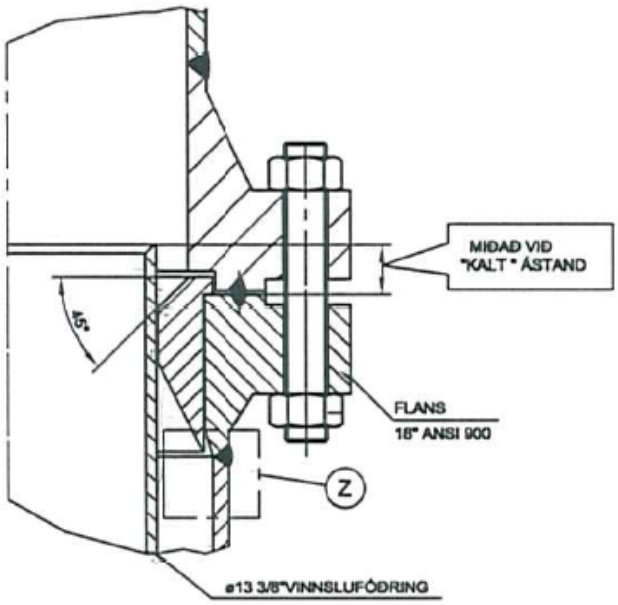

Figure A.3 Casing steering and flange connection[1]

A.2 Measurements of Wellhead HE-46 During and After Charging

Temperature, pressure, displacement and strain measurements of wellhead HE-46 were made in April 2011. Temperature measurements were made at several points, called 1, 2, 3, 4 and 5. Those are shown in numerical order on figure A.4.

Figure A.4 Location of temperature measurements on wellhead HE-46

Strain gages were also fastened to the wellhead. These are shown on figures A.4 and A.5. Unfortunately the strain measurements were unsuccessful, due to malfunction of the strain gages, probably due to the high temperature.

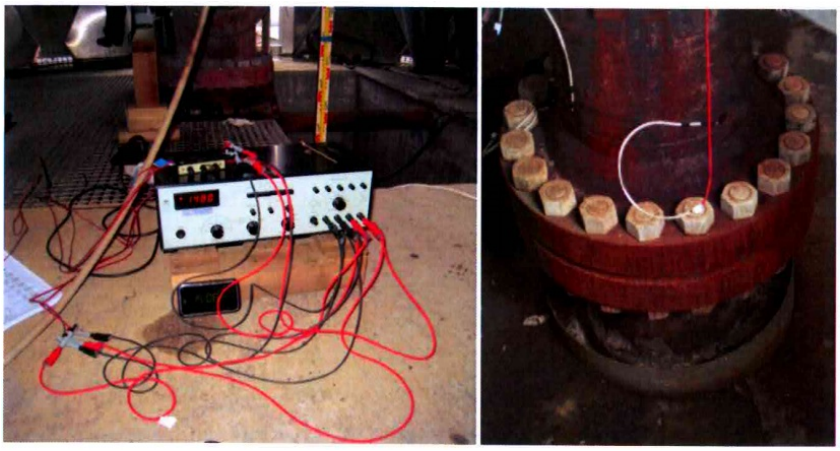

Figure A.5 Strain gages

Figure A.6 shows the pressure that was measured in three ways during charging of the well. The measurement at 13:17 is used as a reference for the setup of the load case "Charging" in the project.

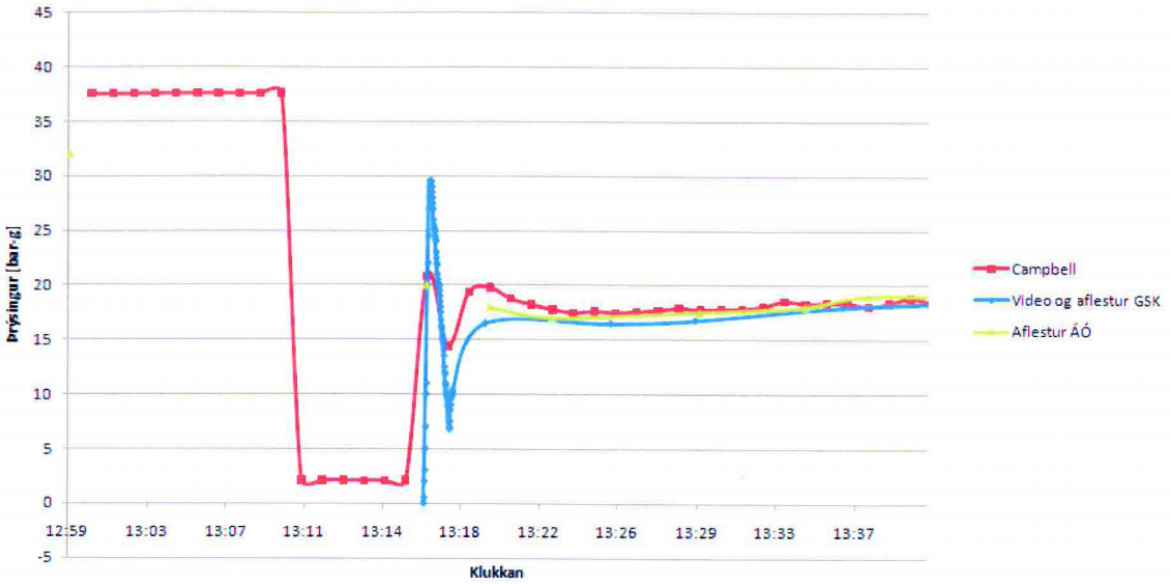

Figure A.6 Pressure inside the wellhead

On figure A.7 the temperature measurements are shown. Points 1-5 are the ones shown on figure A.4.

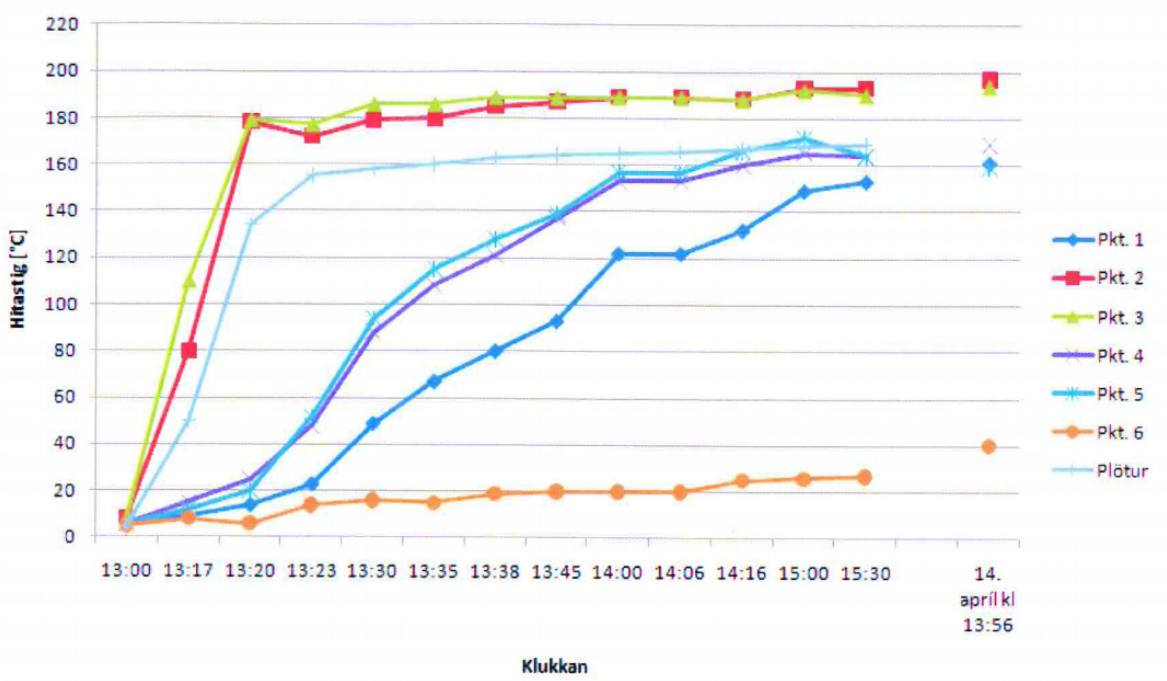

Figure A.7 Temperature measurements on the outside of the wellhead

Finally, expansion of the wellhead from the cellar floor was measured. The results can be seen on figure A.8.

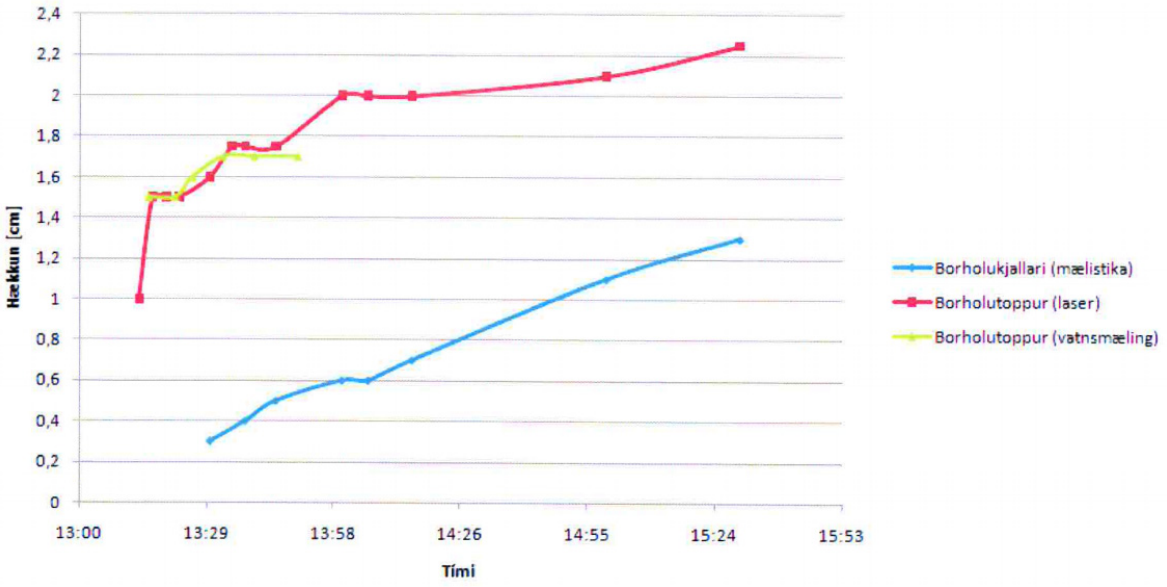

Figure A.8 Expansion of the wellhead from the cellar floor

A.3 Some Production Figures for HE-46

HE-46	Mæld gildi						Reiknuð gildi						Athugasemdir			
Dags kl	Holutopp-þrýstingur P_0 [bar g]	Blenda d [mm]	Blenda P_2 [bar a]	Þvermál stúts D_c [mm]	Kritískur þrýstingur Po [bar a]	Vatns-hlutfall V_h [m³/m³]	Skiljuþrýst. P_{sep} [bar a]	Vatns-rennsli V_r [l/s]	Heildar-vermi H_g [kJ/kg]	Heildar-rennsli Q_{tot} [kg/s]	Gufa við 1 bar G_{stm} [kg/s]	Gufa við skiljuþrýst. G_{sep} [kg/s]	Gufuhlutfl við skiljuþrýst. G_{hlut} [%]	Staða stjórnloka	Athugasemdir	Mælt af	Tenging
02.12.2008	20,19			161	1,82	47,00	8	0,70	2587	17,65	16,95	16,04	90,87			ÍSOR	
03.12.2008	20,66			161	1,87	220,40	8	30,99	1124	45,03	14,07	8,47	18,81			ÍSOR	
04.12.2008	20,11			161	1,85	219,40	8	30,65	1128	44,62	14,01	8,45	18,97			ÍSOR	
04.12.2008	16,00	100	7,00	161	1,90	260	8	46,70	889	58,92	12,26	4,24	7,20			DMM	Hyperlink
05.12.2008	18,53			161	1,93	219,10	8	30,54	1145	44,98	14,47	8,92	19,84			ÍSOR	
06.12.2008	18,59			161	1,88	219,30	8	30,61	1133	44,73	14,15	8,60	19,24			ÍSOR	
07.12.2008	18,35			161	1,95	218,50	8	30,34	1155	44,96	14,66	9,14	20,32			ÍSOR	
08.12.2008	17,92			161	1,84	218,10	8	30,20	1134	44,13	13,97	8,50	19,26			ÍSOR	
09.12.2008	18,20			161	1,89	220,60	8	31,06	1126	45,19	14,16	8,54	18,91			ÍSOR	
10.12.2008	19,04			161	1,95	219,20	8	30,58	1130	44,59	14,05	8,52	19,10			ÍSOR	
11.12.2008	19,17			161	1,89	221,30	8	31,31	1122	45,41	14,14	8,49	18,69			ÍSOR	
11.12.2008	15,50	100	7,50	161	1,70	270	8	51,29	801	61,69	10,45	1,78	2,89			DMM	Hyperlink
12.12.2008	19,05			161	1,85	219,00	8	30,51	1130	44,47	14,00	8,48	19,06			ÍSOR	
13.12.2008	18,65			161	1,91	219,30	8	30,61	1141	44,95	14,37	8,81	19,61			ÍSOR	
14.12.2008	17,69			161	1,85	220,20	8	30,93	1121	44,84	13,95	8,36	18,65			ÍSOR	
15.12.2008	18,46			161	1,90	220,10	8	30,89	1133	45,13	14,28	8,68	19,24			ÍSOR	
16.12.2008	18,53			161	1,95	218,80	8	30,44	1134	44,50	14,10	8,58	19,29			ÍSOR	
17.12.2008	17,73			161	1,93	219,00	8	30,51	1146	44,94	14,47	8,93	19,87			ÍSOR	
18.12.2008	17,28			161	1,90	218,20	8	30,23	1146	44,54	14,34	8,85	19,87			ÍSOR	
18.12.2008	15,50	100	6,70	161	1,70	270	8	51,29	801	61,69	10,45	1,78	2,89			DMM	Hyperlink
19.12.2008	17,46			161	1,87	218,30	8	30,27	1124	43,97	13,74	8,27	18,81			ÍSOR	
20.12.2008	17,45			161	1,84	218,60	8	30,37	1131	44,31	13,98	8,48	19,13			ÍSOR	
21.12.2008	17,89			161	1,90	219,70	8	30,75	1071	43,20	12,49	7,00	16,20			ÍSOR	
22.12.2008	18,13			161	1,91	220,10	8	30,89	1135	45,19	14,34	8,74	19,34			ÍSOR	
23.12.2008	19,19			161	1,87	221,20	8	31,27	1125	45,45	14,21	8,56	18,83			ÍSOR	
24.12.2008	19,92			161	1,90	221,40	8	31,34	1123	45,51	14,21	8,54	18,76			ÍSOR	
25.12.2008	19,81			161	1,84	219,10	8	30,54	1097	43,62	13,11	7,63	17,48			ÍSOR	
26.12.2008	18,65			161	1,87	219,20	8	30,58	1133	44,67	14,13	8,59	19,23			ÍSOR	
27.12.2008	17,86			161	1,84	218,50	8	30,34	1102	43,44	13,14	7,68	17,69			ÍSOR	
28.12.2008	17,11			161	1,83	217,10	8	29,86	1138	43,77	13,95	8,54	19,50			ÍSOR	
29.12.2008	16,34			161	1,87	217,20	8	29,89	1146	44,05	14,19	8,76	19,89			ÍSOR	
30.12.2008	16,31			161	1,90	218,70	8	30,41	1123	44,12	13,75	8,26	18,72			ÍSOR	
31.12.2008	17,14			161	1,86	219,50	8	30,68	1129	44,69	14,05	8,50	19,01			ÍSOR	

Figure A.9 Production figures in december 2008 for well HE-46. The wellhead pressure is normally 18-20 bar

References

[1] Guðmundur Pálmason. *Jarðhitabók*. Hið íslenska bókmenntafélag. 2005.

[2] Ólafur G. Flóvenz. *General Aspects of Geothermal Energy – Lecture notes from Geothermal Systems*. Íslenskar orkurannsóknir, Grensásvegi 9, 108 Reykjavík. 2008.

[3] *Website: www.or.is, Orkuveita Reykjavíkur (e. Reykjavik Energy) site*. May 2011.

[4] Sverrir Þórhallsson. *Geothermal boreholes - Lecture notes from Geothermal Systems*. Íslenskar orkurannsóknir, Grensásvegi 9, 108 Reykjavík. 2008.

[5] Þorleikur Jóhannesson. *Mechanical Design of Geothermal Power Plants – Lecture notes from Geothermal Power Development*. Verkís, Suðurlandsbraut 4, 108 Reykjavík. 2009.

[6] Hagen Hole. *Geothermal Well Design – Casing and Wellhead*. Petroleum Engineering Summer School. Dubrovnik, Croatia. June 2008.

[7] Anna Lilja Oddsdóttir and Einar Gunnlaugsson. *Hellisheiði – Gufuborholur: Afl, vatnsborð og vinnsla*. Orkuveita Reykjavíkur. 2008.

[8] Halldór Pálsson. *Thermodynamics of geothermal power plants – Lecture notes from Geothermal Power Development*. Háskóli Íslands, Hjarðarhaga 2-6, 107 Reykjavík. 2009.

[9] Halldór Pálsson. *Two-phase flow in pipes and boreholes – Lecture notes from Geothermal Systems*. Háskóli Íslands, Hjarðarhaga 2-6, 107 Reykjavík. 2008.

[10] Joseph E. Shigley, Charles R. Mischke and Richard G. Budynas. *Mechanical Engineering Design, Seventh Edition*. McGraw-Hill Companies, Inc., 1221 Avenue of the Americas, New York, NY 10020, 2004.

[11] Mohinder L. Nayyar. *Piping Handbook, Seventh Edition*. McGraw-Hill Companies, Inc., 1221 Avenue of the Americas, New York, NY 10020. 2000.

[12] Takuya Sato and Kenichiro Kado. *Inelastic Analysis of Dissimilar Material Flanges with Metal Ring Gaskets at Elevated Temperatures*. Proceedings of PVP2005 - ASME Pressure Vessels and Piping Division Conference. 2005.

[13] Akli Nechache and Abdel-Hakim Bouzid. *Creep Analysis of Bolted Flange Joints*. International Journal of Pressure Vessels and Piping 84. 2007.

[14] Akli Nechache and Abdel-Hakim Bouzid. *An Analytical Solution for Evaluating Gasket Stress Change in Bolted Flange Connections Subjected to High Temperature Loading*. Journal of Pressure Vessel Technology. 2005.

[15] Sverrir Þórhallsson. *Þróun í hönnun og frágangi hola á háhitasvæðum*. Lecture. Jarðhitafélag Íslands.

[16] Geir Þórólfsson. *Rekstur og viðhald háhitahola*. Lecture. Jarðhitafélag Íslands.

[17] Jr. William D. Callister. *Materials Science and Engineering - An Introduction*. John Wiley & Sons, Inc., 605 Third Avenue, New York, NY 10158-0012, USA, 2003.

[18] Ansel C. Ugural and Saul K. Fenster. *Advanced Strength and Applied Elasticity*. Pearson Education, Inc. Upper Saddle River, New Jersey 07458. 2003.

[19] Michael E. Plesha, Robert D. Cook, David S. Malkus and Robert J. Witt. *Concepts and Applications of Finite Element Analysis, Fourth Edition*. John Wiley & Sons, Inc., 111 River Street, Hoboken, NJ 07030, 2002.

[20] Inc. Ansys. *ANSYS Release 11.0 Documentation*. © 2007 SAS IP, Inc., 2007.

[21] J. P. Holman. *Heat Transfer, Ninth Edition*. McGraw-Hill Companies, Inc., 1221 Avenue of the Americas, New York, NY 10020, 2002.

[22] European standard: *EN-10217-2:2002 – Welded Steel Tubes for Pressure Purposes.*

[23] European standard: *EN-10088:2005 - Stainless Steels.*

[24] Jarðboranir. *Verklagsreglur vegna holutoppa á Reykjanesi – Frágangur á holutoppum*. Hitaveita Suðurnesja. April 2004.